WIRELESS RECEIVER DESIGNS: FROM INFORMATION THEORY TO VLSI IMPLEMENTATION

A Thesis
Presented to
The Academic Faculty

by

Wei Zhang

In Partial Fulfillment
of the Requirements for the Degree
Doctor of Philosophy in the
School of Electrical and Computer Engineering

Georgia Institute of Technology
December 2009

WIRELESS RECEIVER DESIGNS: FROM INFORMATION THEORY TO VLSI IMPLEMENTATION

Approved by:

Professor Xiaoli Ma, Advisor
School of Electrical and Computer Engineering
Georgia Institute of Technology

Professor David V. Anderson
School of Electrical and Computer Engineering
Georgia Institute of Technology

Professor John R. Barry
School of Electrical and Computer Engineering
Georgia Institute of Technology

Professor Kevin T. Kornegay
School of Electrical and Computer Engineering
Georgia Institute of Technology

Professor Xu-Yan Chen
School of Mathematics
Georgia Institute of Technology

Date Approved: 29 September 2009

To my dear family, friends, and my teachers

ACKNOWLEDGEMENTS

A journey is easier when you travel together. This dissertation is the result of more than three years of work during which I have been accompanied and supported by many people. It is a pleasure that I now have the opportunity to express my gratitude for them.

First, I would like to express my deep and sincere gratitude to my advisor Dr. Xiaoli Ma for her guidance and support throughout this work. With her enthusiasm and inspiration, this work has been carried out smoothly. During these years' study, she provided excellent mentoring, but what I benefit most from her is her specially designed training procedures which helped me to develop critical thinking and presenting skills. Her persistent encouragement and insightful advice make me believe in my choice which results in this dissertation. I have been closely working with Dr. Ma for five years, and I am really impressed by her dedication to research. She could not even realize how much I have learned from her. In addition to an excellent supervisor, Dr. Ma is as close as a good friend to me. I am really glad that I have known Dr. Ma in my life.

I am also grateful for the contributions of Dr. David V. Anderson, Dr. John R. Barry, Dr. Xu-Yan Chen, and Dr. Kevin T. Kornegay both as members of my thesis committee and as great teachers, and for their assistance throughout my graduate studies. My sincere appreciation also goes to Dr. Ananthram Swami from Army Research Lab for technical discussions and insightful suggestions. Also, I thank my colleagues in our group, Felix Arnold, Bob Baxley, Giwan Choi, Brian Gestner, Benjamin Hamilton, Qijia Liu, Kun Shi, and Chunming Zhao for their helpful discussions and support through this work. I am also thankful to Jun Ma, Guowang Miao, and

David Milliner for their assistance with technical problems - at all times.

I would like to give my special thanks to my dear wife Xiaoming Li for her love and support, and to my parents for their understanding, endless patience and encouragement. As the only child of the family, I owe them a lot for studying abroad.

I would like to acknowledge the financial support provided by the U.S. Army Research Laboratory and the U.S. Army Research Office under grant no. W911NF-06-1-0090 and through collaborative participation in the Collaborative Technology Alliance for Communications & Networks sponsored by the U.S. Army Research Laboratory under Cooperative Agreement DAAD19-01-2-0011.

TABLE OF CONTENTS

LIST OF TABLES

LIST OF FIGURES

LIST OF SYMBOLS

Upper bold face letters	matrices.
Lower bold face letters	column vectors.
Superscript $^{\mathcal{H}}$	Hermitian.
Superscript ^{T}	transpose.
Superscript *	conjugate.
Superscript †	the Moore-Penrose pseudo-inverse of matrices.
$\lvert \cdot \rvert$	absolute value of a scalar, or, cardinality of a set.
$\lVert \cdot \rVert$	Frobenius norm.
$\lceil \cdot \rceil$	integer ceiling.
$\lfloor \cdot \rfloor$	integer floor.
$\lfloor \cdot \rceil$	integer rounding.
$\langle \cdot, \cdot \rangle$	inner product.
$E[\cdot]$	expectation.
$\mathrm{tr}(\cdot)$	trace of a matrix.
$\det[\cdot]$	determinant of a matrix.
$A_{m,n}$	the $(m,n)^{\text{th}}$ entry of a matrix $\mathbf{A}$.
a_n	the n^{th} entry of the column vector $\mathbf{a}$.
$\mathbf{I}_N$	the $N \times N$ identity matrix.
$\mathbf{1}_{M \times N}$	all-one matrix of size $M \times N$.
$\mathbf{0}_{M \times N}$	all-zero matrix of size $M \times N$.
$\mathrm{diag}[\boldsymbol{x}]$	a diagonal matrix with $\boldsymbol{x}$ on its main diagonal.
$\mathbb{Z}$	the set of integer numbers.
$\mathbb{C}$	the set of complex numbers.
$\mathbb{R}$	the set of real numbers.
j	$\sqrt{-1}$.

$\mathbb{Z}[j]$	Gaussian integer ring, with elements $p + jq$ where $p, q \in \mathbb{Z}$.
$\Re[\cdot]$	the real part.
$\Im[\cdot]$	the imaginary part.
$P(A)$	the probability of event A.
$\sup(\cdot)$	supremum.
$\inf(\cdot)$	infimum.
$\emptyset$	empty set.

GLOSSARY

BER Bit Error Rate.

CCDF Complementary Cumulative Distribution Function.

CDMA Code Division Multiple Access.

CLLL Complex Lenstra-Lenstra-Lovász algorithm.

DFE Decision Feedback Equalizers.

DLLL Dual Lenstra-Lenstra-Lovász algorithm.

DSP Digital Signal Processing.

ECC Error Control Codes.

FMA Fixed Memory-usage Algorithm.

FPA Fixed Points Algorithm.

FRA Fixed Radius Algorithm.

FSD Fixed-complexity Sphere Decoding.

KZ Korkine-Zolotareff reduction algorithm.

LE Linear Equalizer.

LLL Lenstra-Lenstra-Lovász algorithm.

LP-OFDM Linear Precoded Orthogonal Frequency Division Multiplexing.

LR Lattice Reduction.

MIMO Multi-Input Multi-Output.

MLE Maximum-Likelihood Equalizer.

MMSE Minimum Mean-Square Error.

od Orthogonality Deficiency.

OFDM Orthogonal Frequency Division Multiplexing.

RLLL Real Lenstra-Lenstra-Lovász algorithm.

SA Seysen's Algorithm.

SD Sphere Decoding.

SDP Semidefinite Programming.

SIC Successive Interference Cancelation.

SNR Signal-to-Noise Ratio.

SQRD Sorted QR-Decomposition.

V-BLAST Vertical-Bell Laboratories Layered Space Time.

ZF Zero Forcing.

SUMMARY

Receiver design, especially equalizer design, in communications is a major concern in both academia and industry. It is a problem with both theoretical challenges and severe implementation hurdles. While much research has been focused on reducing complexity for optimal or near-optimal schemes, it is still common practice in industry to use simple techniques (such as linear equalization) that are generally significantly inferior. Although digital signal processing (DSP) technologies have been applied to wireless communications to enhance the throughput, the users' demands for more data and higher rate have revealed new challenges. For example, to collect the diversity and combat fading channels, in addition to the transmitter designs that enable the diversity, we also require the receiver to be able to collect the prepared diversity.

Most wireless transmissions can be modeled as a linear block transmission system. Given a linear block transmission model assumption, maximum likelihood equalizers (MLEs) or near-ML decoders have been adopted at the receiver to collect diversity which is an important metric for performance, but these decoders exhibit high complexity. To reduce the decoding complexity, low-complexity equalizers, such as linear equalizers (LEs) and decision feedback equalizers (DFEs) are often adopted. These methods, however, may not utilize the diversity enabled by the transmitter and as a result have degraded performance compared to MLEs.

In this dissertation, we will present efficient receiver designs that achieve low bit-error-rate (BER), high mutual information, and low decoding complexity. Our approach is to first investigate the error performance and mutual information of existing low-complexity equalizers to reveal the fundamental condition to achieve full

diversity with LEs. We show that the fundamental condition for LEs to collect the same (outage) diversity as MLE is that the channels need to be constrained within a certain distance from orthogonality. The orthogonality deficiency (*od*) is adopted to quantify the distance of channels to orthogonality while other existing metrics are also introduced and compared. To meet the fundamental condition and achieve full diversity, a hybrid equalizer framework is proposed. The performance-complexity trade-off of hybrid equalizers is quantified by deriving the distribution of *od*.

Another approach is to apply lattice reduction (LR) techniques to improve the "quality" of channel matrices. We present two widely adopted LR methods in wireless communications, the Lenstra-Lenstra-Lovász (LLL) algorithm and Seysen's algorithm (SA), by providing detailed descriptions and pseudo codes. The properties of output matrices of the LLL algorithm and SA are also quantified. Furthermore, other LR algorithms are also briefly introduced.

After introducing LR algorithms, we show how to adopt them into the wireless communication decoding process by presenting LR-aided hard-output detectors and LR-aided soft-output detectors for coded systems, respectively. We also analyze the performance of proposed efficient receivers from the perspective of diversity, mutual information, and complexity. We prove that LR techniques help to restore the diversity of low-complexity equalizers without increasing the complexity significantly.

When it comes to practical systems and simulation tool, e.g., MATLAB, only finite bits are adopted to represent numbers. Therefore, we revisit the diversity analysis for finite-bit represented systems. We illustrate that the diversity of MLE for systems with finite-bit representation is determined by the number of non-vanishing eigenvalues. It is also shown that although theoretically LR-aided detectors collect the same diversity as MLE in the real/complex field, it may show different diversity orders when finite-bit representation exists. Finally, the VLSI implementation of the complex LLL algorithms is provided to verify the practicality of our proposed designs.

CHAPTER I

INTRODUCTION

1.1 Motivation and State-of-the-art

Wireless communications have become the fastest growing and most ubiquitous industry in almost all areas of our daily life, encompassing everything from radio and television broadcasting to mobile phones and satellite communications. The increasing demand for wireless services for voice, multi-media, and data transmissions results in a continually expanding market. The rapid growth has benefited from the fact that low-cost user terminals and affordable communication devices are feasible because of the development of the solid-state technology and digital signal processing (DSP) devices. More important, however, the globalization of wireless transmission standards has accelerated the spread of wireless services. For example, driven by widespread acceptance of the IEEE 802.11a/b/g standards, wireless local-area networking for computers and other devices is spreading rapidly.

As wireless services spread and become integrated into our daily lives, the expectations of performance and reliability of wireless devices naturally increase. The evolution of standards and systems is driven by the demand for better quality of service, higher data rates, and higher mobility. Now, a generally accepted vision for wireless communications is to provide smaller, faster, better, and cheaper devices that can allow communication anywhere, anytime. As a result, system designers now face more challenges than ever before. Particularly, channel fading effects introduced by variations of the time, frequency, and space domains, introduce challenges in both theoretical analysis and hardware implementation.

Receiver design, especially equalizer design, in communications is a major concern

in both academia and industry. Equalization is the process by which the effects of noise, fading, and dispersion in the channel are mitigated to provide reliable symbol reception. It is a problem with both theoretical challenges and severe implementation hurdles. While much research has been focused on reducing complexity for optimal or near-optimal schemes, it is still common practice in industry to use simple techniques (such as linear equalization) that are generally significantly inferior. Although DSP technologies have been applied to wireless communications to enhance the throughput, the users' demands for more data and higher rate have revealed new challenges. For example, to collect the diversity and combat fading channels, in addition to the transmitter designs that enable the diversity, we also require the receiver to be able to collect the prepared diversity.

Most wireless transmissions, such as orthogonal frequency division multiplexing (OFDM) systems of IEEE 802.11a, multi-antenna multi-input multi-output (MIMO) systems of IEEE 802.11n, and multi-user code division multiple access (CDMA) systems, can be modeled as a linear block transmission system. Therefore, our research is based on a generic linear system model. To quantify the performance of different communication systems, two common but important criteria are the average bit-error-rates (BERs) and ergodic (or outage) capacity [15, 28, 99, 101, 103, 106, 113]. The BER describes how reliable the transmission is and is usually quantified by two parameters: diversity order and coding gain [106, 57, 62, 97]. Diversity is an inherent property of fading channels and is defined as the minus asymptotic slope of the BER versus signal-to-noise ratio (SNR) curve plotted in log-log scale. The higher the diversity, the smaller the error probability at the high SNR regime. To enjoy the diversity from fading channels, we have to design the transmitter properly so that the diversity is enabled, and the receiver that is able to collect the diversity [101, 57, 97]. Most of the existing diversity-enabled schemes adopt the maximum-likelihood equalizer (MLE) at the receiver to collect diversity [106, 57, 62, 97, 100, 111].

Another important criterion to quantify the performance of a receiver is the mutual information when a particular receiver is adopted. Traditionally, capacity is an inherent property of the channel and does not depend on transceiver designs. However, we adopt the word "capacity" here to describe the maximum information rate for a transmission system with a certain equalizer employed at the receiver. The capacity measures how efficiently the transceiver utilizes the channel. Given a random channel, the instantaneous capacity is also random. In this case, to depict the capacity, one needs not only the average capacity, but also the outage capacity [4]. Similarly, the outage diversity is adopted to depict how reliable the transmission is.

In addition to improving the BER and capacity, practical systems also give high priority to reducing receiver complexity. Although MLE enjoys the maximum BER diversity and outage diversity, its exponential decoding complexity makes it infeasible for certain practical systems. Some near-ML schemes (e.g., sphere-decoding [34]) can be used to reduce the decoding complexity. However, at low SNR or when large decoding blocks and/or high signal constellations are employed, the complexity of near-ML schemes is still high [104, 39]. To reduce the decoding complexity, low-complexity equalizers, such as linear equalizers (LEs), decision feedback equalizers (DFEs), and successive interference cancelation (SICs) are often adopted. These methods, however, may not utilize the diversity enabled by the transmitter and as a result have degraded performance relative to the system with MLEs [12, 30, 90, 66, 67]. Lattice reduction (LR) techniques have been introduced to improve the performance of low-complexity equalizers without increasing the complexity significantly [111, 67, 19, 89, 87, 117, 121, 122].

1.2 Objectives

Apparently, the ultimate goal of the receiver design is to achieve

1. low error probability (high BER diversity),

2. high rate (both data rate and information rate),

3. low complexity.

Therefore, our research focuses on the design of low-complexity receivers for wireless systems based on a generic linear system model to achieve these three goals simultaneously. The proposed equalizer designs must be able to achieve high BER diversity for low error probability, and also high outage diversity to guarantee high mutual information for high rate transmissions. Furthermore, when error control codes are adopted to boost the information rate, the proposed designs can be modified to fit the iterative detection and decoding receivers. On the other hand, the proposed scheme should exhibit low-complexity property especially when large block size and/or high constellations are adopted to increase the data rate. Finally, the performance should not be affected much in practical system when finite bits are adopted to represent numbers.

The approach in this dissertation is to first investigate the performance of existing low-complexity equalizers to reveal the fundamental condition to achieve the same diversity as MLE with LEs. Then, we propose different LR algorithms to meet this condition and achieve full diversity with LR-aided equalizers. We also analyze the performance of proposed efficient receivers from the perspective of diversity, complexity, and capacity, respectively. The effect of finite-bit precision in simulations and practical systems has also been investigated. Furthermore, the results of hardware implementation verify the practicality of our proposed receiver designs.

1.3 Outline

The rest of this dissertation is organized as follows.

In Chapter 2, we first present the generic linear system model we adopt in this dissertation. The generic linear block model is general enough to represent many existing designs and practical systems. Two specific wireless communication systems

are also presented as simulation examples in later chapters. Following the system model, the literature research on existing results of different receiver designs is provided. The limitations of existing designs are summarized to motivate the proposed schemes in the following chapters.

In Chapter 3, the fundamental condition with which LEs can collect the same diversity as MLEs do is given. We show that the orthogonality deficiency (*od*) of the channel matrices plays a key role in quantifying the diversity of LEs. Then, we quantify the mutual information for LEs and also the gap from MLEs. The application of these results to receiver design is also given. A hybrid equalizer framework is proposed to achieve the revealed fundamental conditions. To quantify the performance-complexity trade-off of hybrid equalizers, we provide the exact and approximate forms for the distributions of the channel matrix *od*. The decoding complexity of different equalizers is discussed and compared. Then, simulation results are presented to corroborate the theoretical claims on the fundamental limits of LEs on diversity, complexity and mutual information.

In addition to the orthogonality deficiency, there are many other metrics that can be adopted to quantify the orthogonality of matrices. In Chapter 4, we briefly introduce metrics that have been adopted in literatures. We focus on two metrics: the condition number and Seysen's metric. We compare the function of *od* and conditional number in quantifying the diversity of LEs. Furthermore, the general relationship between *od* and Seysen's metric is compared.

In Chapter 5, we introduce lattice reduction algorithms that improve the orthogonality of matrices. Two widely adopted LR methods in wireless communications are the Lenstra-Lenstra-Lovász (LLL) algorithm [51] and Seysen's algorithm (SA) [88]. In this chapter, we focus on these two algorithms by providing detailed descriptions and pseudo codes. The properties of output matrices of the LLL algorithm and SA are also quantified. Furthermore, other LR algorithms are also briefly introduced.

In Chapter 6, we show how to adopt LR algorithms into the wireless communication decoding process. Basically, LR-aided detectors are introduced based on whether an iterative detection and decoding receiver is adopted in the system. For uncoded systems, we provide the detailed process for LR-aided hard-output detectors - LR-aided LEs and LR-aided DFEs (SICs), respectively. For receivers with iterative detection and decoding structure, e.g., in systems with error control codes (ECC), LR-aided soft-output detectors are designed based on the LLL algorithm and SA. Furthermore, the performance of LR-aided detectors is quantified in terms of error probability, mutual information, and complexity, respectively.

When it comes to practical systems and simulation tool, e.g., MATLAB, only finite bits are adopted to represent numbers. Therefore, we revisit the diversity analysis for finite-bit represented systems in Chapter 7. We first analyze the effects of finite-bit representation on the Gaussian channel. We show that the Gaussian complex channel represented by finite bits loses diversity when SNR is high enough. We then study the diversity of different systems with finite-bit representation and MLE. We also compare the sensitivity of different receivers (MLE and LR-aided equalizers) with finite-bit representation. It is shown that although theoretically LR-aided detectors may collect the same diversity as MLE in the real/complex field, it may show different diversity when one considers finite-bit representation. Note that the key player of this analysis is not how good the quantizer is, but lower and upper bounds of the finite-bit representation cause the diversity loss.

The VLSI implementation of the complex LLL algorithms is provided in Chapter 8 to verify the practical value of the proposed LR-aided detectors. Finally, in Chapter 9, we summarize this dissertation and suggest topics for future research.

CHAPTER II

BACKGROUND

In this section, a literature review is presented to emphasize the necessity of designing efficient receivers for wireless systems. We start with a generic linear system model. By summarizing existing results on diversity and complexity of different receivers, the design of efficient receivers has been shown to be well-motivated. Furthermore, the direction of research becomes clear after the literature study on limitations of existing methods.

2.1 Generic Linear System Model

Consider linear block transmissions depicted in Figure 1

$$\boldsymbol{y} = \boldsymbol{H}\boldsymbol{s} + \boldsymbol{w}, \tag{1}$$

where $\boldsymbol{H}$ is the $M \times N$ complex Gaussian channel matrix with zero mean, the $N \times 1$ vector $\boldsymbol{s}$ consists of the information symbols, $\boldsymbol{y}$ is the $M \times 1$ received vector, and $\boldsymbol{w}$ is independent and identically distributed (i.i.d.) complex additive white Gaussian noise with variance σ_w^2. We assume that the channel matrix $\boldsymbol{H}$ is known at the receiver, but unknown at the transmitter. Note that the channel matrix $\boldsymbol{H}$ is general enough to represent a number of cases, e.g., multi-antenna MIMO [97], precoded OFDM [57], single-carrier Toeplitz channels [100, 108], and multiuser channels [103]. The results and analysis in the following sections are based on this linear model, and thus can be easily applied to the specific wireless systems whose input/output (I/O) relationship can be expressed as the general system model in (1). In the following, we introduce two specific transmission systems of which the system model is characterized as in (1). These two systems will be adopted as simulation examples in later chapters.

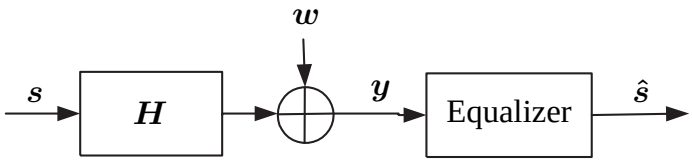

Figure 1: Block diagram of linear transmission system model

MIMO i.i.d. Channels: Consider a multi-antenna system with N transmit-antennas and M receive-antennas. For Vertical-Bell Laboratories Layered Space Time (V-BLAST) transmissions in [15, 27], the data stream is divided into N sub-streams and transmitted through N antennas. The channel matrix $\boldsymbol{H}$ consists of $M \times N$ independent and identically distributed (i.i.d.) complex Gaussian coefficients with zero mean and unit variance. We assume a flat-fading quasi-static environment where the channel coefficients are invariant during a frame and change independently from frame to frame. We also assume that the channel matrix $\boldsymbol{H}$ is known at the receiver, but unknown at the transmitter.

Linear Precoded OFDM Systems: Another example is the linear precoded OFDM (LP-OFDM) system in [57], where the N_c subcarriers of OFDM systems are split into N_g groups, each of size K, so that the g^{th} group is $\boldsymbol{s}_g = [s(gK), \ldots, s(gK+K-1)]^T$. Group $\boldsymbol{s}_g$ is linearly precoded by a $K \times K$ full-rank square precoder $\boldsymbol{\Theta}$, and the entries of the precoded sub-block $\boldsymbol{u}_g = \boldsymbol{\Theta}\boldsymbol{s}_g$ are transmitted through K equi-spaced sub-carriers. Some designs of precoder $\boldsymbol{\Theta}$ can be found in [57] and references therein. Therefore, we can express the I/O relationship for the g^{th} group as

$$\boldsymbol{y}_g = \boldsymbol{D}_{H,g}\boldsymbol{\Theta}\boldsymbol{s}_g + \boldsymbol{w}_g = \boldsymbol{H}_{equ}\boldsymbol{s}_g + \boldsymbol{w}_g, \tag{2}$$

where $\boldsymbol{D}_{H,g} = \text{diag}[H(g), H(g+N_g), \ldots, H(g+(K-1)N_g)]$, $H(n) = \sum_{\ell=0}^{L} h_\ell e^{-j2\pi\ell n/N_c}$ is the channel response at subcarrier n, and $\boldsymbol{w}_g$ is the corresponding white complex Gaussian noise for the g^{th} group with zero mean and variance $\sigma_w^2\boldsymbol{I}$. In this case, the maximum multipath diversity order is $G_d = \min(K, \rho_h)$, which is less than or equal to $L+1$ [57].

Given the linear block transmission model in (1), there are various ways to decode the transmitted symbol vector $\boldsymbol{s}$ from the observation $\boldsymbol{y}$. Here, we generalize the term "equalizer" as the one to equalize the channel effect. Different equalizers lead to different system performance. To quantify the performance of different communication systems, two common but important criteria are the average BER and outage capacity [15, 28, 99, 101, 103, 106, 113]. The BER describes the reliability of the transmission while the capacity measures how efficiently the transceiver utilizes the channel. The BER performance of wireless transmissions over fading channels is usually quantified by two parameters: diversity order and coding gain. Diversity order is defined as the negative asymptotic slope of the BER versus SNR curve plotted in log-log scale. It describes how fast the error probability decays with SNR. The coding gain further measures the SNR gap among different coding schemes that have the same diversity. The higher the diversity is, the smaller the error probability is when SNR is high. Therefore, diversity-enriched transmitters and receivers have well-appreciated merits to cope with the deleterious fading effects on the performance [57, 97, 101].

To quantify the outage capacity of the transmission system when a particular receiver is adopted, we employ the outage diversity. The outage diversity is defined as the negative asymptotic slope of the outage capacity versus SNR curve plotted in log-log scale. Similar to the diversity of BER, outage diversity measures how fast the outage capacity decays with SNR. Higher outage diversity leads to smaller probability that the instantaneous capacity is less than the threshold. We summarize these two types of diversity as follows.

Definition 1 (Diversity) *Suppose that the error probability is* $P_e = P(\hat{\boldsymbol{s}} \neq \boldsymbol{s})$ *and the signal-to-noise ratio is* SNR*. The diversity order of a given system is defined as:*

$$G_d = \lim_{SNR \to \infty} -\frac{\log P_e}{\log(SNR)}. \tag{3}$$

Suppose that $P(C < C^{th})$ is the probability that the instantaneous capacity C is less than a threshold C^{th} for a certain system. The outage diversity order G_o is defined as:

$$G_o = \lim_{SNR\to\infty} -\frac{\log P(C < C^{th})}{\log(SNR)}. \tag{4}$$

Note that G_d and G_o quantify different aspects of the performance of a system: one is error performance, and the other is the mutual information. The maximum diversity is determined by the degrees of freedom of the channels. Different channels provide different diversity flavors, e.g., frequency-selective channels provide multipath diversity [57], multi-antenna channels provide spatial diversity [97]. To enjoy the diversity from fading channels, we must design both the transmitter and receiver appropriately. In this dissertation, we focus on the receiver designs that can collect the prepared diversity with low complexity. In the following, we first briefly review the existing equalizer designs.

2.2 Optimal and Near Optimal Equalizers

One often used and also optimal detector (If there is no prior information about the symbols and/or symbols are treated as deterministic parameters) is the maximum-likelihood equalizer (MLE), which is based on an exhaustive search among all $N \times 1$ symbol vectors as

$$\hat{\boldsymbol{s}}_{ml} = \arg\min_{\tilde{\boldsymbol{s}}\in\mathcal{S}^N} \|\boldsymbol{y} - \boldsymbol{H}\tilde{\boldsymbol{s}}\|^2, \tag{5}$$

where $\mathcal{S}$ is the finite alphabet of the symbols. MLE in (5) provides optimal error performance with the price paid on high decoding complexity ($\mathcal{O}(|\mathcal{S}|^N)$). Some near-ML equalizers have also been proposed to reduce the complexity and achieve near-ML performance. For example, the sphere-decoding (SD) method [34] formulates the decoding process into a tree search and reduces the average complexity to polynomial when N is small and the SNR is high [34], but the variance of the complexity remains

high [104]. Another example is the semidefinite programming (SDP) detector [61], which is based on semi-definite relaxation of the original ML problem. The worst-case polynomial complexity of SDP is theoretically proven to be $\mathcal{O}(N^{3.5})$. However, the complexity of (near-) MLEs is especially high when the size of the channel matrix and/or the constellation size is large. Furthermore, early termination and fixed memory considerations for hardware implementations may degrade the performance of near-MLEs.

Some algorithms have been proposed to reduce the complexity of the SD method by pruning the tree structure. The K-best algorithm proposed in [115] adopts the breadth-first search strategy to reduce the complexity but does not guarantee the full diversity. Recently, the fixed-complexity SD (FSD) has been proposed to reduce the decoding complexity while maintaining near-ML performance [6], by splitting the N detection layers into full expansion and single expansion stages. It has been shown in [38] that when the number of layers detected in full expansion is greater than or equal to $\lfloor\sqrt{N}\rfloor$, the diversity of FSD is the same as that of MLE. However, the complexity is still high when it comes to systems with large channel matrices, since the decoding complexity is still not polynomial. Some suboptimal detection methods also exist, e.g., the improved M-algorithm in sequential decoding [73], though none of them has analytically proved the diversity. The major disadvantages of these tree-search algorithms are two folds: (1) the complexity depends on SNR and the constellation size and thus can be infeasible when it comes to systems with large channel matrices and large constellations; (ii) the tree-search algorithm is executed whenever new signal comes in even when the channel stays the same. Therefore, people are looking to low-complexity detection methods for practical implementation purpose.

2.3 Low-complexity Equalizers

There are some equalizers that are usually characterized and referred to as low-complexity equalizers: linear equalizers (LEs) and decision feedback equalizers (DFEs). LEs, as depicted in Figure 2, are in the form

$$\hat{\boldsymbol{s}} = \mathcal{Q}(\boldsymbol{G}\boldsymbol{y}), \tag{6}$$

where $\mathcal{Q}(\cdot)$ corresponding to the "Decision" block in Figure 2 denotes element-wise quantization to the nearest constellation point for a given modulation scheme. Two often adopted LEs are the zero-forcing (ZF) equalizer and the linear minimum mean-square error (MMSE) equalizer. Given the model in (1), the ZF-LE is given as

$$\boldsymbol{x}_{zf} = \boldsymbol{G}\boldsymbol{y} = \boldsymbol{H}^{\dagger}\boldsymbol{y} = \boldsymbol{s} + \boldsymbol{H}^{\dagger}\boldsymbol{w} = \boldsymbol{s} + \boldsymbol{\eta}, \tag{7}$$

where $\boldsymbol{G} = \boldsymbol{H}^{\dagger} = (\boldsymbol{H}^{\mathcal{H}}\boldsymbol{H})^{-1}\boldsymbol{H}^{\mathcal{H}}$ denotes the Moore-Penrose pseudo-inverse of the channel matrix $\boldsymbol{H}$ and $\boldsymbol{\eta} := \boldsymbol{H}^{\dagger}\boldsymbol{w}$ is the noise after equalization. Another often adopted LE, the linear MMSE-LE, is defined as

$$\boldsymbol{x}_{mmse} = \boldsymbol{G}\boldsymbol{y} = \left(\boldsymbol{H}^{\mathcal{H}}\boldsymbol{H} + \sigma_w^2\boldsymbol{I}_N\right)^{-1}\boldsymbol{H}^{\mathcal{H}}\boldsymbol{y}, \tag{8}$$

followed by the quantization step. Here, we notice that, with the definition of an extended system (also shown in [117, 33]):

$$\bar{\boldsymbol{H}} = \begin{bmatrix} \boldsymbol{H} \\ \sigma_w\boldsymbol{I}_N \end{bmatrix} \qquad \text{and} \qquad \bar{\boldsymbol{y}} = \begin{bmatrix} \boldsymbol{y} \\ \boldsymbol{0}_{N\times 1} \end{bmatrix}, \tag{9}$$

the MMSE equalizer in (8) can be rewritten as $\boldsymbol{x}_{mmse} = \bar{\boldsymbol{H}}^{\dagger}\bar{\boldsymbol{y}}$. Thus, the MMSE-LE has the same form as the ZF-LE in (7) with respect to this extended system. The analysis based on the ZF equalizer in (7) can be extended to MMSE equalizer accordingly.

From Eqs. (7) and (8), we can see that the ZF equalizer aims to cancel the channel effect by assuming a noiseless environment, while the MMSE equalizer further takes

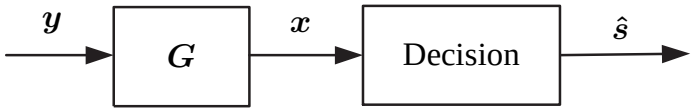

Figure 2: Block diagram of linear equalizers

into account the noise effect. Thus, the MMSE-LE achieves better performance in general, but requires an estimate of the noise variance at the receiver. The complexities of both equalizers are dominated by matrix inversion, which requires polynomial complexity $\mathcal{O}(N^3)$ via Gaussian elimination.

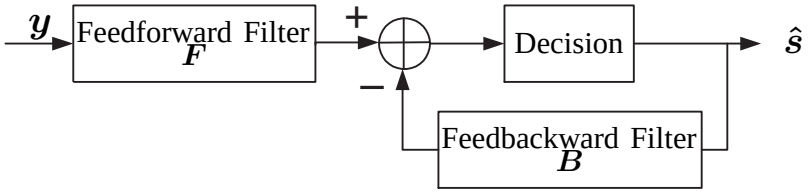

Figure 3: Block diagram of decision feedback equalizers

To improve the performance, successive-interference-cancelation (SIC) equalizers are proposed [27]. Since the DFEs have been shown to be equivalent to SICs in [24], we consider them as one category of low-complexity equalizers. The block diagram of DFEs (SICs) is depicted in Figure 3. The major difference between DFEs and LEs is the feedback of the detected symbols through a feedback matrix $\boldsymbol{B}$, which is an upper triangular matrix. The equalization procedure is described in Table 1. According to

Table 1: Equalization process of DFEs (SICs)

(1)	$\boldsymbol{x} = \boldsymbol{F}\boldsymbol{y}$;
(2)	for n=N:(-1):1
(3)	s(n) = $\mathcal{Q}\left(x(n) - \sum_{k=n+1}^{N} B(n,k)s(k)\right)$;
(4)	end

the equalization method, DFEs are divided into two categories: ZF-DFE (ZF-SIC) and MMSE-DFE (MMSE-SIC). The specific designs of the feedforward matrix $\boldsymbol{F}$ and the feedback matrix $\boldsymbol{B}$ for both DFEs can be found in [24, 41]. Different from

LEs, matrix decompositions, e.g., QR-decomposition, comprise the major part of the DFEs' complexity. Such algorithms are usually associated with the complexity of $\mathcal{O}(MN^2)$. Compared to LEs, the corresponding DFEs achieve better performance. However, the performance of DFEs is greatly affected by the decoding order and the error propagation. To improve the performance of DFEs and to mitigate the complexity overhead introduced by the feedback filter, optimum ordering is usually adopted in DFEs. For example, V-BLAST ordering optimizes the BER performance but the complexity is sub-optimal [41].

2.4 Limitations of Existing Designs

To see the limitations of current receiver designs, we first provide a comparison of low-complexity equalizers with (near-) MLEs. We find the SNR of different equalizers to achieve the target BER by searching the SNR with step size 0.05 dB. The corresponding complexity of different equalizers is calculated in terms of average arithmetic operations (including real additions and real multiplications). The results are given in Table 2 for QPSK constellation and i.i.d. complex channels for different sizes, where the SNR is defined as the symbol energy per transmit dimension versus noise power spectral density. The complexity of ZF-LE is based on the Gaussian elimination of square matrices, while the complexity of SICs is obtained from the QR-decomposition approach. Furthermore, the complexity of MMSE (MMSE-SIC) equalizer does not include the procedure of estimating the noise variance. The SD method is implemented as in [34]. For higher QAM constellation, the complexity of SD increases dramatically while the complexity of LEs and DFEs stays the same. From Table 2, it is obvious that the low-complexity equalizers need higher SNR to achieve a certain BER though their complexity is quite low. Another example is the linear precoding (a.k.a. linear complex-field coding) techniques for OFDM systems in [57]. We plot the performance of five equalizers: ZF-LE, ZF-SIC, MMSE-LE, MMSE-SIC and SD, for

Table 2: Comparison of different equalizers for i.i.d. complex channels with QPSK modulation

		$M=N=4$		$M=N=6$		$M=N=8$	
Target BER		10^{-3}	10^{-4}	10^{-3}	10^{-4}	10^{-3}	10^{-4}
SD	SNR (dB)	8.25	11.05	5.05	7.35	3.05	5.0
	Complexity	3662	3550	16019	14090	55957	54150
ZF-LE	SNR (dB)	27.1	37.05	27.05	37.35	27.00	37.05
	Complexity	298		869		1892	
MMSE-LE	SNR (dB)	22.4	32.45	20.1	30.25	18.20	28.25
	Complexity	812		2618		6040	
ZF-SIC	SNR (dB)	23.75	33.15	23.15	33.60	22.50	32.80
	Complexity	748		2401		5546	
MMSE-SIC	SNR (dB)	19.75	29.65	16.85	27.10	14.60	24.75
	Complexity	1284		4333		10266	

Table 3: Diversity of different transmission systems

	Diversity of (near-) MLEs	Diversity of LEs and DFEs
V-BLAST in [27] with i.i.d. channels	M	M-N+1
OSTBC in [97] with i.i.d. channels	MN	MN
Golden code in [123] for 2×2 systems	4	1
uncoded OFDM systems	1	1
LP-OFDM in [57] with square encoding matrices	min(K, ρ_h)	1
LP-OFDM in [106] with tall encoding matrices	ρ_h	ρ_h
FDFR MIMO-OFDM in [63]	MNρ_h	M-N+1
STF MIMO-OFDM in [64]	MNρ_h	MN

the linear precoded (LP-) OFDM system in [57]. We assume the multipath channel has channel order $L = 3$, which means the maximum multipath diversity is $L+1 = 4$. From Figure 4 we can see that low-complexity equalizers only collect diversity 1, while the SD method exploit the full diversity.

From Table 2 and Figure 4, we can see that the main drawback of the foremen-tioned low-complexity equalizers is that these equalizers usually cannot collect the same diversity as (near-) MLEs. For example, the diversity order collected by LEs and DFEs is only $M - N + 1$ for spatial multiplexing systems with i.i.d. channels, while (near-) MLE exploits diversity M [67]. The impact of the lack of diversity order becomes especially severe when the channel matrix is square, e.g., $M = N$ as

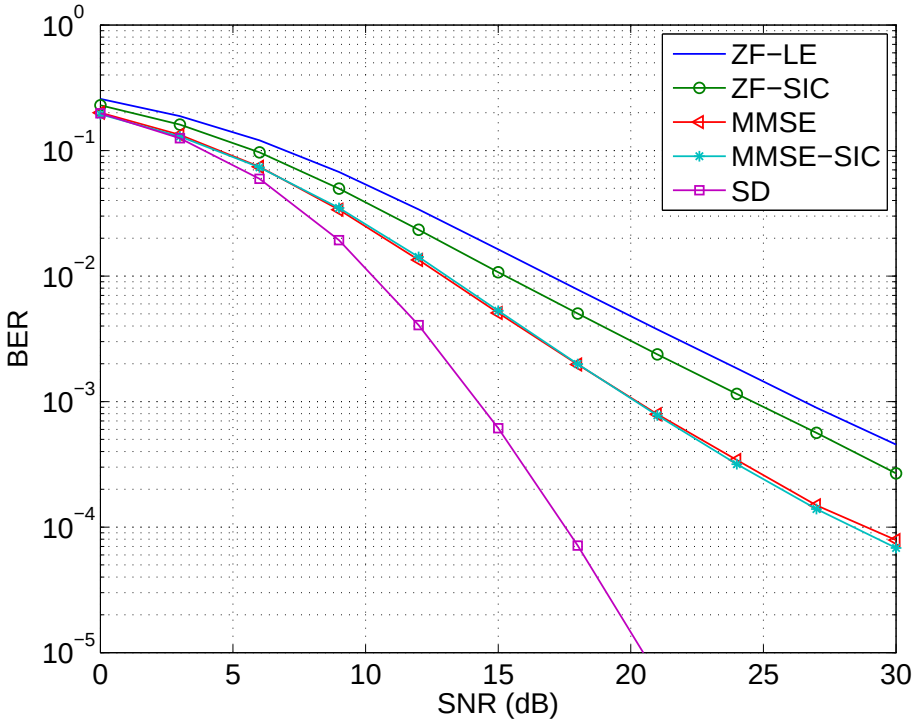

Figure 4: Performance of LP-OFDM with channel order $L = 3$

shown in Table 2. Furthermore, as shown in [41], optimal ordering cannot increase the diversity order collected by DFEs, but only improves the performance in terms of coding gain. We summarized the existing results on the diversity of different wireless systems collected by different equalizers in Table 3, where ρ_h represents the rank of the covariance matrix of frequency-selective channel taps. From the table we can see that for most systems low-complexity equalizers cannot exploit the same diversity as that of (near-) MLEs. However, since (near-) MLEs exhibit either high average complexity or high complexity variance, the cubic order complexity makes LEs and DFEs widely adopted in practical systems. A natural question is whether the complexity reduction is worth the performance sacrifice. Or in other words, is there a way to keep the complexity low while improving the performance in terms of coding gain or even diversity order?

CHAPTER III

FUNDAMENTAL LIMITS OF LINEAR EQUALIZERS

One major reason that prevents LEs from getting more attention in theory and practice is that their performance loss is not quantified in general. For specific cases, it has been shown that LEs lose diversity and capacity relative to MLEs for MIMO V-BLAST systems [12, 30, 67]. It has also been shown that LEs collect full diversity for precoded OFDM systems in [100] and orthogonal space-time block coding schemes in [97]. Therefore, we are interested in the fundemental condition with which LEs can collect the full diversity enabled by the transmitter. Or in other words, under what condition LEs will exploit the same diversity as that of (near-) MLEs.

In the following, we introduce a parameter – orthogonality deficiency (*od*) – for the channel matrix $\boldsymbol{H}$ as [96], which is critical to quantify the performance gap between LEs and MLEs as we will show later.

Definition 2 (Orthogonality Deficiency) *For an $M \times N$ matrix $\boldsymbol{H} = [\boldsymbol{h}_1, \boldsymbol{h}_2, \ldots, \boldsymbol{h}_N]$, with $\boldsymbol{h}_n$ being $\boldsymbol{H}$'s n^{th} column, its orthogonality deficiency ($od(\boldsymbol{H})$) is defined as:*

$$od(\boldsymbol{H}) = 1 - \frac{\det(\boldsymbol{H}^{\mathcal{H}}\boldsymbol{H})}{\prod_{n=1}^{N} \|\boldsymbol{h}_n\|^2}, \tag{10}$$

where $\|\boldsymbol{h}_n\|, 1 \le n \le N$ is the norm of the n^{th} column of $\boldsymbol{H}$[1].

Note that $0 \le od(\boldsymbol{H}) \le 1$, $\forall \boldsymbol{H}$. If $\boldsymbol{H}$ is singular, $od(\boldsymbol{H}) = 1$, and if the columns of $\boldsymbol{H}$ are orthogonal, $od(\boldsymbol{H}) = 0$. The smaller $od(\boldsymbol{H})$ is, the more orthogonal $\boldsymbol{H}$ is. Given the model in (1), if $od(\boldsymbol{H}) = 0$, i.e., $\boldsymbol{H}^{\mathcal{H}}\boldsymbol{H}$ is diagonal, then LEs have the same performance as that of MLEs. Furthermore, for the MMSE equalizer in (9), we

[1] *od has also been defined as $\frac{\prod_{n=1}^{N_t} \|\boldsymbol{h}_n\|}{|\det(\boldsymbol{H})|}$ in [42], which is equivalent to* (10) *when $\boldsymbol{H}$ is square, but is unbounded.*

obtain the following result on $od(\bar{\boldsymbol{H}})$.

Lemma 1 *With the extended system defined in* (9)*, for all possible* $\boldsymbol{H}$ *and* σ_w^2*, if* $\sup_{\boldsymbol{H}}(od(\boldsymbol{H})) = \epsilon$*, then* $\sup_{\sigma_w^2, \boldsymbol{H}}(od(\bar{\boldsymbol{H}})) = \epsilon'$*, where* $\epsilon' = 1$*, when* $\epsilon = 1$ *and* $\epsilon' < 1$*, when* $\epsilon < 1$.

Proof: See Appendix A.

Thus, with this lemma, the following analysis and claims on ZF equalizer can be extended to MMSE equalizer[2].

3.1 The Diversity of Linear Equalizers

In this section, we study the BER performance of LEs in terms of diversity order. The results for different systems with MLEs are well-known. However, the ones for LEs are not well established. With the definitions of diversity in (3) and $od(\boldsymbol{H})$ in (10), we present the condition with which LEs collect the same diversity as MLEs do.

Theorem 1 *Consider a linear system in* (1)*, where the entries of the channel matrix are complex Gaussian distributed with zero mean, and the information symbols are drawn from integer lattice (Gaussian integer ring). The linear equalizers in* (7) *and* (8) *collect the same diversity as MLE does* (5) *if there exists a constant* $\epsilon \in [0, 1)$ *such that* $\forall \boldsymbol{H}$, $od(\boldsymbol{H}) \leq \epsilon$*, i.e.,* $\sup(od(\boldsymbol{H})) = \epsilon$.

Proof: See Appendix B.

Theorem 1 reveals the fundamental relationship between the *od* of the channel matrix $\boldsymbol{H}$ and the diversity order collected by LEs. If the supremum of $od(\boldsymbol{H})$ is 1 (i.e., $\sup(od(\boldsymbol{H})) = 1$), i.e., there is no $\epsilon < 1$ such that $od(\boldsymbol{H}) \leq \epsilon$, $\forall \boldsymbol{H}$, then in general, LEs lose diversity relative to MLEs.

[2]Since MMSE equalizer may be biased, a diagonal matrix $\boldsymbol{D}_{sc}$ may be multiplied to $\boldsymbol{x}_{mmse}$ to reduce the bias. It is not difficult to verify that $od(\bar{\boldsymbol{H}}\boldsymbol{D}_{sc}^{-1}) = od(\bar{\boldsymbol{H}})$. Thus, the claims hold true for this scaled MMSE equalizer.

The same claim can be made for the MMSE equalizer based on the definition in (9) and Lemma 1. Furthermore, Theorem 1 and our proof are general enough even for correlated non-Gaussian channels. Thus, Theorem 1 can be extended as:

Corollary 1 *Given a random channel matrix* $\boldsymbol{H}$*, when* $od(\boldsymbol{H}) \leq \epsilon$*,* $\forall \boldsymbol{H}$ *and* $\epsilon \in (0, 1)$*, then LEs collect the same diversity as MLE does.*

Proof: The proof for general channels is quite similar to the one for Gaussian channel case in Theorem 1. The major difference is at Eqs. (92) and (93). For general channels with pdf given in [106, Eq. (7)], it can be verified that LEs collect the diversity $\sum_{d=1}^{D_n}(t_{n,d}+1)$ where $t_{n,d}$ comes from the series form of the pdf of $|\tilde{h}_{n,d}|^2$. For Gaussian case, $t_{n,d} = 0$. Similarly, MLE collects the same diversity. Therefore, the claim in Corollary 1 holds true. ■

A well-known special case of Corollary 1 is:

Corollary 2 *When* $od(\boldsymbol{H}) = 0$*, ZF equalizer has the same performance as MLE does.*

In the following, we give some examples to verify Theorem 1. The diversity orders of these transmission systems using LEs have already been derived in the literature. However, we show that applying Theorem 1 to these systems also provides the same results but in a simpler way compared with the original approaches.

Example 3.1 (Toeplitz Channel Matrix): Consider an $M \times N$ tall Toeplitz channel matrix $\boldsymbol{H}$ generated by the first column $[h_1, h_2, \ldots, h_L, 0, ..., 0]^T$ and the first row $[h_1, 0, \ldots, 0]$, where $M \geq N + L$ and $N > L$[3]. One example for this kind of transmissions is the zero-padding (ZP-) only transmission in [108]. Apparently, if the block size N is large, the complexity of MLE becomes prohibitive. Likewise, as

[3]These are necessary conditions if one wants to guarantee a reasonable transmission rate $\frac{N}{M}$.

the channel length L becomes high, decoding with Viterbi algorithm (which is also optimal in this case) becomes excessively complex. Therefore, in this case, applying LEs is well justified. Using Theorem 1, we obtain that:

Corollary 3 *If the channel matrix* $\boldsymbol{H}$ *in* (1) *with size* $M \geq N + L$ *and* $N > L$ *is Toeplitz with first column* $[h_1, h_2, ..., h_L, 0, ..., 0]^T$ *and first row* $[h_1, 0, ..., 0]$*, LEs collect the same diversity as MLE does.*

Proof: Since $\boldsymbol{H}$ is Toeplitz, then $\det(\boldsymbol{H}^{\mathcal{H}}\boldsymbol{H}) > 0$ for any non-zero channel response, i.e., h_ℓ's are not equal to zero simultaneously. Suppose $m = \arg\max_{\ell\in[1,L]} |h_\ell|^2$, and then $|h_m|^2 > 0$. The Toeplitz matrix $\boldsymbol{H}$ can be split into three submatrices as $\boldsymbol{H} = [\boldsymbol{H}_{o1}^T, \boldsymbol{H}_m^T, \boldsymbol{H}_{o2}^T]^T$, where matrix $\boldsymbol{H}_{o1}$ consists of the first $(m-1)$ rows of $\boldsymbol{H}$, $\boldsymbol{H}_{o2}$ has the last $(L-m)$ rows, and $\boldsymbol{H}_m$ is of size $N \times N$ with h_m on the diagonal entries. Therefore, we have $\boldsymbol{H}^{\mathcal{H}}\boldsymbol{H} = \boldsymbol{H}_{o1}^{\mathcal{H}}\boldsymbol{H}_{o1} + \boldsymbol{H}_m^{\mathcal{H}}\boldsymbol{H}_m + \boldsymbol{H}_{o2}^{\mathcal{H}}\boldsymbol{H}_{o2}$. According to the expression of matrix determinant in [45, p. 11] and the structure of $\boldsymbol{H}_m$, it is ready to show that $\det(\boldsymbol{H}_m^{\mathcal{H}}\boldsymbol{H}_m) = (|h_m|^2)^N$ when $N > L$. Thus, we bound $\det(\boldsymbol{H}^{\mathcal{H}}\boldsymbol{H})$ as

$$\det(\boldsymbol{H}^{\mathcal{H}}\boldsymbol{H}) \geq \det(\boldsymbol{H}_m^{\mathcal{H}}\boldsymbol{H}_m) = \left(\max_{\ell\in[1,L]}(|h_\ell|^2)\right)^N, \tag{11}$$

where the inequality holds true since $\boldsymbol{H}_m^{\mathcal{H}}\boldsymbol{H}_m$ is positive definite while $\boldsymbol{H}_{o1}^{\mathcal{H}}\boldsymbol{H}_{o1}$ and $\boldsymbol{H}_{o2}^{\mathcal{H}}\boldsymbol{H}_{o2}$ are positive semi-definite (see [108, Appendix B] for the proof). In this case, we can verify that $od(\boldsymbol{H})$ is strictly less than 1 and can be bounded as

$$od(\boldsymbol{H}) \leq 1 - \frac{(\max_{\ell\in[1,L]}(|h_\ell|^2))^N}{\left(\sum_{\ell=1}^{L}|h_\ell|^2\right)^N} \leq 1 - \frac{1}{L^N}. \tag{12}$$

Therefore, according to Theorem 1, we claim that LEs collect the same diversity as MLE does. ■

Our result in Corollary 3 is consistent with the result in [100].

Example 3.2 (Orthogonal Channel Matrix): Consider that the channel matrix in (1) is orthogonal, e.g., the orthogonal space-time block codes in [97]. In this case,

$od(\boldsymbol{H}) = 0$ for any non-zero realization of $\boldsymbol{H}$. Thus, the LEs exploit the same diversity as MLE does. Another example is diagonal $\boldsymbol{H}$ in OFDM systems. In this case, again the LEs collect the same diversity order as MLE does [106] and both of them have diversity 1.

Example 3.3 (i.i.d. Channel Matrix): When channel matrix $\boldsymbol{H}$ has i.i.d. Gaussian entries, it has been shown that LEs lose diversity [30, 29, 67, 37]. In this case, it can be verified that $\sup(od(\boldsymbol{H})) = 1$, i.e., there is no ϵ which is strictly less than 1. This also verifies Theorem 1.

Example 3.4 (FDFR Channel Matrix): By defining $\boldsymbol{\mathcal{H}} := \boldsymbol{I}_N \otimes \boldsymbol{H}$ with $\boldsymbol{H}$ having i.i.d. complex Gaussian entries, and a well-designed unitary matrix $\boldsymbol{\Phi}$ (see [17, 63, 123] for details), the full-diversity full-rate (FDFR) transmissions can be represented compactly as:

$$\boldsymbol{y} = \boldsymbol{H}_{eq}\boldsymbol{s} + \boldsymbol{w} = \boldsymbol{\mathcal{H}}\boldsymbol{\Phi}\boldsymbol{s} + \boldsymbol{w}. \tag{13}$$

In the literature (e.g., [17, 63, 123]), it has been shown that the FDFR design in (13) achieves full diversity (MN) if MLE is adopted at the receiver. However, when LEs are employed, the diversity order is only $M - N + 1$ as shown in [68], which is the same as V-BLAST transmissions with LEs (as shown in Fig. 5 for 2×2 case). Furthermore, for the model in (13), we can verify that

$$od(\boldsymbol{H}_{eq}) = 1 - (1 - od(\boldsymbol{H}))^N .$$

Based on Example 3, we know that $\sup(od(\boldsymbol{H})) = 1$, and thus, $\sup(od(\boldsymbol{H}_{eq})) = 1$ for FDFR case. This also verifies our Theorem 1.

In summary, Theorem 1 quantifies the diversity order collected by LEs for linear systems. Furthermore, the proof of Theorem 1 implies that, if ϵ (the upper bound of $od(\boldsymbol{H})$) is smaller, i.e., the channel is more orthogonal, the upper bound of BER in (141) also becomes smaller, which indicates that LEs may achieve better performance in this case. Later, we will verify this by simulations.

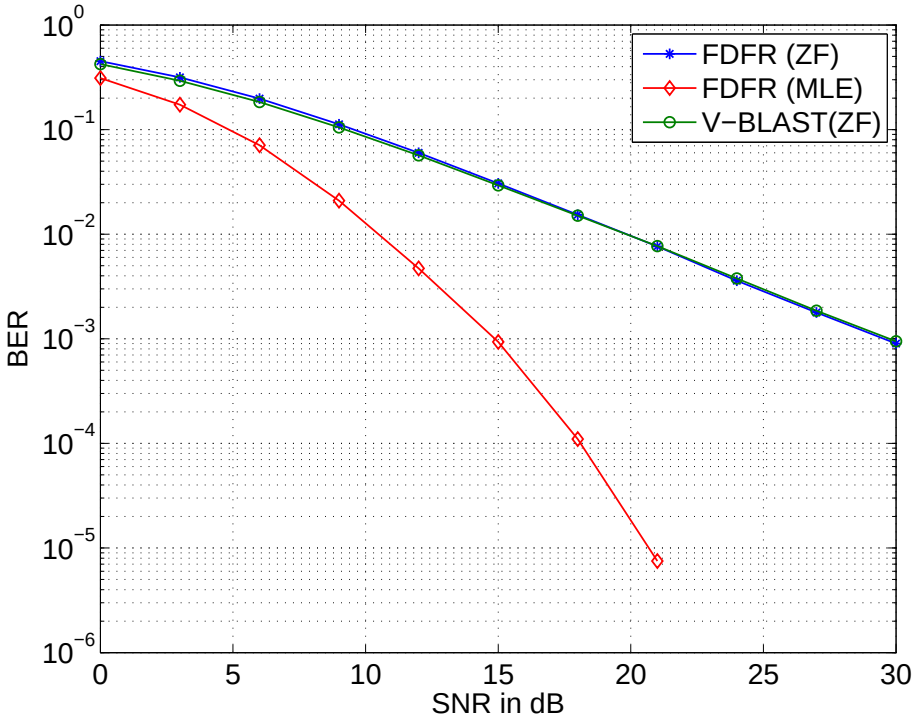

Figure 5: Performance of FDFR design with $M = N = 2$

3.2 The Outage Diversity of Linear Equalizers

In addition to error probability, mutual information is another important metric when comparing the performance of different receivers, since it measures how efficiently the receivers utilize the channels. The word "capacity" here denotes the maximum mutual information when a certain transceiver is adopted. Given a random channel, the instantaneous capacity is also random. In this case, to depict the capacity, one needs not only average capacity, but also outage capacity [4]. In this section, we compare the outage capacity of ZF equalizer with that of MLE. The results can be easily extended to other LEs.

Let us first revisit the capacity when no channel state information is available at the transmitter, and MLE is adopted at the receiver. Given the linear model in (1), the mutual information is given as (say e.g., [30, 29, 99])

$$\mathcal{I}(\boldsymbol{y};\boldsymbol{s}|\boldsymbol{H}) = \mathcal{H}(\boldsymbol{s}|\boldsymbol{H}) - \mathcal{H}(\boldsymbol{s}|\boldsymbol{y};\boldsymbol{H}), \tag{14}$$

where $\mathcal{H}(\cdot)$ denotes the entropy. It is not difficult to show that

$$\mathcal{H}(\boldsymbol{s}|\boldsymbol{H}) \leq \log_2 \det(\pi e \boldsymbol{R}_s), \tag{15}$$

where the equality holds when $\boldsymbol{s}$ is Gaussian and $\boldsymbol{R}_s = E[\boldsymbol{s}\boldsymbol{s}^{\mathcal{H}}]$. Since the noise is Gaussian, we obtain

$$\begin{aligned}\mathcal{H}(\boldsymbol{s}|\boldsymbol{y};\boldsymbol{H}) &= \log_2 \det(\pi e \boldsymbol{R}_{s|y;H}) \\ &= \log_2 \det\left[\pi e \left(\boldsymbol{R}_s^{-1} + \frac{1}{\sigma_w^2}\boldsymbol{H}^{\mathcal{H}}\boldsymbol{H}\right)^{-1}\right]. \end{aligned} \tag{16}$$

Suppose that the information symbols $\boldsymbol{s}$ are Gaussian distributed with zero mean and covariance matrix $\boldsymbol{R}_s = \boldsymbol{I}_N$. The instantaneous capacity achieved by MLE is given as (see also [99])

$$\begin{aligned}C_{ML}(\boldsymbol{H}) &= \log_2\left[\det\left(\boldsymbol{I}_M + \frac{1}{\sigma_w^2}\boldsymbol{H}\boldsymbol{R}_s\boldsymbol{H}^{\mathcal{H}}\right)\right] \\ &= \log_2\left[\det\left(\boldsymbol{I}_N + \frac{1}{\sigma_w^2}\boldsymbol{H}^{\mathcal{H}}\boldsymbol{H}\right)\right]. \end{aligned} \tag{17}$$

The closed form of the average capacity of MLE for i.i.d. MIMO channels can be found in [90].

When ZF equalizer is adopted at the receiver, the covariance matrix of the equivalent noise vector $\boldsymbol{\eta}$ from (7) is $\sigma_w^2\boldsymbol{R}_\eta$ with

$$\boldsymbol{R}_\eta = \mathrm{diag}[C_{1,1}, C_{2,2}, \ldots, C_{N,N}] \tag{18}$$

and $C_{i,i}$ being the $(i,i)^{\text{th}}$ entry of matrix $\boldsymbol{C} = (\boldsymbol{H}^{\mathcal{H}}\boldsymbol{H})^{-1}$. Here because of symbol-by-symbol detection for ZF equalizer, the covariance matrix of the noise is diagonal. Given $\boldsymbol{H}$, what we call "ZF capacity" is defined as the maximum mutual information between $\boldsymbol{x}_{zf}$ and $\boldsymbol{s}$, $\mathcal{I}(\boldsymbol{x}_{zf};\boldsymbol{s}|\boldsymbol{H})$ with symbol-by-symbol detection. Following the similar procedure as the derivation of the capacity of MLE, the instantaneous capacity of ZF equalizer given $\boldsymbol{H}$ can be expressed as

$$C_{ZF}(\boldsymbol{H}) = \log_2\left[\det\left(\boldsymbol{I}_N + \frac{1}{\sigma_w^2}\boldsymbol{R}_\eta^{-1}\right)\right]. \tag{19}$$

The closed form of the average capacity of ZF equalizer is derived for i.i.d. MIMO channels in [12]. Here, for generality, we keep the instantaneous forms.

Now, let us check the relationship between the ML capacity in (17) and ZF capacity in (19). When the SNR is high, we can simplify the expressions in (17) and (19) as

$$\begin{aligned} C_{ML}(\boldsymbol{H}) &\approx \log_2 \left[\det \left(\frac{1}{\sigma_w^2} \boldsymbol{H}^{\mathcal{H}} \boldsymbol{H} \right) \right] \\ &= \log_2 \left[\det \left(\boldsymbol{H}^{\mathcal{H}} \boldsymbol{H} \right) \right] - N \log_2 \sigma_w^2, \end{aligned} \tag{20}$$

$$\begin{aligned} C_{ZF}(\boldsymbol{H}) &\approx \log_2 \left[\det \left(\frac{1}{\sigma_w^2} \boldsymbol{R}_\eta^{-1} \right) \right] \\ &= \log_2 \left[\det \left(\boldsymbol{R}_\eta^{-1} \right) \right] - N \log_2 \sigma_w^2. \end{aligned} \tag{21}$$

Based on Hadamard inequality and the definition of $\boldsymbol{R}_\eta$ in (18), it can be verified that (see also [12])

$$C_{ZF}(\boldsymbol{H}) \leq C_{ML}(\boldsymbol{H}), \tag{22}$$

where the equality holds if and only if $\boldsymbol{H}^{\mathcal{H}}\boldsymbol{H}$ is diagonal, i.e., $od(\boldsymbol{H}) = 0$. This is consistent with the diversity analysis in Corollary 2. Furthermore, we quantify the difference between $C_{ZF}(\boldsymbol{H})$ and $C_{ML}(\boldsymbol{H})$ for each realization of $\boldsymbol{H}$ as

$$\begin{aligned} C_{ML}(\boldsymbol{H}) - C_{ZF}(\boldsymbol{H}) &\approx -\log_2 \left[\frac{\det \left((\boldsymbol{H}^{\mathcal{H}} \boldsymbol{H})^{-1} \right)}{\det(\boldsymbol{R}_\eta)} \right] \\ &= -\log_2 \left(1 - od(\boldsymbol{H}(\boldsymbol{H}^{\mathcal{H}} \boldsymbol{H})^{-1}) \right), \end{aligned} \tag{23}$$

where od is defined in (10) and $\boldsymbol{H}(\boldsymbol{H}^{\mathcal{H}}\boldsymbol{H})^{-1}$ is $(\boldsymbol{H}^{\dagger})^{\mathcal{H}}$. Surprisingly, the capacity difference between ZF and MLEs is also related to the od of the channel matrix. Based on (23), we observe that as $od((\boldsymbol{H}^{\dagger})^{\mathcal{H}})$ decreases, i.e., the inverse of the channel matrix is more orthogonal, then the capacity gap between ML and ZF equalizers decreases. Before we introduce the statistical properties of ZF capacity, let us revisit the definition of outage diversity.

Definition 3 (Outage diversity) *Suppose that $P(C < C_{th})$ is the probability that the instantaneous capacity is less than a threshold for a certain system. The outage*

diversity order G_o is defined as:

$$G_o = \lim_{SNR\to\infty} -\frac{\log P(C < C_{th})}{\log(SNR)}. \tag{24}$$

With the definitions of outage diversity in (24) and $od(\boldsymbol{H})$ in (10), we present the condition with which LEs have the same outage diversity as MLEs do.

Theorem 2 *Given the system model in* (1) *with channel state information at the receiver but not at the transmitter, in the high SNR regime, the capacity gap between ML and ZF equalizers is determined by* $od((\boldsymbol{H}^\dagger)^{\mathcal{H}})$ *in* (23)*. If* $od((\boldsymbol{H}^\dagger)^{\mathcal{H}}) \leq \epsilon, \forall \boldsymbol{H}$ *and* $\epsilon \in (0, 1)$*, ZF equalizers have the same outage diversity* (24) *as that of MLEs.*

Proof: See Appendix C.

Note that the conditions on *od* numbers in Theorems 1 and 2 are different. To unify them, we need the following lemma.

Lemma 2 *Suppose that* $\boldsymbol{H}$ *is a random matrix with* $od(\boldsymbol{H}) < \epsilon < 1$*. There exists* $\epsilon' < 1$ *such that* $od((\boldsymbol{H}^\dagger)^{\mathcal{H}}) < \epsilon' < 1$*, and vice versa.*

Proof: See Appendix .

With Lemma 2, we can modify Theorem 2 as follows.

Corollary 4 *Given the system model in* (1)*, if* $od(\boldsymbol{H}) \leq \epsilon, \forall \boldsymbol{H}$ *and* $\epsilon \in (0, 1)$*, then at high SNR regime, ZF equalizers collect the same outage diversity as that of MLEs, i.e., the cumulative density functions (CDFs) of the instantaneous capacity* $P(C < C_{th})$ *with ML and ZF equalizers are parallel in the log-log scale plot.*

In this section, we have shown that the mutual information loss between ZF equalizer and MLE also depends on the *od* of the channel matrix. When the *od* of the channel matrix has an upper bound which is strictly less than one, the performance diversity in (3) and the outage diversity in (24) of ZF equalizer are the same as those of MLE. Now a natural question is what if the *od* of the channel matrix does not have an upper bound.

3.3 Applying Theorems 1 and 2

In Section 3.1, we have shown that for some particular transmission systems, $od(\boldsymbol{H})$ has an upper bound which is strictly less than 1. However, in most practical systems, $od(\boldsymbol{H})$ does not have an upper bound less than 1. For example, when the channel matrix has independent entries (Example 3 in Sec. 3.1), $od(\boldsymbol{H})$ does not have an upper bound less than 1. As shown in [66], for these systems, LEs have inferior performance relative to MLEs due to loss of diversity. Thus, to collect the same diversity as MLE does and reduce the capacity gap, channel matrix $\boldsymbol{H}$ needs some "modification" to upper bound $od(\boldsymbol{H})$ by a constant less than 1. One approach is to design the transmitter properly so that at the receiver $od(\boldsymbol{H})$ has an upper bound, e.g., space-time orthogonal coding [97]. Another approach is to modify the receiver which we will focus on in the following.

One way to apply Theorem 1 is to design a hybrid equalizer that combines LEs with other full-diversity detectors based on the *od* of the channel matrix $\boldsymbol{H}$. Unlike the combined ZF-ML equalizer in [77], our hybrid equalizers are able to guarantee the same diversity as MLE does. Our hybrid equalizers are also different from the equalizer proposed in [13] which combines decision feedback equalizer and ML detector for every single realization of the channel matrix $\boldsymbol{H}$. Here, we only apply one kind of equalizer for one realization of the channel $\boldsymbol{H}$.

We summarize our framework in the following proposition.

Proposition 1 *Consider the model in* (1) *and a constant* $\epsilon_{th} \in (0, 1)$. *A hybrid equalizer is designed as: If* $od(\boldsymbol{H}) \leq \epsilon_{th}$, *LEs are employed; otherwise, MLE (or any other decoder with maximum diversity) is adopted. This hybrid equalizer collects the same diversity order as pure MLE does and exploits the same outage diversity of the capacity as that of MLE, but requires lower complexity.*

Obviously, the average complexity of this hybrid equalizer is lower than that of

MLE or near-MLE that is adopted, but higher than the pure LEs, since only some realizations of $\boldsymbol{H}$ are dealt with MLE. Furthermore, we notice that by selecting ϵ_{th}, we can balance the trade-off between the complexity and the performance. That means, when ϵ_{th} is small, more realizations of $\boldsymbol{H}$ are dealt with by (near-)MLE, and then the complexity of this hybrid equalizer is higher, while the performance is also better with larger coding gain.

The hybrid equalizer framework is general enough to accommodate different designs. A special case is worth mentioning. An attractive hybrid equalizer is a hybrid using LEs and the SD method [34] as

$$\begin{cases} \text{LEs} & \text{if } od(\boldsymbol{H}) \leq \epsilon_{th} \\ \text{SD method} & \text{if } od(\tilde{\boldsymbol{H}}) > \epsilon_{th} \end{cases} . \tag{25}$$

The reason to combine these two equalizers is not only to achieve the full diversity, but also to improve the performance of pure LEs and reduce the complexity of the SD-only method. Since LEs are usually adopted as preprocessing of the SD method, it is natural to combine these two without introducing extra hardware complexity. The computational complexity of this kind of hybrid LEs is close to LEs when ϵ_{th} is close to 1 (but not exactly 1), but the diversity is always the same as MLE's. Note that each burst of data may experience one realization of the channel and then employ an equalizer (either LE or (near-)MLE). Different decoders may result in different decoding delay since they have different complexity. However, this does not create an obstacle to implementing our equalizer in practical systems, because usually there is enough guard period between two bursts.

For our hybrid equalizers, selecting ϵ_{th} can trade between performance and complexity, since by choosing ϵ_{th} we can determine the probability to adopt LEs or (near-)MLEs. To further quantify the trade-off (e.g., control the percentage of the usage of (near-)MLEs), we need the distribution of $od(\boldsymbol{H})$ which will be discussed in the next section.

3.4 The Distribution of $od(\boldsymbol{H})$

Since the channel matrix $\boldsymbol{H}$ is random, $od(\boldsymbol{H})$ is also random. The distribution of $od(\boldsymbol{H})$ affects the performance. In this section, we focus on the general Gaussian random channel $\boldsymbol{H}$ where $\sup(od(\boldsymbol{H})) = 1$ to study the distribution of $od(\boldsymbol{H})$.

3.4.1 i.i.d. Gaussian Channels

First, we consider channel coefficients of $\boldsymbol{H}$ in (1) with i.i.d. complex Gaussian entries with zero mean and unit variance. Two practical examples of this kind of channels are V-BLAST multi-antenna transmissions in [15] and multiuser transmissions in [103]. To find the distribution of $od(\boldsymbol{H})$ for i.i.d. Gaussian channels, we need the following lemma:

Lemma 3 [102, Lemma 2.1] *Suppose that $\boldsymbol{H}$ is an $M \times N$ matrix, whose entries are i.i.d. complex Gaussian random variables with zero mean and unit variance. Denote the QR decomposition of $\boldsymbol{H}$ by $\boldsymbol{H} = \boldsymbol{Q}\boldsymbol{R}$, where $\boldsymbol{Q}$ is a unitary matrix, and $\boldsymbol{R}$ is an upper triangular matrix with real diagonal entries. Then the entries of $\boldsymbol{R}$ are independent of each other and its diagonal entries, $R_{n,n}$, for $n \in [1, 2, \ldots, N]$, are such that $2R_{n,n}^2$ are Chi-square random variables with $2(M-n+1)$ degrees of freedom (DOF). The off-diagonal entries, $R_{m,n}$ for $m < n$, are complex Gaussian distributed with zero-mean and unit variance.*

With this lemma, we obtain the following theorem on the exact distribution of $od(\boldsymbol{H})$ of i.i.d. Gaussian channels.

Theorem 3 *Suppose that $\boldsymbol{H}$ is an $M \times N$ matrix with all the entries i.i.d. complex Gaussian distributed with zero mean and unit variance. Then, $od(\boldsymbol{H})$ in* (10) *is a*

random variable with the probability density function (PDF) expressed as

$$f(x) = \left(\prod_{n=1}^{N} \frac{(M-1)!}{(M-n)!}\right) \sum_{k=1}^{N-1}\sum_{\ell=0}^{k-1} \frac{\rho_{k,\ell}(1-x)^{M-N+k-1}(-\ln(1-x))^{k-1-\ell}}{(k-1-\ell)!\ell!} \tag{26}$$

where

$$\rho_{k,0} = \prod_{q=1, q\neq k}^{N-1} (q-k)^{-q} \qquad \text{and}$$

$$\rho_{k,\ell} = \sum_{r=0}^{\ell-1} \prod_{q=1, q\ \neq k}^{N-1} (-1)^{r+1} \binom{\ell-1}{r} \frac{r!\cdot q\cdot \rho_{k,\ell-1-r}}{(q-k)^{r+1}} \tag{27}$$

Proof: See Appendix E.

The expression in (26) is still complicated and the number of parameters increases as the size of $\boldsymbol{H}$ increases. Fortunately, it has been shown in [14] that the product of Beta variables can be well approximated by another Beta variable which only needs two parameters. Thus, we establish the following proposition about the simple expression of the distribution of $od(\boldsymbol{H})$ for i.i.d. channels.

Proposition 2 *Given the system model in* (1)*, if the channels are i.i.d. complex Gaussian distributed with zero mean and unit variance, then* $od(\boldsymbol{H})$ *is approximated by a Beta distributed random variable with parameters* (a, b)*, which are determined as*

$$a = \frac{(\Phi-\Psi)(1-\Phi)}{\Psi-\Phi^2}, \qquad b = \frac{(\Phi-\Psi)\Phi}{\Psi-\Phi^2}, \tag{28}$$

where

$$\Phi = \prod_{n=1}^{N} \frac{M-n+1}{M}, \Psi = \prod_{n=1}^{N} \frac{(M-n+1)(M-n+2)}{M(M+1)}. \tag{29}$$

3.4.2 General Gaussian Channels

If the channels are not i.i.d. but still complex Gaussian distributed, e.g., correlated channels, $od(\boldsymbol{H})$ can still be approximated as a Beta random variable, because $1 - od(\boldsymbol{H})$ is still a product of N Beta random variables. Though these Beta random variables may be correlated with each other, the product can still be approximated by a Beta random variable.

One example of this kind of general Gaussian channels is the precoded OFDM system in [57]. In this case, the channel matrix $\boldsymbol{H} = \boldsymbol{D}_H\boldsymbol{\Theta}$, where $\boldsymbol{D}_H = \text{diag}[H(0), H(1), \ldots, H(N-1)]$ with $H(n) = \sum_{l=0}^{L} h_l e^{-j2\pi ln/N}$ being the channel response of the n^{th} subcarrier of the OFDM system, h_l's are complex Gaussian distributed with zero mean, and $\boldsymbol{\Theta}$ is the $N \times N$ unitary complex encoder. Thus, we can express the od for the equivalent channel matrix $\boldsymbol{D}_H\boldsymbol{\Theta}$ as [cf. the definition of od in (10)]

$$od(\boldsymbol{H}) = od(\boldsymbol{D}_H\boldsymbol{\Theta}) = 1 - \frac{\prod_{n=0}^{N-1} |H(n)|^2}{\left(\frac{1}{N}\sum_{n=0}^{N-1} |H(n)|^2\right)^N}. \tag{30}$$

From this expression, we know that $od(\boldsymbol{H})$ does not have an upper bound in $(0, 1)$, since $\sup(od(\boldsymbol{H})) = 1$ when any one of $H(n)$ approaches 0, which means deep fading on that subcarrier. Here it is difficult to obtain the exact distribution of $od(\boldsymbol{H})$ if the channel response of the subcarriers are correlated with each other. Since $H(n)$'s are still Gaussian distributed, according to [47], the second term in (30) is the product of N random variables which are jointly Dirichlet distributed. However, $1 - od(\boldsymbol{H})$ can still be approximated by a Beta random variable, since $\frac{|H(m)|^2}{\sum_{n=0}^{N-1} |H(n)|^2}$ is Beta distributed.

Thus, in practical systems, we may treat $od(\boldsymbol{H})$ as Beta distributed again. We summarize the results regarding the distribution of $od(\boldsymbol{H})$ as follows.

Corollary 5 *Suppose that $\boldsymbol{H}$ is complex Gaussian distributed with zero mean and $\sup(od(\boldsymbol{H})) = 1$. Then $od(\boldsymbol{H})$ is approximately a Beta random variable with two parameters.*

Table 4: Distribution of the $od(\boldsymbol{H})$ for i.i.d. channels

n	Exact Distribution $f(1-x)$	Approximate $\beta(a,b)$
2	1	(1, 1)
3	$4(1-x)+4x\ln(x)$	(3.1818, 0.9091)
4	$13.5+216x-229.5x^2+(108x+135x^2)\ln x-27x^2\ln^2 x$	(7.4529, 0.7710)
5	$\frac{128}{3}+6912x-58752x^2+\frac{155392}{3}x^3+1728x\ln x-20736x^2\ln x$ $-25792x^3\ln x-6912x^2\ln^2 x+4992x^3\ln^2 x-384x^3\ln^3 x$	(16.1011, 0.6430)

Using the distribution of $od(\boldsymbol{H})$ obtained by estimating the two parameters of Beta distribution, one has more control on the system design, e.g., one can trade-off between the performance and the complexity by designing the equalizer appropriately as we have shown in Section 3.3. Also the distribution of $od(\boldsymbol{H})$ will be helpful for further analyzing the performance and capacity of LEs.

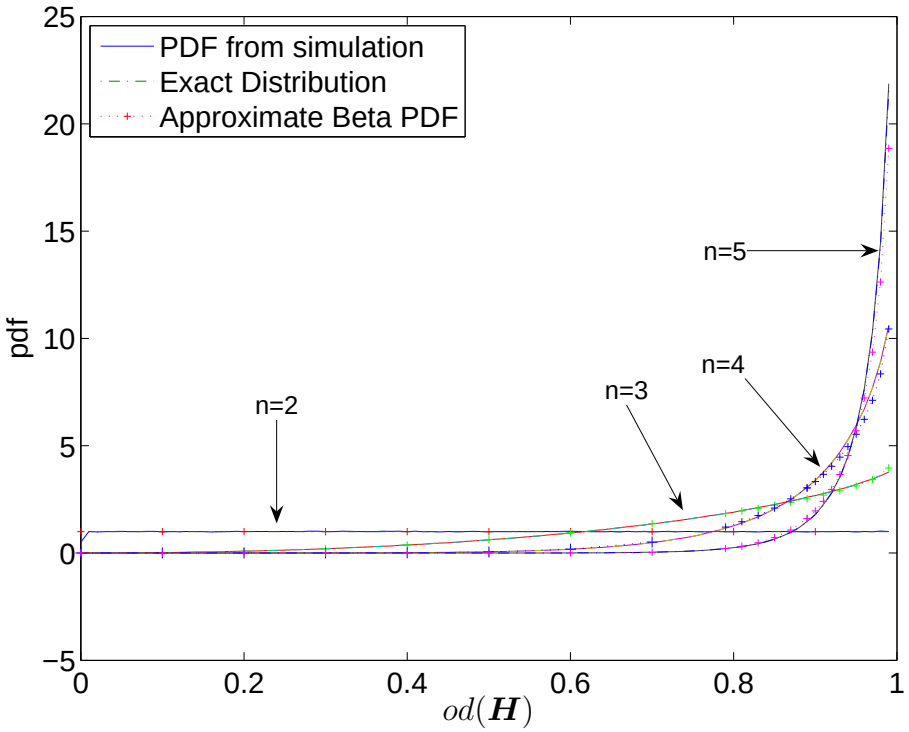

Figure 6: PDF of $od(\boldsymbol{H})$ for i.i.d. channels

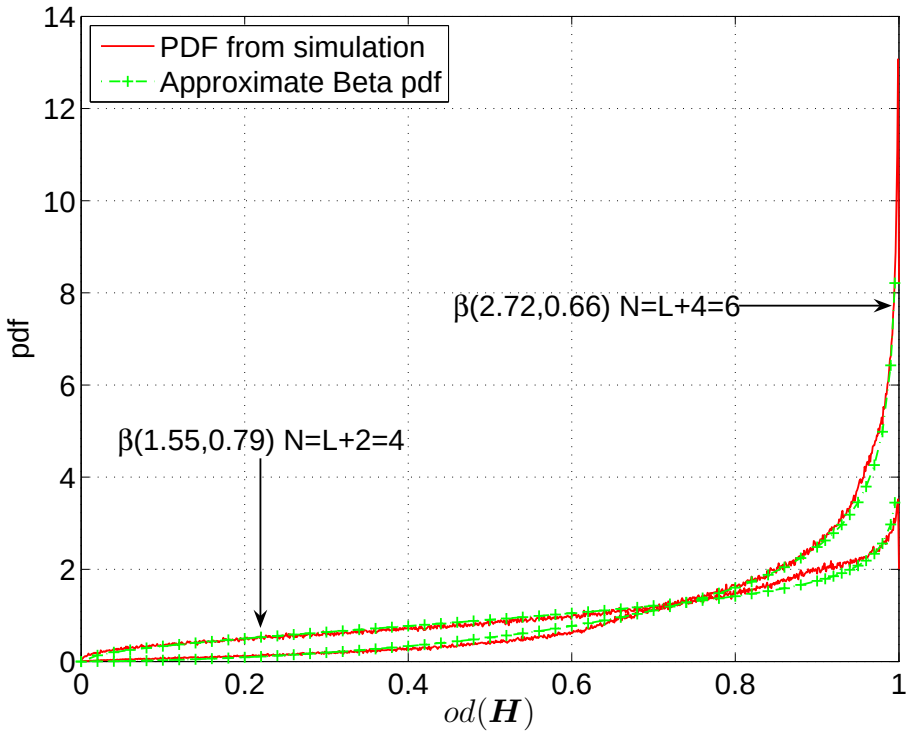

Figure 7: PDF of $od(\boldsymbol{H})$ for precoded OFDM systems

Example 3.5 (The distribution of $od(\boldsymbol{H})$): After analytically finding the distribution of $od(\boldsymbol{H})$, we now use some numerical examples to verify the results in Theorem 3, Proposition 2, and Corollary 5. First, we specialize the expressions of the exact and approximate distributions of $od(\boldsymbol{H})$ for i.i.d. channels to $N = M = n$ for $n = 2, 3, 4, 5$ in Table 4. We approximate the PDF of $od(\boldsymbol{H})$ for i.i.d. channels by plotting histograms in Fig. 6. The histograms are obtained by recording $od(\boldsymbol{H})$ for more than $1,000,000$ random realizations of i.i.d. Rayleigh fading channels. In the same figure, the distributions in Table 4 (both exact and approximate expressions) are also plotted. It is observed that the theoretical results match the simulation results very well. For general Gaussian channels, we choose the precoded OFDM system in [57] as an example. As stated in Corollary 5, we do not have the exact PDF of the *od* for the equivalent channel matrix. We only know it is approximately Beta distributed. We plot the PDF histograms of $od(\boldsymbol{D}_H\boldsymbol{\Theta})$ as in (30), for block size

$N = 4$ and 6 respectively, and the order of the frequency-selective channels $L = 2$. Then, we approximate these curves using Beta distributions. From Fig. 7, we can see, for $N = 4$, $\beta(1.55, 0.79)$ fits the simulation results, while $\beta(2.72, 0.66)$ works well for $N = 6$ case.

Instead of histogram, parameters (a, b) for Beta distributions can be obtained from the mean and variance of $od(\boldsymbol{H})$. Suppose the mean and the variance of $od(\boldsymbol{H})$ are μ and σ^2 respectively. Then, we have [78]

$$\mu = \frac{a}{a+b}, \qquad \text{and} \qquad \sigma^2 = \frac{ab}{(a+b)^2(a+b+1)}. \tag{31}$$

Thus, we can find parameters a and b as

$$a = \left(\frac{\mu(1-\mu)}{\sigma^2} - 1\right)\mu, \text{ and } b = \left(\frac{\mu(1-\mu)}{\sigma^2} - 1\right)(1-\mu).$$

In practice, the mean and variance of $od(\boldsymbol{H})$ can be obtained as the channel mean and variance are obtained.

3.5 Complexity of Linear Equalizers

In practical systems, the decoding complexity is usually given high priority. Thus, the decoding complexity is an important metric to compare different equalizers. In this section, we discuss the complexity of the commonly used equalizers, and then address that the overhead paid by our hybrid equalizers to compute *od* is negligible compared with the equalization complexity.

3.5.1 Complexity Comparison among Different Equalizers

To quantify the decoding complexity of different equalizers, we count the average number of arithmetic operations needed to estimate $\boldsymbol{s}$ in (1). This number of arithmetic operations takes into account the numbers of real multiplications and real additions. Though usually the SD method and other tree-search algorithms use the number of possible end nodes to represent the decoding complexity, we do not adopt it here because it is impossible to compare the complexity of a tree-search based algorithm with

that of other non-search methods (e.g., LEs) in this way. We focus on analyzing the difference in complexity among different equalizers and how the various parameters (e.g., M, N, $|\mathcal{S}|$ or $od(\boldsymbol{H})$) influence the complexity.

The major advantage of LEs is their low decoding complexity. Using ZF equalizer in (7) as an example, the complexity results from computing $\boldsymbol{H}^{\dagger} = (\boldsymbol{H}^{\mathcal{H}}\boldsymbol{H})^{-1}\boldsymbol{H}^{\mathcal{H}}$ using the QR decomposition and calculating $\boldsymbol{H}^{\dagger}\boldsymbol{y}$. As shown in [77], the number of real multiplication for ZF equalizer is $\mathcal{O}(N^3)+\mathcal{O}(N^2M)+\mathcal{O}(NM^2)$ while the number of real addition is also $\mathcal{O}(N^3) + \mathcal{O}(N^2M) + \mathcal{O}(NM^2)$. There is no need to calculate $od(\boldsymbol{H})$ when linear equalization is performed, though it determines the performance of LEs.

As shown in [34], the SD method generally requires an exponential worst-case complexity, whereas the heuristic search methods require only $\mathcal{O}(N^3)$ computations in average. Note that this complexity does not include the complexity from any preprocessing (e.g., QR decomposition) and it is an average. Simulation results in [113] show that SD method still has a high complexity compared with conventional LEs. It is not surprising to see this result, since LEs are used as the preprocessing step. Later, in our simulation, we count the average arithmetic operations of the SD method in [34], including the preprocessing step.

The optimum equalizer, MLE in (5), consumes the highest complexity among these equalizers. As shown in [77], both the number of arithmetic operations is $\mathcal{O}(|\mathcal{S}|^N MN)$.

3.5.2 Complexity Overhead of Hybrid Equalizers

Now, let us revisit our proposed hybrid equalizers in Proposition 1 to verify the complexity. Compared with the original LEs (say in (7)), the main complexity overhead the hybrid equalizer pays is to compute $od(\boldsymbol{H})$. To compute $od(\boldsymbol{H})$, we need

$(4M^2N + 8N^2 - 7N)$ real multiplications and $(4M^2N - 2MN + 4N^2 - 4)$ real additions. However, most of the operations to compute $od(\boldsymbol{H})$ are already required for the equalization process in (7). Since QR decomposition is also needed in the SD method, for the channel matrices that need the SD method, the overhead to compute $od(\boldsymbol{H})$ becomes $(2N^2 + 4N)$ real multiplications and $(2N^2 - 2N + 1)$ real additions. For the other channel matrices where only LEs are employed, the extra complexity to compute $od(\boldsymbol{H})$ is $2N$ real multiplications and 1 real addition, because $\boldsymbol{H}^{\mathcal{H}}\boldsymbol{H}$ is also needed when applying LEs. For both cases, the overhead of computing od is negligible compared with the equalization complexity, not to mention the situation when MLE is employed. Thus, the complexity of the hybrid equalizers is lower than that of (near-) optimum equalizer but higher than the conventional LEs, since only some realizations of $\boldsymbol{H}$ are decoded by the conventional LEs. Our hybrid equalizer provides a feasible approach to trade-off between performance (coding gain) and complexity while enjoying ML diversity.

3.6 Simulation Results

In this section, we use computer simulations to verify our theoretical claims on the diversity, capacity and complexity. QPSK is adopted as modulation scheme and channels are complex Gaussian distributed.

Test case 3.1 (Bounded *od* values): In this example, we verify Theorem 1 and Corollary 1 for i.i.d. Gaussian channels with $M = N = 4$. As we have shown, $od(\boldsymbol{H})$ for this kind of channels does not have an upper bound in $(0, 1)$. However, in simulations, by only counting the channel realizations of which od is less than ϵ, we upper-bound the od of the channel matrix by ϵ. In Fig. 8, we plot the BERs of the ZF and MMSE equalizers with $\epsilon = 0.8, 0.99$ respectively. The BERs of the ZF and MMSE with unconstrained $od(\boldsymbol{H})$ (without discarding those $od(\boldsymbol{H}) > \epsilon$ realizations), and MLEs are also plotted as references. From Fig. 8, we observe that,

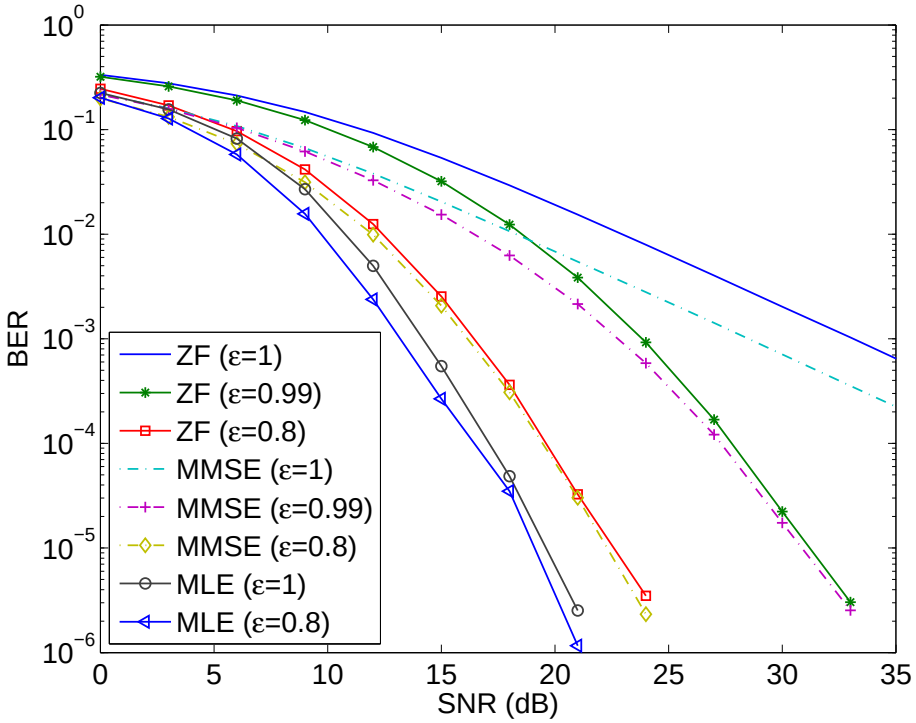

Figure 8: Performance of LEs for i.i.d. channels

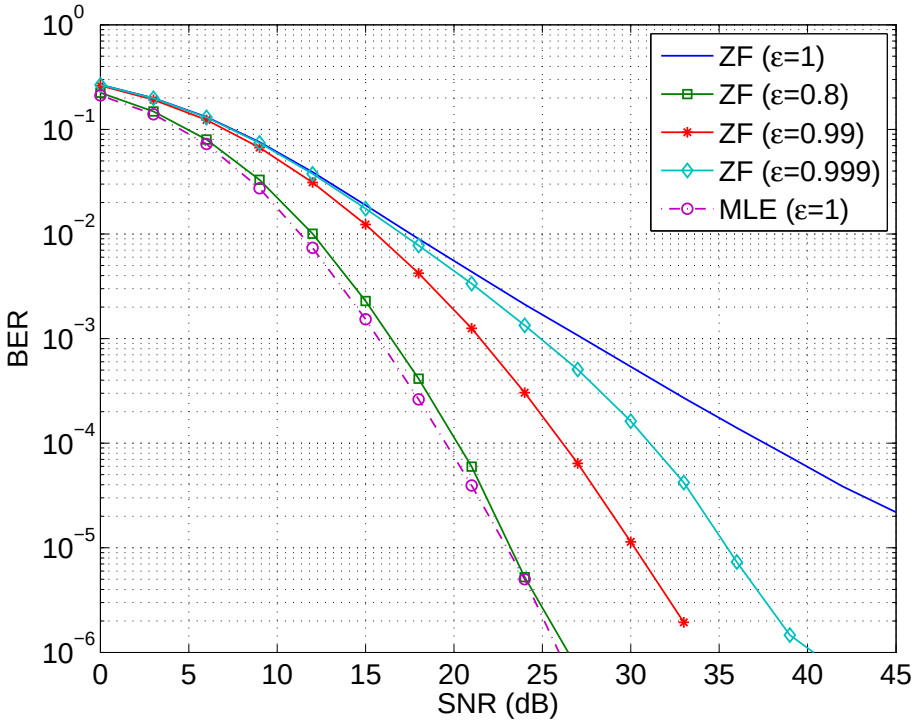

Figure 9: Performance of ZF equalizer for precoded OFDM systems

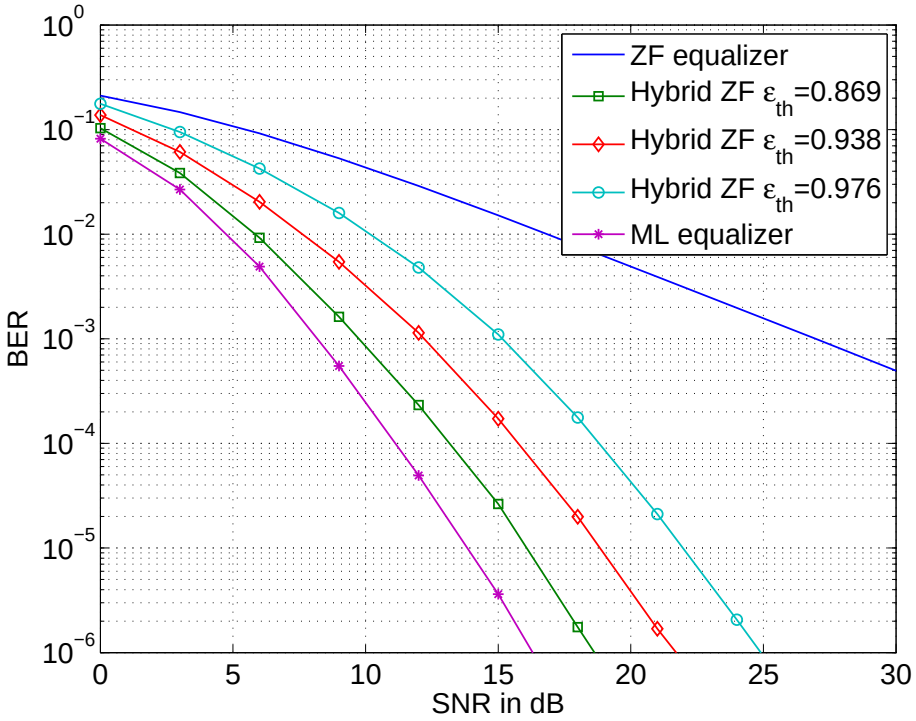

Figure 10: Performance of hybrid ZF equalizer for i.i.d. channels with $M = N = 4$

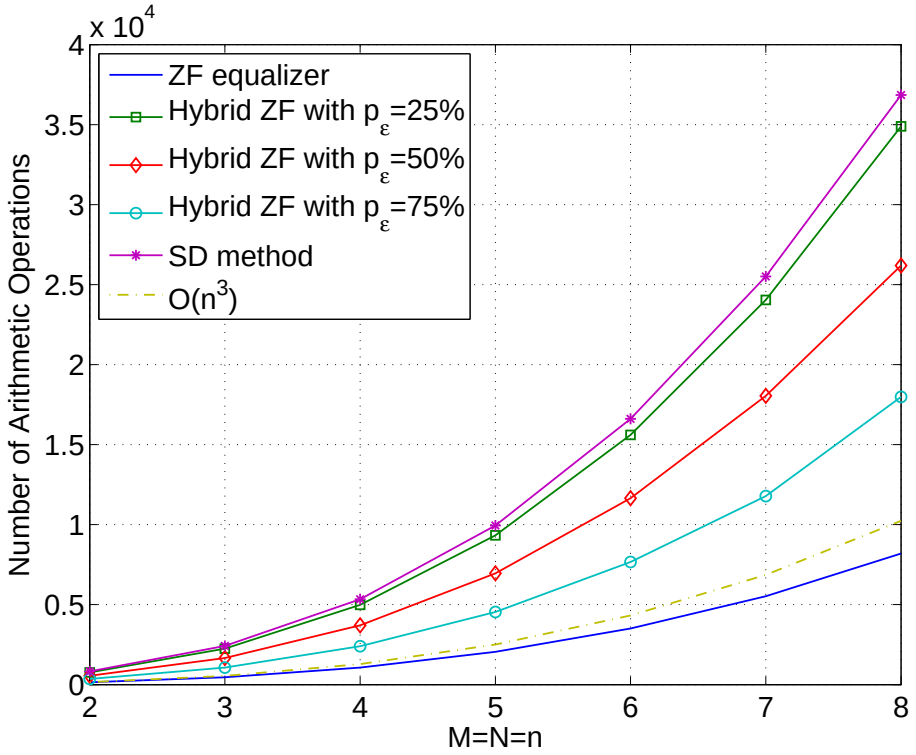

Figure 11: Complexity of hybrid equalizers with $N = M = n$

if $od(\boldsymbol{H}) \leq \epsilon < 1$, LEs collect the same diversity order as MLE does, which is 4 here, while the LEs without the *od* bound only collect diversity 1. On the contrary, the performance of MLEs is not highly influenced by $od(\boldsymbol{H})$. We also notice that when ϵ is smaller, the gap between LEs and MLE is smaller. This is consistent with the analysis, when ϵ is smaller, the upper bound of the BER performance in (141) also becomes smaller. In general, for LEs, a smaller $od(\boldsymbol{H})$ bound indicates higher coding gain while the diversity is the same as that collected by MLE. To further show the effect of $od(\boldsymbol{H})$ on performance, we depict another specific case for precoded OFDM systems in [57]. The frequency-selective channel order L is fixed to be 2 and the block size $M = N = 4$, which means the maximum diversity order is 3.

In Fig. 9 we plot the performance of the ZF equalizer for the channel realizations whose *od* is upper bounded by $\epsilon = 0.8, 0.99, 0.999$ respectively. For reference, the BER curve of ZF equalizer for all the channel realizations is also plotted. From the figure, we know that, if $od(\boldsymbol{H})$ of the channel matrix has an upper bound, ZF equalizers collect the same diversity order as MLE, while unconstrained case only collects diversity 1.

Test case 3.2 (Performance and complexity comparisons of hybrid equalizers): In this example, we illustrate the performance and the complexity of our two hybrid equalizers for i.i.d. channels with $N = M = 4$. In Fig. 10, we plot the BER curves for the hybrid equalizer which combines ZF equalizer and SD method as in Proposition 1 (referred as "Hybrid ZF") with $\epsilon_{th} = 0.869, 0.938, 0.976$, for which the percentage of channel realizations that are decoded by ZF equalizer are $p_\epsilon = 25\%, 50\%, 75\%$ respectively. The performance of ZF and SD equalizers is also plotted as references. From the figure, we know that the diversity of the hybrid ZF equalizer is 4 in this example. We also notice that the diversity orders of all three hybrid ZF equalizers are the same as that of MLE, and the one with $\epsilon_{th} = 0.869$ has

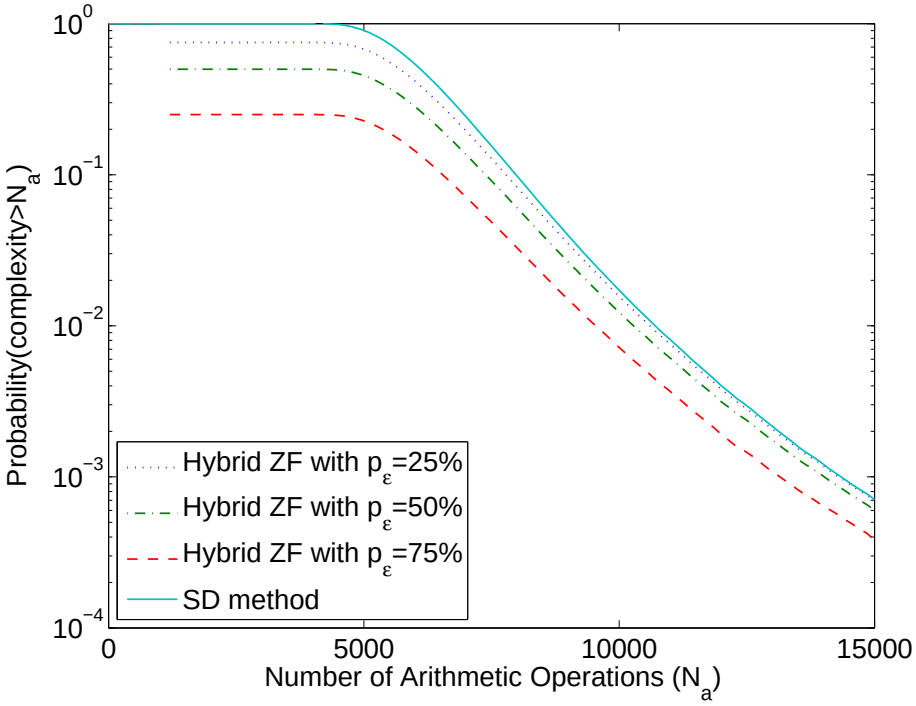

Figure 12: Outage complexity of hybrid equalizers with $N = M = 4$ and SNR=30dB

the best performance, since for this equalizer, only 25% of all the realizations of $\boldsymbol{H}$ are decoded by ZF equalizer. By adjusting ϵ_{th}, the hybrid ZF equalizer bridges the performance gap between LEs and SD.

With the comparable performance, we are interested in the complexity of these hybrid ZF equalizers. In Fig. 11, we plot the complexity of the hybrid ZF equalizers with ϵ_{th} satisfying the percentages of channel realizations that are decoded by LEs are $p_\epsilon = 25\%, 50\%, 75\%$, as $N = M = n$ increases. We fix the search radius of the SD method as 4 and SNR=30dB. From this figure, we observe that the complexity of our hybrid ZF equalizers is between that of ZF and SD. The smaller ϵ_{th} is, the higher the complexity of the hybrid equalizers is. This is because in general, smaller ϵ_{th} means more realizations of $\boldsymbol{H}$ are decoded by SD. Thus, we can see that ϵ_{th} plays an important role in hybrid equalizers. We also plot the curve of $\mathcal{O}(n^3)$ in the same figure to give a reference.

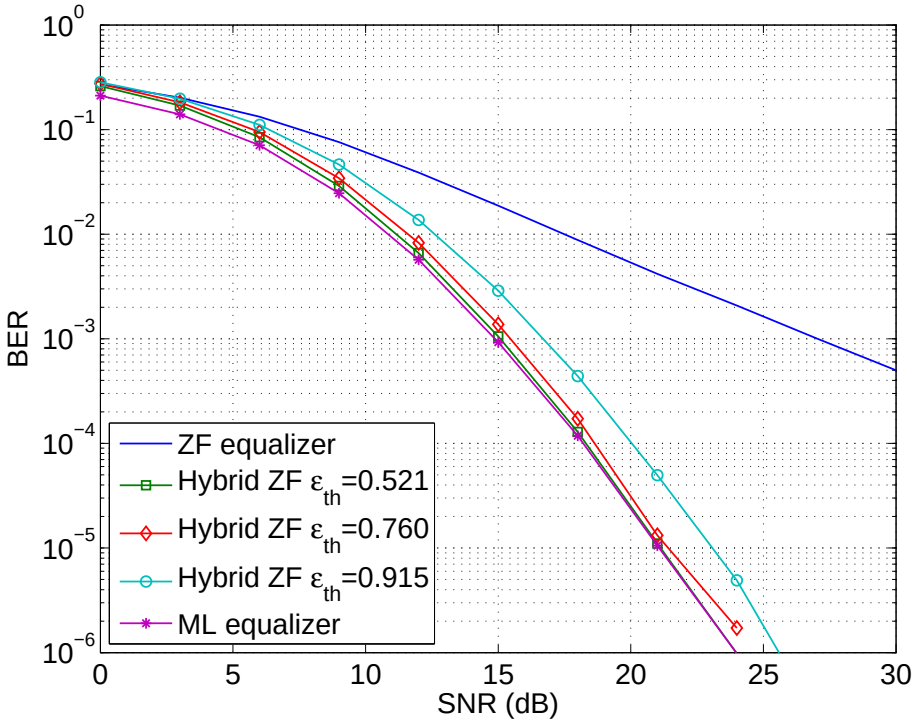

Figure 13: Performance of hybrid ZF equalizer for precoded OFDM with $L = 3$

Besides the average complexity, the outage complexity (the probability that the complexity is higher than a threshold value) is another important metric to compare different equalizers. We plot the outage complexity of these hybrid ZF equalizers with $p_\epsilon = 25\%, 50\%, 75\%$ by fixing $M = N = 4$ and SNR=30dB in Fig. 12. The outage complexity of the SD method with radius 4 is also plotted. From the figure, we observe that, there is a gap between the SD method and hybrid ZF equalizers. This shows that the probability that worst cases (high complexity) happen is reduced by applying hybrid equalizers. Furthermore, the gap increases as p_ϵ increases, which means increasing the percentage of the usage of ZF equalizer will not only reduce the average complexity but also the probability that worst cases show up.

The same experiments are tested on precoded OFDM systems in [57]. Fig. 13 shows the performance of hybrid ZF equalizers with $\epsilon_{th} = 0.521, 0.760, 0.915$, for which the percentage of the channel realizations that are decoded by ZF equalizer is

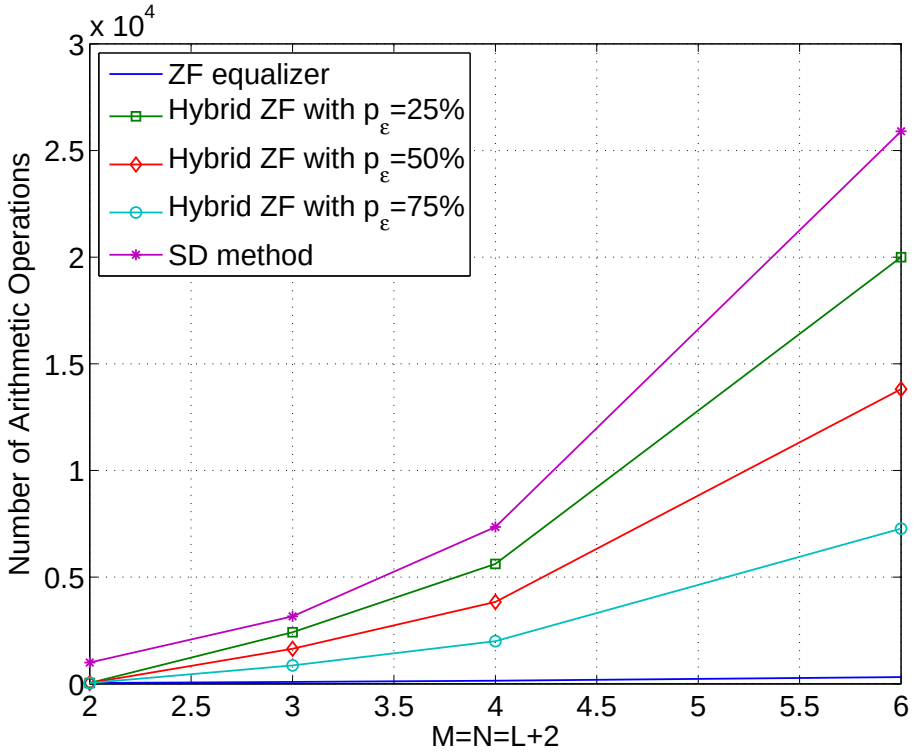

Figure 14: Complexity of hybrid equalizers with different channel order L

$p_\epsilon = 25\%, 50\%$, and 75%, respectively. The complexity versus $M = N = L + 2$ is plotted in Fig. 14. This figure shows that the complexity of the hybrid equalizers can be tuned by selecting ϵ_{th}.

Test case 3.3 (Capacity of different LEs): In Fig. 28, we plot the average capacity of i.i.d. channels with $M = N = 4$ and different equalizers: ZF ($\epsilon = 1$ and 0.976), Hybrid ZF ($\epsilon_{th} = 0.976$) and MLEs. From the figure, we notice that all these curves are parallel to each other. This confirms the observation in (23) that in the mid to high SNR region, the difference between capacities does not depend on SNR but on $od(\boldsymbol{H})$. When $\epsilon = 0.976$, the average $od(\boldsymbol{H})$ decreases, and thus the average capacity is higher. The CDFs of the capacity with these equalizers are depicted in Fig. 37 with SNR = 20 dB. Outage probabilities of the capacity versus SNR are

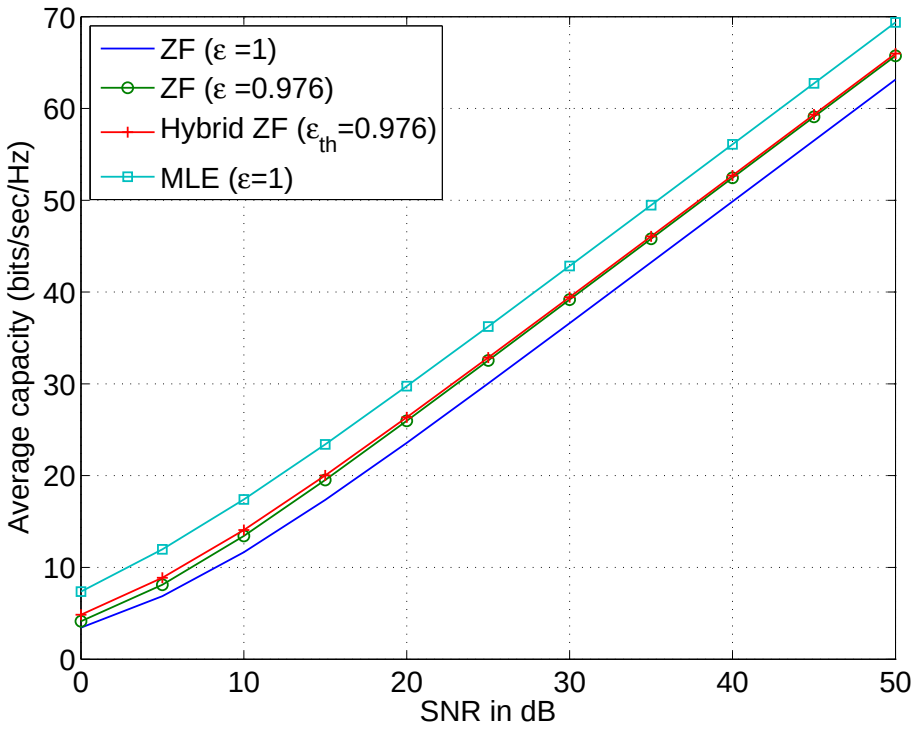

Figure 15: Average capacity vs. SNR

plotted in Fig. 38 with $C_{th} = 20$ bits/sec/Hz. Comparing Figs. 37 and 38, we notice that (i) when $\sup(od((\boldsymbol{H}^{\dagger})^{\mathcal{H}})) = 1$ (ZF with $\epsilon = 1$ case) LE loses outage diversity (i.e., the curve of LE is not parallel with the one of MLE); this is different from the average capacity in Fig. 28; and (ii) when $od((\boldsymbol{H}^{\dagger})^{\mathcal{H}})$ has an upper bound which is less than 1 (ZF with $\epsilon = 0.976$ case), the outage probability curves of LEs become parallel with those of MLEs. This is consistent with Theorem 2 and our analysis in Section 3.3.

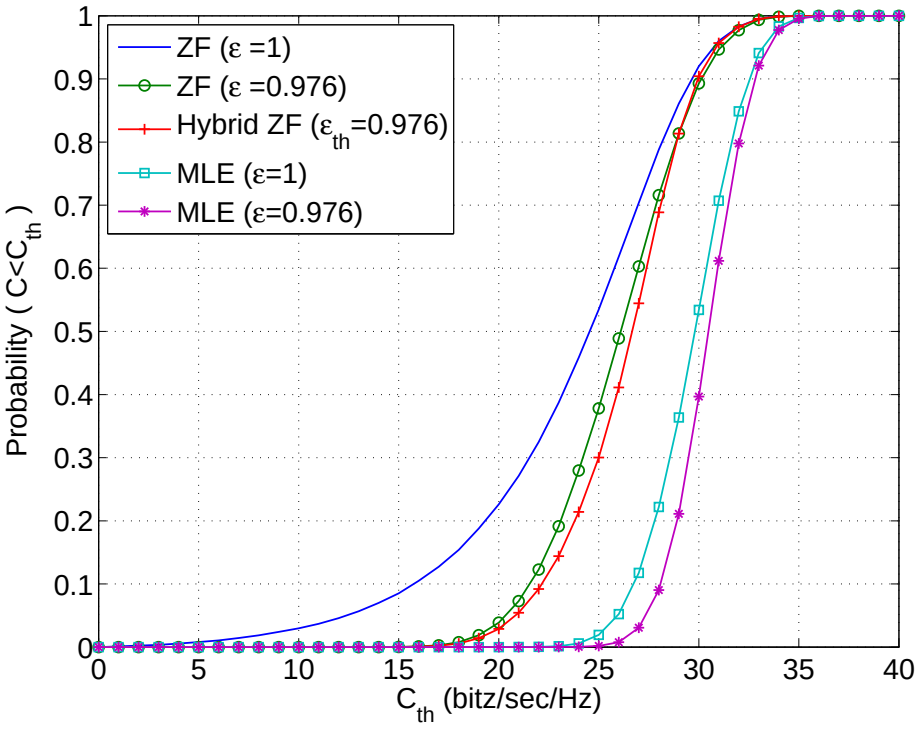

Figure 16: CDF of the capacity based on different equalizers

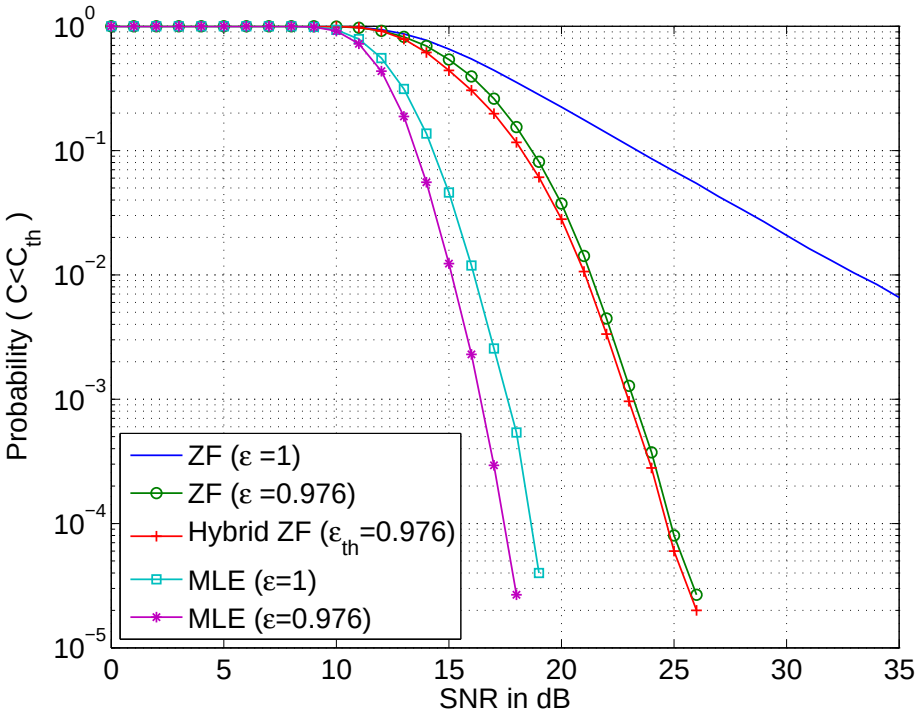

Figure 17: Outage probability vs. SNR

CHAPTER IV

QUANTIFYING THE ORTHOGONALITY OF MATRICES

Now, one may ask whether there exists other metrics to quantify the orthogonality of a channel matrix and corresponding LR algorithms to reduce it. The answer is positive. There are several metrics that have been adopted to measure the "quality" of a matrix and further judge whether the fundamental condition is met. In addition to *od* in (10), condition number and Seysen's metric also quantify the distance to orthogonality. We summarize these metrics as follows.

- **Condition Number** : $\kappa(\boldsymbol{H}) = \|\boldsymbol{H}^{-1}\| \cdot \|\boldsymbol{H}\|$; $\kappa(\boldsymbol{H}) \in [1, \infty)$; $\kappa(\boldsymbol{H}) = 1$ for unitary $\boldsymbol{H}$; and $\kappa(\boldsymbol{H}) = \infty$ for singular $\boldsymbol{H}$
- **Orthogonality Deficiency** : $od(\boldsymbol{H}) = 1 - \frac{\det(\boldsymbol{H}^{\mathcal{H}}\boldsymbol{H})}{\prod_{n=1}^{N}\|\boldsymbol{h}_n\|^2}$; $od(\boldsymbol{H}) \in [0, 1]$; $od(\boldsymbol{H}) = 0$ for orthogonal $\boldsymbol{H}$; $od(\boldsymbol{H}) = 1$ for singular $\boldsymbol{H}$
- **Seysen's Metric** : $S(\boldsymbol{H}) = \sum_{n=1}^{N}\|\boldsymbol{h}_n\|^2\|\boldsymbol{a}_n^T\|^2$; $S(\boldsymbol{H}) \in [N, \infty)$; $S(\boldsymbol{H}) = N$ for unitary $\boldsymbol{H}$; $S(\boldsymbol{H}) = \infty$ for singular $\boldsymbol{H}$

where $\boldsymbol{h}_n$ is the n^{th} column of $\boldsymbol{H}$ and $\boldsymbol{a}_n^T$ is the n^{th} row of $\boldsymbol{H}^{\dagger}$.

4.1 od or Condition Number

In the literature, a condition number of the channel matrix is an often-used criterion to judge the condition of the channel matrix. For the condition number, the analysis in [71] shows LEs collect the same diversity as that of MLE when $\kappa(\boldsymbol{H})$ has a finite upper bound. The reason that we adopt channel *od* number instead of condition number as in [77] is two-fold: (i) the performance gap between ZF and ML equalizers is not due to condition number because when channel is diagonal, ZF equalizer has

the same performance as MLE no matter the condition number is large or small; and (ii) as we have shown, performance diversity and outage capacity of the LEs depend on the *od* of the channel matrix instead of channel condition number. Thus, in this dissertation, we focus on the study of $od(\boldsymbol{H})$ on the fundamental limits of LEs.

4.2 od and Seysen's Metric

Seysen's metric further balances the orthogonality between the matrix and the inverse matrix. Following similar procedures in Appendix B for Theorem 1 in Chapter 3, we arrive at the following result.

Theorem 4 *Consider a linear system in* (1)*, where the entries of the channel matrix are complex Gaussian distributed with zero mean, and the information symbols are drawn from integer lattice (Gaussian integer ring). The linear equalizers in* (7) *and* (8) *collect the same diversity as MLE in* (5) *does if there exists a finite constant* ξ *such that* $\forall \boldsymbol{H}$, $S(\boldsymbol{H}) \leq \xi$*, i.e.,* $\sup(S(\boldsymbol{H})) = \xi$.

Proof: See Appendix G.

Furthermore, we find the general relationships between $od(\boldsymbol{H})$ and $S(\boldsymbol{H})$ in the following two propositions.

Proposition 3 *For a lattice basis* $\boldsymbol{B}$ *with size* $M \times N$*, if* $od(\boldsymbol{B})$ *is upper bounded by* $1-\epsilon$*, then* $S(\boldsymbol{B})$ *is also upper bounded by* $\frac{N}{\epsilon}$.

Proof: From [96] we know that for a lattice basis $\{\boldsymbol{b}_i\}$ and its dual lattice basis $\{\boldsymbol{b}'_i\}$ the following inequality holds

$$\|\boldsymbol{b}_i\|^2 \|\boldsymbol{b}'_i\|^2 \leq \frac{1}{1-od(\boldsymbol{B})} \leq \frac{1}{\epsilon}, \qquad i = 1, .., N. \tag{32}$$

Thus, for Seysen's metric, we have

$$S(\boldsymbol{B}) = \sum_{i=1}^{N} \|\boldsymbol{b}_i\|^2 \|\boldsymbol{b}'_i\|^2 \leq \frac{N}{\epsilon}. \tag{33}$$

■

Proposition 4 *For a lattice basis $\boldsymbol{B}$ with size $M \times N$, if $S(\boldsymbol{B})$ is upper bounded by ξ, then $od(\boldsymbol{B})$ is also upper bounded by $1 - \frac{1}{(\xi - N)^{N-1}}$.*

Proof: Let α_i represent the angle between $\boldsymbol{b}_i$ and $\boldsymbol{b}'_i$. Seysen's metric $S(\boldsymbol{B})$ can be rewritten as

$$S(\boldsymbol{B}) = \sum_{i=1}^{N} \frac{1}{\cos^2(\alpha_i)}. \tag{34}$$

Note here, for a two-dimensional (2-D) lattice, $\boldsymbol{b}_1, \boldsymbol{b}_2, \boldsymbol{b}'_1$ and $\boldsymbol{b}'_2$ are in the same plane as depicted in Figure 18, since $[\boldsymbol{b}'_1, \boldsymbol{b}'_2]^{\mathcal{H}}$ forms the pseudo-inverse (inverse with the shortest Euclidean norm) of $\boldsymbol{B}$. Thus, we have $\alpha_1 = \alpha_2 = \alpha$.

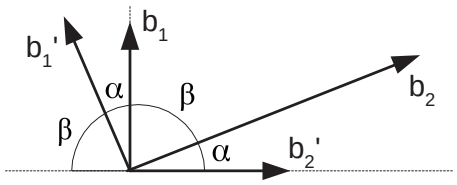

Figure 18: Sketch of lattice and dual lattice basis vectors for 2-D real case

With the expression of $S(\boldsymbol{B})$ in (34), we have

$$S(\boldsymbol{B}) = \sum_{i=1}^{N} \frac{1}{\sin^2(\beta_{H,i})} \leq \xi, \qquad i = 1, .., N. \tag{35}$$

Thus, it is ready to see $\sin^2(\beta_{H,i}) \geq \frac{1}{\xi - N}$ for $i \in \{1, .., N\}$. Furthermore, we can rewrite $od(\boldsymbol{B})$ as

$$od(\boldsymbol{B}) = 1 - \frac{\det(\boldsymbol{B}^{\mathcal{H}}\boldsymbol{B})}{\prod_{i=1}^{N} \|\boldsymbol{b}_i\|^2} = 1 - \frac{\prod_{i=1}^{N} \sin^2(\phi_{H,i}) \|\boldsymbol{b}_i\|^2}{\prod_{i=1}^{N} \|\boldsymbol{b}_i\|^2} = 1 - \prod_{i=1}^{N} \sin^2(\phi_{H,i}) \tag{36}$$

where $\phi_{H,i}$ is the Hermitian angle between $\boldsymbol{b}_i$ and the hyper plane spanned by $\boldsymbol{b}_1, ..., \boldsymbol{b}_{i-1}$ and $\sin(\phi_{H,1}) = 1$ [53]. Because $\beta_{H,i}$ is the Hermitian angle between $\boldsymbol{b}_i$ and the hyper plane spanned by $\boldsymbol{b}_1, ..., \boldsymbol{b}_{i-1}, \boldsymbol{b}_{i+1} ..., \boldsymbol{b}_N$, it is straightforward to see that $\beta_{H,i} \leq \phi_{H,i}$. Thus, we can bound $od(\boldsymbol{B})$ as

$$od(\boldsymbol{B}) \leq 1 - \prod_{i=2}^{N} \sin^2(\beta_{H,i}) < 1 - \frac{1}{(\xi - N)^{N-1}}. \qquad \blacksquare$$

Corollary 6 *Given a 2-D lattice with basis* $\boldsymbol{B}$*, the following relationship holds true:*

$$od(\boldsymbol{B}) = 1 - \frac{2}{S(\boldsymbol{B})} \tag{37}$$

Proof: For lattices in two dimensions, we have $\beta_{H,2} = \phi_{H,2}$. With the expressions of $S(\boldsymbol{B})$ in (35) and $od(\boldsymbol{B})$ in (36) it is straightforward to obtain the relationship in (37). ■

In addition to these metrics, other metrics exist that help quantify the performance gap between a specific low-complexity equalizer and MLE. For example, the proximity factor in [52] is a function of not only the channel matrix but also the specific low-complexity equalizer adopted. However, for most practical systems, no matter which metric is adopted the "quality" of the channel matrix does not have a lower bound for the worst case, which means the channel matrices can be arbitrarily close to singular. For example, when the channel matrix has i.i.d. entries, $od(\boldsymbol{H})$ does not have an upper bound less than 1. For these transmissions, low-complexity equalizers usually have inferior performance relative to MLEs because of the loss of diversity [67, 68]. Thus, to collect the same diversity as MLE does using low-complexity equalizers and reduce the capacity gap, besides adopting hybrid equalizers proposed in Proposition 1, we can "modify" the channel matrix $\boldsymbol{H}$ to upper bound the orthogonality metrics by a constant and thus make sure $\boldsymbol{H}$ cannot be arbitrarily close to singularity. One approach is to design the transmitter properly so that $od(\boldsymbol{H})$ has an upper bound, e.g., space-time orthogonal coding [97]. Another approach is to modify the receiver by adopting lattice reduction algorithms, which we will focus on in the following.

CHAPTER V

LATTICE REDUCTION ALGORITHMS

In the linear block transmission model in (1), the received signal vector $\boldsymbol{y}$ is the noisy observation of the vector $\boldsymbol{Hs}$, which is in the lattice spanned by the columns of $\boldsymbol{H}$ since all the entries of $\boldsymbol{s}$ can be transformed to complex integers by shifting and scaling. In general, a lattice has more than one set of basis vectors. There exist some bases that span the same lattice as $\boldsymbol{H}$ but are closer to orthogonality than $\boldsymbol{H}$. The process of finding a basis closer to orthogonality is called lattice reduction (LR). Theoretically, finding an optimal set of bases (closest to orthogonality) in a lattice is computationally expensive. Thus, the ultimate goal of LR algorithms is to find a "better" channel matrix $\tilde{\boldsymbol{H}} = \boldsymbol{HT}$ where $\boldsymbol{T}$ as a unimodular matrix, which means that all the entries of $\boldsymbol{T}$ and $\boldsymbol{T}^{-1}$ are complex integers and the determinant of $\boldsymbol{T}$ is ± 1 or $\pm j$. The restrictions on the matrix $\boldsymbol{T}$ ensure that the lattice generated by $\tilde{\boldsymbol{H}}$ is the same as that of $\boldsymbol{H}$. Note that the equivalence of the two lattices spanned by $\boldsymbol{H}$ and $\tilde{\boldsymbol{H}}$ is based on the assumption that all the entries of $\boldsymbol{s}$ belong to the whole complex integer set.

LR techniques have been studied by mathematicians for decades, and many LR algorithms have been proposed. Gaussian reduction, Minkowski reduction and Korkine-Zolotareff (KZ) reduction algorithms find the optimal basis for a lattice based on the successive minimal criteria, but these algorithms are highly complex and therefore infeasible for communications systems [121, 46, 84]. The well-known Lenstra-Lenstra-Lovász (LLL) algorithm does not guarantee to find the optimal basis with minimal *od*, but it guarantees in polynomial time to find a basis within a factor to the optimal one [40, 52, 51, 121]. Seysen's algorithm (SA) reduces Seysen's metric to perform LR

[87]. A simplified Brun's algorithm is proposed and implemented in [10] to reduce complexity but also sacrifices performance. For the worst cases these LR algorithms may not terminate, but simulations have shown that this never occurs in practice (see [121, p. 62] and [40]).

Given the array of LR algorithms in the literature, it is difficult to justify which one is better in terms of both performance and complexity. In the following, we look into two well-adopted LR algorithms: the SA and the LLL algorithm since they are known to be able to reduce $od(\boldsymbol{H})$ and $S(\boldsymbol{H})$. We will find the property of the output matrices, e.g., whether the conditions in Theorems 1 and 4 are met. We will also briefly introduce other LR algorithms for readers' interest.

5.1 The Complex Lenstra-Lenstra-Lovász Algorithm

So far, the most popular LR algorithm is the Lenstra-Lenstra-Lovász (LLL) algorithm [51]. The LLL algorithm does not guarantee to find the optimal basis, but it guarantees in polynomial average time to find a basis within a factor to the optimal one [121, 51, 40, 54]. The results in [54] theoretically proved the upper bound on the average complexity of LLL is $\mathcal{O}(N^3 \log N)$. Furthermore, [40] reduces the upper bound on the average complexity to $\mathcal{O}(N^2 \log(\frac{N}{M-N+1}))$. We need to note that the worst-case complexity of the LLL algorithm can be infinite, since we can build a special structure that needs exactly certain number of iterations to finish the LLL algorithm [121, 40]. However, the probability that a system meets such a special structure in practice or simulations is zero, not to mention the probability that we meet it many times. Thus, though theoretically the worst-case complexity of the LLL algorithm is not upper bounded, the complexity is still polynomial in practice and simulations.

The real LLL (RLLL) algorithm is first applied by extending the system model in (1) into an equivalent real system and use the real LR-aided equalizers [96, 111, 117].

Table 5: The complex LLL algorithm (using MATLAB notation)

INPUT: $\boldsymbol{H}$; OUTPUT: $\tilde{\boldsymbol{Q}}$, $\tilde{\boldsymbol{R}}$, $\boldsymbol{T}$

(1) $[\tilde{\boldsymbol{Q}},\tilde{\boldsymbol{R}}]$ = QR Decomposition($\boldsymbol{H}$);
(2) $\delta \in (\frac{1}{2}, 1)$;
(3) $m = size(\boldsymbol{H}, 2)$;
(4) $\boldsymbol{T} = \boldsymbol{I}_m$;
(5) $k = 2$;
(6) while $k \leq m$
(7) for $n = k-1 : -1 : 1$
(8) $u = round((\tilde{\boldsymbol{R}}(n,k)/\tilde{\boldsymbol{R}}(n,n)))$;
(9) if $u \sim= 0$
(10) $\tilde{\boldsymbol{R}}(1:n,k) = \tilde{\boldsymbol{R}}(1:n,k) - u \cdot \tilde{\boldsymbol{R}}(1:n,n)$;
(11) $\boldsymbol{T}(:,k) = \boldsymbol{T}(:,k) - u \cdot \boldsymbol{T}(:,n)$;
(12) end
(13) end
(14) if $\delta|\tilde{\boldsymbol{R}}(k-1,k-1)|^2 > |\tilde{\boldsymbol{R}}(k,k)|^2 + |\tilde{\boldsymbol{R}}(k-1,k)|^2$
(15) Swap the $(k-1)^{\text{th}}$ and k^{th} columns in $\tilde{\boldsymbol{R}}$ and $\boldsymbol{T}$
(16) $\boldsymbol{\Theta} = \begin{bmatrix} \alpha^* & \beta \\ -\beta & \alpha \end{bmatrix}$ where $\alpha = \frac{\tilde{\boldsymbol{R}}_{(k-1,k-1)}}{\|\tilde{\boldsymbol{R}}_{(k-1:k,k-1)}\|}$; $\beta = \frac{\tilde{\boldsymbol{R}}_{(k,k-1)}}{\|\tilde{\boldsymbol{R}}_{(k-1:k,k-1)}\|}$;
(17) $\tilde{\boldsymbol{R}}(k-1:k, k-1:m) = \boldsymbol{\Theta}\tilde{\boldsymbol{R}}(k-1:k, k-1:m)$;
(18) $\tilde{\boldsymbol{Q}}(:, k-1:k) = \tilde{\boldsymbol{Q}}(:, k-1:k)\boldsymbol{\Theta}^{\mathcal{H}}$;
(19) $k = \max(k-1, 2)$;
(20) else
(21) $k = k+1$;
(22) end
(23) end

The complex LLL (CLLL) algorithm is proposed in our paper [67] based on the QR decomposition and [19] based on the Gram-Schmidt orthogonalization. The definition of a reduced basis in the complex field is given as follows.

Definition 4 *An $M \times N$ complex matrix $\tilde{\boldsymbol{H}}$ is called a reduced basis of a lattice if the QR-decomposition $\tilde{\boldsymbol{H}} = \tilde{\boldsymbol{Q}}\tilde{\boldsymbol{R}}$ satisfies the following two conditions:*

$$|\Re[\tilde{R}_{i,k}]| \leq \frac{1}{2}|\tilde{R}_{i,i}|, \quad |\Im[\tilde{R}_{i,k}]| \leq \frac{1}{2}|\tilde{R}_{i,i}|, \qquad \text{for} \;\; 1 \leq i < k \leq N, \tag{38}$$

$$\delta|\tilde{R}_{i-1,i-1}|^2 \leq |\tilde{R}_{i,i}|^2 + |\tilde{R}_{i-1,i}|^2, \qquad \text{for} \;\; i = 2, \ldots N, \tag{39}$$

where the parameter δ now is arbitrarily chosen from $(\frac{1}{2}, 1)$, and $\tilde{R}_{i,k}$ is the $(i,k)^{\text{th}}$ entry of $\tilde{\boldsymbol{R}}$.

The detailed pseudo-code of the CLLL algorithm can be found in Table 5. The parameter δ controls the complexity and performance of the LLL algorithm and the bigger δ is, the higher the complexity is. Compared with the RLLL algorithm in [116, 117], the major differences of the CLLL algorithm are: (i) at Step (8), the rounding equation is on complex numbers; and (ii) at Step (16), a complex unitary $\boldsymbol{\Theta}$ is adopted. It has been shown that the CLLL algorithm reduces the complexity of the RLLL algorithm without sacrificing performance [19, 67]. This may counter intuition since the matrix dimensions are doubled in RLLL, but only real operations are required. As shown in Table 6, the RLLL algorithm requires more basis updates than the CLLL algorithm. One basis update is defined as the process that updates the n^{th} basis vector using the m^{th} basis as $\boldsymbol{h}_n \leftarrow \boldsymbol{h}_n + a_{m,n}\boldsymbol{h}_m$. Furthermore, the sorted QR-decomposition (SQRD) in [117] is introduced into the LLL process to further reduce the complexity as shown in Table 6. The CLLL algorithm has been applied to the dual basis of the channel matrix and the performance is further improved [52]. The complexity of the LLL algorithm depends on the specific realization of the channel but has an polynomial upper bound on average [40].

Table 6: Number of basis updates needed for different LR algorithms for i.i.d. channels

$M = N = n$		2	4	6	8	10
Greedy SA	Average	1.0733	5.4579	11.1725	16.9698	22.0766
	Std. deviation	0.6378	2.3032	4.4139	6.9265	9.3423
Real LLL	Average	3.5204	19.0711	46.5706	84.7531	132.36
	Std. deviation	2.7614	9.6056	21.5811	39.5851	61.8293
Complex LLL	Average	1.1151	6.6624	16.2276	29.0076	44.2684
	Std. deviation	0.6963	3.0824	7.0284	12.6450	19.4835
Complex LLL with SQRD	Average	1.0505	5.7555	13.4083	23.3189	35.2554
	Std. deviation	0.6208	2.6426	5.9486	10.3063	15.5275

Following the CLLL algorithm, we find a "better" channel matrix $\tilde{\boldsymbol{H}} = \boldsymbol{HT}$ from

the original channel matrix $\boldsymbol{H}$. Adopting *od* as the orthogonality metric, we quantify the condition of the output matrix $\tilde{\boldsymbol{H}}$ of the CLLL algorithm as follows.

Proposition 5 *Given a matrix $\boldsymbol{H} \in \mathbb{C}^{M\times N}$ with rank N, $\tilde{\boldsymbol{H}}$ is obtained after applying the CLLL algorithm in Table 5 for a given parameter $\delta \in (\frac{1}{2}, 1)$. Then, the od of $\tilde{\boldsymbol{H}}$ satisfies:*

$$\sqrt{1 - od(\tilde{\boldsymbol{H}})} \geq 2^{\frac{N}{2}} \left(\frac{2}{2\delta - 1}\right)^{-\frac{N(N+1)}{4}} := c_\delta. \tag{40}$$

Proof: See Appendix F.

For real $\boldsymbol{H}$, the upper bound in (40) is consistent with the result in [51, Proposition 1.8]. Here, we extend it to the complex field according to the CLLL algorithm in Table 5. If $\boldsymbol{H}$ is singular, i.e., $\text{rank}(\boldsymbol{H}) < N$, then the upper bound in (40) does not hold true since $\boldsymbol{H}$ is not a basis any more. In this case, we need to reduce the size of $\boldsymbol{H}$ and then apply the CLLL algorithm. From Eq. (40), we can see that the CLLL algorithm does not guarantee to reduce the *od* for every realization of $\boldsymbol{H}$, but the new basis $\tilde{\boldsymbol{H}}$ now has an upper bound on *od* which is strictly less than 1. Later, we show that thanks to this upper bound on *od*, the LLL based equalizers collect the same diversity as MLEs. Furthermore, according to Proposition 3, we know the Seysen's metric of the output matrix $\tilde{\boldsymbol{H}}$ is also upper bounded by a finite number.

Test Case 5.1 (Effects of LLL on the distribution of $od(\boldsymbol{H})$): We use this example to verify the effect of LR on $od(\boldsymbol{H})$ for both i.i.d. channels and correlated Gaussian channels. For i.i.d. Rayleigh fading channels, we plot the PDFs of $od(\boldsymbol{H})$ and $od(\tilde{\boldsymbol{H}})$ obtained after the CLLL algorithm in Fig. 19. The histograms are obtained by recording the *od* samples over $1,000,000$ different realizations of $\boldsymbol{H}$ for $n = M = N = 3$ and 4, respectively. It is shown that the LR algorithm not only upper-bounds the *od* of the equivalent channel matrix, but also changes its distribution. Most realizations of the channel matrix now have a smaller *od*, since the PDF of $od(\tilde{\boldsymbol{H}})$ after LR is no longer concentrated near 1. For general correlated Gaussian

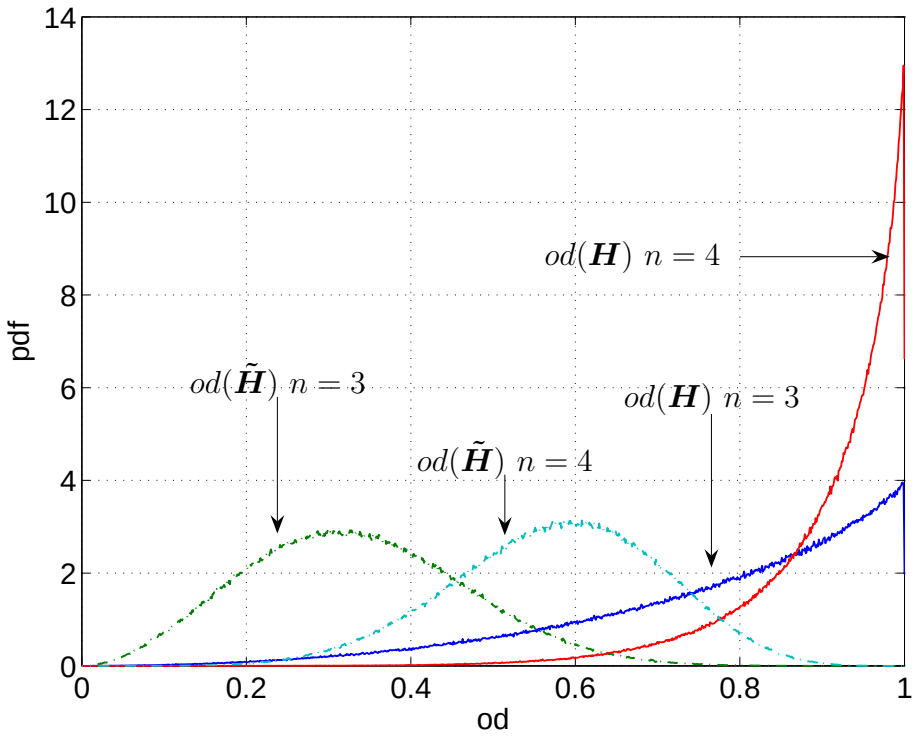

Figure 19: PDF of $od(\boldsymbol{H})$ for i.i.d. channels

channels, we choose the precoded OFDM system in [57] as an example. We plot the average $od(\boldsymbol{H})$ versus channel order L in Fig. 20, when $M = N = L + 1$. From the figure we observe that the average $od(\boldsymbol{H})$ increases as L (or N) increases, because as the size of the channel matrix increases, it becomes more difficult for the random matrix to be close to orthogonal. In the same figure, we also plot the average $od(\tilde{\boldsymbol{H}})$ and the *od* bound from Proposition 5. It can be seen that LR reduces the average $od(\boldsymbol{H})$ and thus improves the performance.

5.2 Seysen's Algorithm

As an alternative to the LLL algorithm, SA is an iterative method to reduce the lattice based on the Seysen's metric [50, 88]. The Seysen's metric that SA adopts to quantify the orthogonality of matrices is defined as follows (see e.g., [50, 88]).

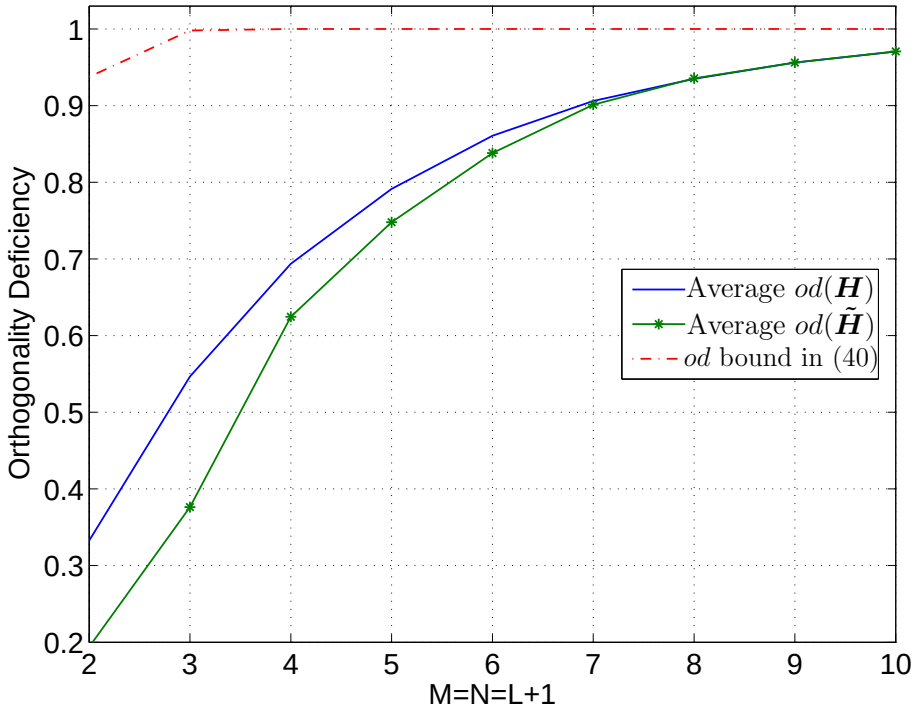

Figure 20: Average $od(\boldsymbol{H})$ for precoded OFDM systems

Definition 5 *For an $M \times N$ matrix $\boldsymbol{H}$, the Seysen's metric ($S(\boldsymbol{H})$) is defined as*

$$S(\boldsymbol{H}) = \sum_{n=1}^{N} \|\boldsymbol{h}_n\|^2 \|\boldsymbol{a}_n\|^2, \tag{41}$$

where $\boldsymbol{h}_n$ is the n^{th} column of $\boldsymbol{H}$ and $\boldsymbol{a}_n^T$ is the n^{th} row of $\boldsymbol{H}^\dagger$.

For any $\boldsymbol{H}$, $S(\boldsymbol{H}) \geq N$, with equality when $\boldsymbol{H}$ is a unitary matrix. In general, smaller $S(\boldsymbol{H})$ indicates that $\boldsymbol{H}$ is closer to being a unitary matrix. Compared with the definition of od in (10), we can see that $S(\boldsymbol{H})$ optimizes the orthogonality of both $\boldsymbol{H}$ and $\boldsymbol{H}^{\mathcal{H}}$, while $od(\boldsymbol{H})$ focuses on the orthogonality of $\boldsymbol{H}$ only.

The ultimate goal of SA is to find a set of bases $\tilde{\boldsymbol{H}}$, of which the Seysen's metric cannot be reduced anymore. The lazy method and the greedy method are first proposed to implement SA [50], while a simplified greedy implementation is proposed in [87] to further reduce the complexity. The lazy implementation of SA guarantees to find the optimal bases that minimize $S(\tilde{\boldsymbol{H}})$ but requires extremely high complexity.

The greedy implementation requires much fewer operations, but the algorithm may stop at a certain set of bases $\tilde{\boldsymbol{H}}$ with suboptimal $S(\tilde{\boldsymbol{H}})$ (a local minimum).

SA adopts iterative basis updates to generate $\tilde{\boldsymbol{H}}$ whose $S(\boldsymbol{H})$ cannot be reduced any more. The new basis and the unimodular matrix are initialized as $\tilde{\boldsymbol{H}} = \boldsymbol{H}$ and $\boldsymbol{T} = \boldsymbol{I}_N$. In each basis update, an index pair (m, n) and an integer $\lambda_{m,n}$ are found to update $\tilde{\boldsymbol{H}}$ and $\tilde{\boldsymbol{H}}^\dagger$ as

$$\tilde{\boldsymbol{h}}_m \leftarrow \tilde{\boldsymbol{h}}_m + \lambda_{m,n}\tilde{\boldsymbol{h}}_n \qquad \text{and} \qquad \tilde{\boldsymbol{a}}_n^T \leftarrow \tilde{\boldsymbol{a}}_n^T - \lambda_{m,n}^*\tilde{\boldsymbol{a}}_m^T, \tag{42}$$

where $\tilde{\boldsymbol{h}}_m$ is the m^{th} column of $\tilde{\boldsymbol{H}}$ and $\tilde{\boldsymbol{a}}_n^T$ is the n^{th} row of $\tilde{\boldsymbol{H}}^\dagger$, and the unimodular matrix $\boldsymbol{T}$ is also updated correspondingly as $\boldsymbol{t}_m \leftarrow \boldsymbol{t}_m + \lambda_{m,n}\boldsymbol{t}_n$ [50, 87]. According to [50, 88], given the indices m and n, the integer $\lambda_{m,n}$ is chosen as

$$\lambda_{m,n} = \left\lfloor 0.5 \left(\frac{\tilde{\boldsymbol{a}}_n^T \tilde{\boldsymbol{a}}_m^*}{\|\tilde{\boldsymbol{a}}_m\|^2} - \frac{\tilde{\boldsymbol{h}}_n^{\mathcal{H}} \tilde{\boldsymbol{h}}_m}{\|\tilde{\boldsymbol{h}}_n\|^2} \right) \right\rceil \tag{43}$$

to maximize the reduction of $S(\boldsymbol{H})$, where $\lfloor \cdot \rceil$ is the rounding operator that rounds the real and imaginary parts to the nearest integers. The corresponding reduction of $S(\boldsymbol{H})$ is expressed as

$$\Delta_{m,n} = 2\|\tilde{\boldsymbol{h}}_m\|^2 \|\tilde{\boldsymbol{a}}_n^T\|^2 \left(\Re\left(\lambda_{m,n}^* \left(\frac{\tilde{\boldsymbol{a}}_n^T \tilde{\boldsymbol{a}}_m^*}{\|\tilde{\boldsymbol{a}}_m\|^2} - \frac{\tilde{\boldsymbol{h}}_n^{\mathcal{H}} \tilde{\boldsymbol{h}}_m}{\|\tilde{\boldsymbol{h}}_n\|^2} \right) \right) - |\lambda_{m,n}|^2 \right). \tag{44}$$

The algorithm continues updating the bases as in (42) until no more reduction can be made on $S(\boldsymbol{H})$, i.e., all the entries of the matrix $\boldsymbol{\Delta}$ defined in (44) are zero. However, the algorithm may stop at $\tilde{\boldsymbol{H}}$ with suboptimal $S(\boldsymbol{H})$ (a local minimum). Only when the right index pairs are chosen in the right order, can the global optimal $\tilde{\boldsymbol{H}}$ (i.e., $\tilde{\boldsymbol{H}}$ with minimum $S(\boldsymbol{H})$) be found. Thus, how to choose the index pairs to update the bases is the crucial problem of SA. As shown in [50, 87], the index pair (m, n) is chosen randomly in the lazy implementation of SA, while in the greedy implementation, $(m, n) = \arg \max_{m,n=1,\ldots,N} \Delta_{m,n}$. In the following, we propose a tree-search algorithm to choose index pairs based on the corresponding reduction in $S(\boldsymbol{H})$.

We design our implementation of SA by formulating the choice of index pairs into a spanning tree. The tree is composed of different versions of $\boldsymbol{H}$ as

(i) the tree roots at the initialization $\tilde{\boldsymbol{H}} = \boldsymbol{H}$;

(ii) the p^{th} level of the tree denotes the p^{th} basis update;

(iii) each leaf node on the p^{th} level of the tree represents a candidate of $\tilde{\boldsymbol{H}}$ after basis updating with a selected index pair of its parent and is associated with the corresponding $S(\tilde{\boldsymbol{H}})$; and

(iv) each end node with a path from the origin represents a candidate of $\tilde{\boldsymbol{H}}$ after a series of basis updates.

Thus, finding the optimal $\tilde{\boldsymbol{H}}$ in terms of $S(\tilde{\boldsymbol{H}})$ is equivalent to finding the end node with the smallest $S(\tilde{\boldsymbol{H}})$ of this spanning tree. This is a regular tree where every interior node has $N(N-1)$ children. There are many existing search strategies to go through the tree and find the optimal end node, e.g., depth-first, breadth-first, and best-first tree-search algorithms. However, we need to note that, this tree is built up by $\boldsymbol{H}$'s and thus is random. This is different from the setup of other tree-search algorithms, e.g., the sphere-decoding method [34], where the spanning tree is based on the symbol constellation and thus fixed for every $\boldsymbol{H}$. Therefore, depth-first and best-first strategies are not computationally efficient for our problem here since we even cannot predict how many levels this tree has for a given $\boldsymbol{H}$. To simplify the tree-search process, we adopt the breadth-first approach.

In the p^{th} basis update, instead of updating only one pair of basis indices as in the greedy implementation, we find the best K_c index pairs (K_c nodes with the smallest $S(\boldsymbol{H})$ at the p^{th} level of the tree), which give us at most K_c different candidates of $\tilde{\boldsymbol{H}}$, $\{\tilde{\boldsymbol{H}}_k\}_{k=1}^{K_c}$. For each candidate $\tilde{\boldsymbol{H}}_k$, we check K_ℓ children nodes (the largest K_ℓ entries in the $\boldsymbol{\Delta}_{m,n}^{(k)}$ matrix associated with the current candidate). Then from these K_cK_ℓ children nodes, we again choose the best K_c nodes with the smallest $S(\boldsymbol{H})$. In other words, we select K_c nodes on each level of the tree, which are from the K_cK_ℓ children nodes of the K_c nodes we chose in the previous level. The program stops

Table 7: The tree-search implementation for SA (using MATLAB notation).

INPUT: $\boldsymbol{H}$, K_c, K_ℓ ; OUTPUT: $\tilde{\boldsymbol{H}}$, $\boldsymbol{T}$

Initialization:
(1) $\tilde{\boldsymbol{H}} = \boldsymbol{H}$;
(2) $\boldsymbol{T} = \boldsymbol{I}_N$;
(3) Calculate $\tilde{\boldsymbol{H}}^\dagger$;
(4) Calculate $\boldsymbol{\lambda}_{m,n}$ and $\boldsymbol{\Delta}_{m,n}$ matrices as in Eqs. (43) and (44);
(5) Find K_c index pairs associated with the K_c largest value in $\boldsymbol{\Delta}$;
(6) for $k = 1 : K_c$
(7) Update $\tilde{\boldsymbol{H}}_k$, $\tilde{\boldsymbol{H}}_k^\dagger$, and $\boldsymbol{T}_k$ as in Eq. (42)
(8) Update $\boldsymbol{\lambda}_{m,n}^{(k)}$ and $\boldsymbol{\Delta}_{m,n}^{(k)}$ matrices based on Eqs. (43) and (44);
(9) end

Iteration:
(10) while there exists $\boldsymbol{\lambda}_{m,n}^{(k)} \neq 0$
(11) for $k = 1 : K_c$
(12) Find K_ℓ index pairs associated with the K_ℓ largest value in $\boldsymbol{\Delta}_{m,n}^{(k)}$;
(13) end
(14) Find K_c index pairs among $K_c K_\ell$ index pairs with the smallest $S(\boldsymbol{H})$;
(15) for $c = 1 : K_c$
(16) Update $\tilde{\boldsymbol{H}}_k$, $\tilde{\boldsymbol{H}}_k^\dagger$, and $\boldsymbol{T}_k$ as in Eq. (42);
(17) Update $\boldsymbol{\lambda}_{m,n}^{(k)}$ and $\boldsymbol{\Delta}_{m,n}^{(k)}$ matrices based on Eqs. (43) and (44);
(18) end
(19) end
(20) Find $\tilde{\boldsymbol{H}}$ with the smallest $S(\tilde{\boldsymbol{H}})$ among K_c candidates $\{\tilde{\boldsymbol{H}}_k\}_{k=1}^{K_c}$

when none of the candidates has children nodes, i.e., $\boldsymbol{\Delta}$ matrix is zero. Then, we can choose the end node with the smallest $S(\boldsymbol{H})$ as the output $\tilde{\boldsymbol{H}}$. One major advantage of SA over the LLL algorithm is that it reduces the metric $S(\boldsymbol{H})$ by $\Delta_{m,n}$ in each basis update whereas the LLL algorithm does not guarantee reduction of $od(\boldsymbol{H})$.

Specifically, if $K_c = K_\ell = 1$, the tree-search SA becomes the greedy method [50, 87]. If $K_c = \infty$ and $K_\ell = N(N-1)$, it is the lazy implementation of SA, which is also the implementation that achieves optimal $S(\boldsymbol{H})$ [50, 87]. The detailed algorithm chart is given in Table 7. With this tree-search implementation of SA, we can adjust K_c and K_ℓ according to the complexity that we can afford. The larger K_c and K_ℓ are,

the higher is the probability that the global optimal $\tilde{\boldsymbol{H}}$ ($\tilde{\boldsymbol{H}}$ with the smallest $S(\tilde{\boldsymbol{H}})$) is found, while the complexity is also higher.

Different from the LLL algorithm, SA needs a fixed number of arithmetic operations in each basis update, though the number of basis updates is still random. Another difference between SA and the LLL algorithm is that SA does not require QR decomposition but needs to compute the channel matrix inverse at the preprocessing stage, while the LLL algorithm needs to compute the matrix inverse after $\tilde{\boldsymbol{H}}$ is found. As shown in Table 6, the number of basis updates needed by simplified greedy SA in [87] is less than that needed by the CLLL algorithm and even CLLL with SQRD, in both average and standard deviation. However, the number of arithmetic operations needed by SA in each basis update ($16M + 104N - 90$) is far more than that of the CLLL algorithm (at most $(28M+46N+6)$ even if δ condition is violated), which leads to higher algorithm complexity. Another major drawback of SA is that it requires more memory storage during the updating process.

The analysis on the final condition ($\lambda_{mn} = 0$) reveals that for any two-dimensional (2-D) lattice, Seysen's reduced basis is the same as the Gaussian reduced basis (up to signs).

Proposition 6 *For any 2-D lattice, Seysen's reduced basis is the same as the Gaussian reduced basis (up to signs).*

Proof: See Appendix H.

Because SA and the Gaussian algorithm yield the same reduced basis, the same performance can be expected in a 2x2 MIMO communication system. Furthermore, for a 2-D lattice, the following results on the output matrices of SA is obtained.

Proposition 7 *For any 2-D lattice, Seysen's reduced basis is the same as the Gaussian reduced basis (up to signs). Furthermore, for a 2-D lattice, Seysen's metric of a Seysen reduced basis is upper bounded by* $\frac{8}{3}$ *if the lattice is real, and by* 4 *if the lattice*

is complex.

Proof: See Appendix I.

Because SA and the Gaussian reduction algorithm yield the same reduced basis, the same performance can be expected for applications (e.g., for 2x2 MIMO communication systems). Furthermore, the bounds in Proposition 7 guarantee the resulting basis is within a certain distance from orthogonality, which may be applied to further quantify the performance of applications of SA (e.g., diversity in MIMO communication systems). According to Proposition 4, we know the output matrices of SA also has an upper bound on $od(\boldsymbol{H})$ for 2-D lattices. In general, there is no theoretical result on whether the Seysen's metric is also upper bounded for N-D lattices with $N > 2$. However, the complementary cumulative distribution function (CCDF) of $S(\boldsymbol{H})$ of the output matrices of SA obtained in simulations shows the existence of a finite upper bound.

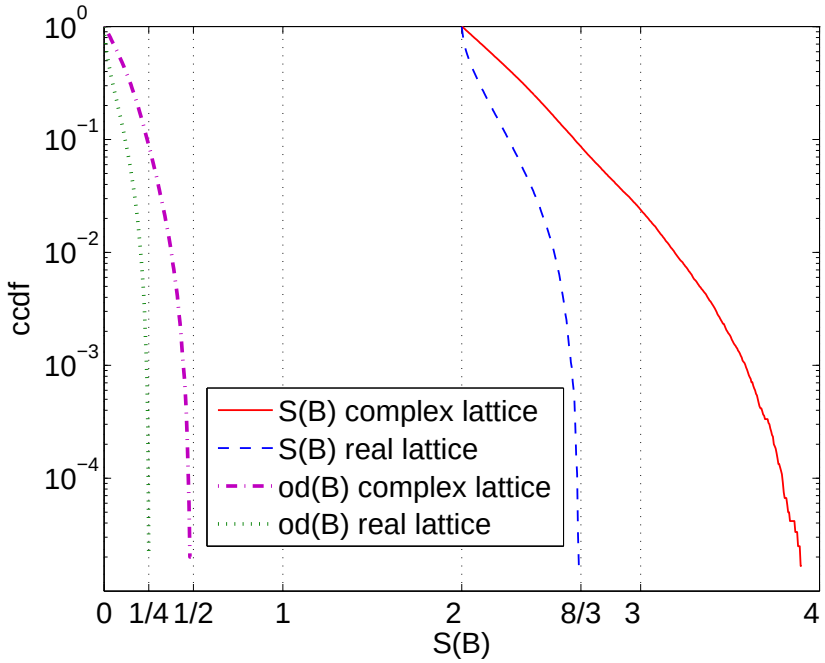

Figure 21: CCDF of $S(\boldsymbol{B})$ and $od(\boldsymbol{B})$ after SA for real and complex lattices

Figure 21 serves as a numerical verification for Proposition 7. The CCDF after LR is plotted. The real (complex) 2×2 lattice basis matrix $\boldsymbol{B}$ used in the simulation has i.i.d. real (complex) Gaussian distributed entries. It can be observed that $S(\boldsymbol{B})$ is bounded by $\frac{8}{3}$ and 4, respectively.

However, for N-D lattices with $N > 2$, the situation is not clear. Here, we numerically show that $S(\tilde{\boldsymbol{H}})$ also has a finite upper bound even with the greedy SA. When K_c and K_ℓ are greater than 1, the $S(\tilde{\boldsymbol{H}})$ of the output matrices is further reduced compared with greedy SA. To facilitate visualization of the results, we transform the range of $S(\boldsymbol{H})$ from $[N, +\infty)$ to $[0, 1]$ by defining

$$S'(\boldsymbol{H}) = 1 - \frac{N}{S(\boldsymbol{H})}. \tag{45}$$

Obviously, $S'(\boldsymbol{H})$ is monotonically increasing with $S(\boldsymbol{H})$, which means that if $S(\boldsymbol{H})$ has a finite upper bound, then $S'(\boldsymbol{H})$ has an upper bound that is strictly less than 1.

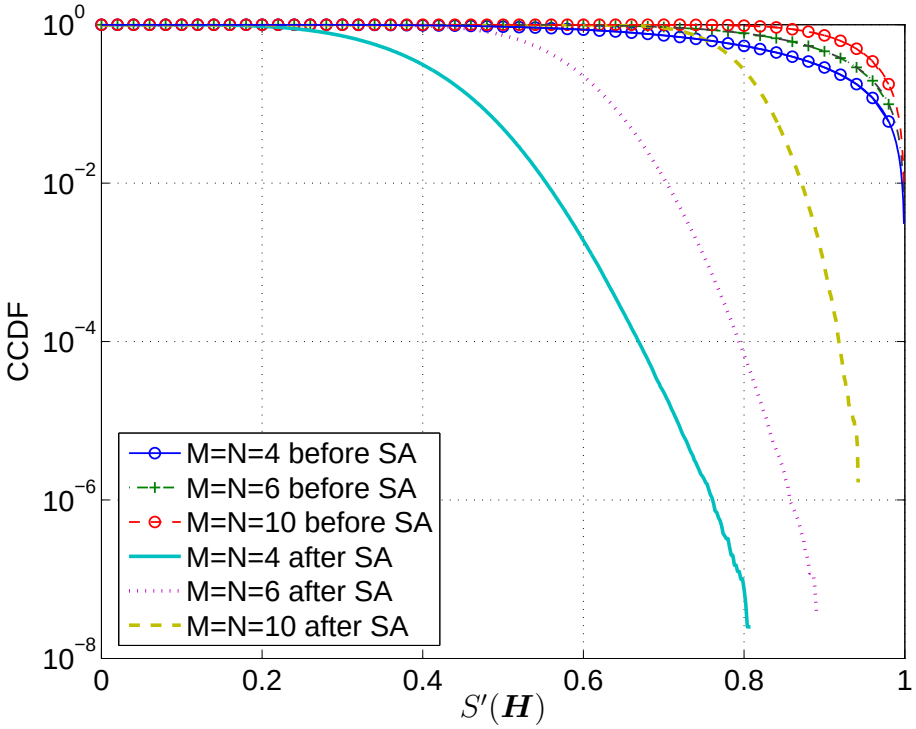

Figure 22: CCDF of $S'(\boldsymbol{H})$ and $S'(\tilde{\boldsymbol{H}})$ after SA

Test case 5.2 (Effect of SA): We consider a $N \times N$ channel matrix H whose elements are independent complex Gaussian variables with zero mean and unit variance. We simulate 10^8 channel realizations, which amount to over 60 days nonstop communications for pedestrian at 3km per hour, or 6 days nonstop communications for vehicle traveling at 30km per hour, considering IEEE 802.11g systems as an example. We plot the resulting empirical CCDF of $S'(\tilde{\boldsymbol{H}})$ for the channel matrix $\boldsymbol{H}$ and the output matrix $\tilde{\boldsymbol{H}}$ of greedy SA, i.e., $K_c = K_\ell = 1$, by fixing $M = N = 4$, 6, and 10. From Fig. 22, we see that the upper bound on $S'(\tilde{\boldsymbol{H}})$ is strictly less than 1, which means a finite upper bound for $S(\tilde{\boldsymbol{H}})$ exists. Therefore, we can consider the finite upper bound on $S(\tilde{\boldsymbol{H}})$ for practical performance analysis. Furthermore, the bound in Fig. 22 increases with N, as expected.

5.3 Other LR Algorithms

In addition to the LLL algorithm and SA, many other LR algorithms have been proposed in the literature. The Gaussian reduction [32, 125], Minkowski reduction, and Korkine-Zolotareff (KZ) reduction algorithms [46] find the optimal basis for a lattice based on the successive minimal criteria. However, the Gaussian reduction method is only for 2×2 systems and has been shown to be equivalent to SA [125]. The Minkowski and the KZ algorithms do not have polynomial time implementation and therefore infeasible for communications systems (see [121] and references therein). Furthermore, it has been shown that for LR-aided equalizers, the KZ algorithm only achieves performance similar to that of the LLL algorithm [111].

A simplified Brun's algorithm is proposed and implemented in [10] to reduce complexity but also sacrifices performance. Based on the approximation of eigenvectors of $\boldsymbol{H}$, the complexity of the simplified Brun's algorithm is even lower than the LLL algorithm. However, the performance of the simplified Brun's algorithm is much

worse than that of the LLL algorithm as shown in [10]. Furthermore, the property of resulting matrices of the Brun's algorithm is not studied analytically. Thus, whether LR-aided equalizers based on the simplified Brun's algorithm can collect the same diversity as LLL based equalizers is not clear. In next chapter, we provide the performance of LR-aided equalizers based on the simplified Brun's algorithm.

CHAPTER VI

LATTICE REDUCTION AIDED DETECTORS AT THE RECEIVER

LR algorithms find a better basis $\tilde{\boldsymbol{H}} = \boldsymbol{HT}$ that is more orthogonal than $\boldsymbol{H}$ based on different metrics. For example, the CLLL algorithm upper bounds the *od* of output matrices while SA generates a new matrix with a reduced Seysen's metric. Note that the equivalence of the two lattices spanned by $\boldsymbol{H}$ and $\tilde{\boldsymbol{H}}$ is based on the assumption that all the entries of $\boldsymbol{s}$ belong to the complex integer set. In the following, we show how to adopt LR algorithms into the wireless communication decoding process.

With the new channel matrix $\tilde{\boldsymbol{H}}$ generated by applying LR algorithms onto the channel matrix, the system model in (1) can be written as

$$\boldsymbol{y} = \boldsymbol{HT}\left(\boldsymbol{T}^{-1}\boldsymbol{s}\right) + \boldsymbol{w} = \tilde{\boldsymbol{H}}\boldsymbol{z} + \boldsymbol{w}. \tag{46}$$

Since all the entries of $\boldsymbol{T}^{-1}$ and the signal constellation belong to Gaussian integer ring, the entries of $\boldsymbol{z}$ are also Gaussian integers. Basically, LR-aided equalization is to apply traditional equalizers like LEs and DFEs onto the system model in (65) to obtain the estimate of $\boldsymbol{z}$ and then the estimate of $\boldsymbol{s}$. Furthermore, when error control codes are applied onto the system, soft-output detectors are usually adopted for iterative detection and decoding (Turbo equalization) receivers. Compared with hard-output detectors which only obtain the estimate of the transmitted signal, soft-output detectors also generate the reliability information for the estimate. In the following, we introduce the LR-aided hard-output detectors and LR-aided soft-output detectors, respectively.

6.1 Lattice-Reduction-Aided Hard-Output Detectors

Hard-output detectors are adopted to obtain the estimate of the transmitted signals, e.g, $\hat{\boldsymbol{s}}$. Depending on the traditional equalizer that is adopted to estimate $\boldsymbol{z}$, LR-aided hard-output equalizers are divided into two major categories: LR-aided LEs and LR-aided DFEs (SICs). We now provide the detailed process for these two hard-output detectors, respectively.

6.1.1 LR-aided LEs

Based on the general system model in (1), we first introduce LR-aided LEs using LR-aided ZF-LE as an example. Since the MMSE-LE agrees with the ZF-LE with respect to the extended system in (9), to perform LR-aided MMSE-LE, it is equivalent to perform LR-aided ZF-LE on the extended system. For LR-aided ZF-LE, we first apply the ZF equalizer in (7) onto the system in (65) to obtain $\hat{\boldsymbol{z}}$, the estimate of $\boldsymbol{z}$, by taking the constellation of $\boldsymbol{z}$ as the whole Gaussian integer ring. After obtaining $\hat{\boldsymbol{z}}$, we recover $\boldsymbol{s}$ by mapping $\boldsymbol{T}\hat{\boldsymbol{z}}$ to the original signal constellation. These two hard decoding steps consist of the LR-aided low-complexity equalizers for linear block transmission systems.

Note that the possible values of $\boldsymbol{z}$ are determined by the original signal constellation and the unimodular matrix $\boldsymbol{T}$. Given a specific constellation of $\boldsymbol{s}$, the actual constellation of $\boldsymbol{z}$ is random due to the randomness of $\boldsymbol{H}$. To simplify the estimation of $\boldsymbol{z}$, we assume that all the entries of $\boldsymbol{z}$ belong to Gaussian integer ring. Since $\boldsymbol{T}$ is random, the assumption is valid if the real and imaginary parts of $\boldsymbol{s}$ belong to consecutive integer sets. However, for $\mathcal{M}$-QAM symbols, the real and imaginary parts of each symbol are drawn from the set $\{-(\sqrt{\mathcal{M}}-1), \cdots, -1, 1, \cdots, \sqrt{\mathcal{M}}-1\}$, which is not a consecutive integer set. Therefore, we need to shift and/or scale the constellation to make sure the real/imaginary part of the constellation belong to a consecutive integer set. For example, by applying $(\boldsymbol{s} - (1+j)\mathbf{1})/2$, we transfer the

real and imaginary parts of the $\mathcal{M}$-QAM constellation to a consecutive integer set $\{-\sqrt{\mathcal{M}}/2, \cdots, -1, 0, 1, \cdots, (\sqrt{\mathcal{M}}-2)/2\}$, which makes the real and imaginary parts of $\boldsymbol{z}$ are also consecutive integers. Therefore, the quantization to obtain $\hat{\boldsymbol{z}}$ is now as simple as rounding to the nearest complex integer. Furthermore, the scaling and shifting operation on signal constellations must be considered when obtaining the estimate of $\boldsymbol{s}$. Using LR-aided ZF-LE as an example, the estimate $\hat{\boldsymbol{s}}$ is expressed as

$$\hat{\boldsymbol{s}} = 2\bar{\mathcal{Q}}\left(\boldsymbol{T}\left\lfloor\frac{1}{2}\left(\boldsymbol{x} - \boldsymbol{T}^{-1}(1+j)\mathbf{1}\right)\right\rceil\right) + (1+j)\mathbf{1}, \tag{47}$$

where $\boldsymbol{x} = \tilde{\boldsymbol{H}}^{\dagger}\boldsymbol{y}$ and $\bar{\mathcal{Q}}$ denotes the quantization operation that maps the real and imaginary parts to the nearest integer in the set $\{-\sqrt{\mathcal{M}}/2, \cdots, -1, 0, 1, \cdots, (\sqrt{\mathcal{M}}-2)/2\}$.

Table 8: LR-aided LEs with QAM constellations (using MATLAB notation).

INPUT: $\boldsymbol{y}, \boldsymbol{H}$ for ZF-LE $\quad (\bar{\boldsymbol{y}} = [\boldsymbol{y}; \mathbf{0}_{N\times 1}], \bar{\boldsymbol{H}} = [\boldsymbol{H}; \sigma_w \boldsymbol{I}_N]$ for MMSE-LE); OUTPUT: $\hat{\boldsymbol{s}}$;
(1) $[\tilde{\boldsymbol{H}}, \boldsymbol{T}] = \mathrm{LR}(\boldsymbol{H})$; (2) $\boldsymbol{x} = \tilde{\boldsymbol{H}}^{\dagger}\boldsymbol{y}$; (3) $\hat{\boldsymbol{x}} = (\boldsymbol{x} - \boldsymbol{T}^{-1}(1+j)\mathbf{1})/2$; (4) $\hat{\boldsymbol{z}} = \mathrm{round}(\hat{\boldsymbol{x}})$; (5) $\hat{\boldsymbol{s}} = 2\bar{\mathcal{Q}}(\boldsymbol{T}\hat{\boldsymbol{z}}) + (1+j)\mathbf{1}$;

We summarize the main steps of the LR-aided LEs for QAM signals in Table 8. The inputs are $\boldsymbol{y}$ and $\boldsymbol{H}$ for LR-aided ZF-LE, and $\bar{\boldsymbol{y}}$ and $\bar{\boldsymbol{H}}$ as in (9) for LR-aided MMSE-LE. In step (3), we manually shift and scale the original constellation to make sure that the constellation of $\boldsymbol{z}$ is in the whole complex integer set. Therefore, the estimation of $\boldsymbol{z}$ in step (4) is a simple rounding operation. The quantization operation $\bar{\mathcal{Q}}$ in step (5) is the same as the one in (47). Other constellations like PSK that belong to the Gaussian integer ring and can be transferred to consecutive integer sets through

scaling/shifting can also be adopted. The shifting and scaling operations in steps (3) and (5) need to be modified accordingly.

6.1.2 LR-aided DFEs

LR-aided DFEs (SICs) can be obtained by replacing the linear estimation of $\boldsymbol{z}$ in LR-aided LEs by the DFEs (SICs). Here, we introduce the detailed process of LR-aided ZF-DFE, while LR-aided MMSE-DFE can be obtained by applying LR-aided DFE onto the extended system in (9). For the system model in (65) obtained by applying LR algorithms onto the channel matrix $\boldsymbol{H}$, ZF-DFE with the feedforward matrix $\boldsymbol{F} = \tilde{\boldsymbol{Q}}^{\mathcal{H}}$ and the feedback matrix $\boldsymbol{B} = \tilde{\boldsymbol{R}}$ is applied to obtain the estimate of $\boldsymbol{z}$ by assuming the constellation of $\boldsymbol{z}$ to be the whole complex integer set. $\tilde{\boldsymbol{Q}}$ and $\tilde{\boldsymbol{R}}$ are the QR decomposition of the new channel matrix $\tilde{\boldsymbol{H}}$. For readers' convenience, we summarize the equalization process of the LR-aided ZF-DFE in Table 9. Note that the quantization in step (7) is the same as the mapping operation in (47).

Table 9: LR-aided DFEs with QAM constellations (using MATLAB notation).

INPUT: $\boldsymbol{y}, \boldsymbol{H}$ for ZF-DFE $\quad (\bar{\boldsymbol{y}} = [\boldsymbol{y}; \boldsymbol{0}_{N\times 1}], \bar{\boldsymbol{H}} = [\boldsymbol{H}; \sigma_w \boldsymbol{I}_N]$ for MMSE-DFE);
OUTPUT: $\hat{\boldsymbol{s}}$;

(1) $[\tilde{\boldsymbol{Q}}, \tilde{\boldsymbol{R}}, \boldsymbol{T}] = \mathrm{LR}(\boldsymbol{H})$;
(2) $\boldsymbol{x} = \tilde{\boldsymbol{Q}}^{\mathcal{H}} \boldsymbol{y}$;
(3) $\hat{\boldsymbol{x}} = \left(\boldsymbol{x} - \tilde{\boldsymbol{R}}\boldsymbol{T}^{-1}(1+j)\boldsymbol{1}\right)/2$;
(4) for $\quad n = N : (-1) : 1$
(5) $\qquad \hat{z}(n) = \lfloor (\hat{x}(n) - \sum_{k=n+1}^{N} \tilde{\boldsymbol{R}}(n,k)\hat{z}(k))/\tilde{\boldsymbol{R}}(n,n) \rceil$;
(6) end
(7) $\hat{\boldsymbol{s}} = 2\bar{\mathcal{Q}}(\boldsymbol{T}\hat{\boldsymbol{z}}) + (1+j)\boldsymbol{1}$;

6.1.3 Dual LR-aided Equalizers

The above LR-aided equalizers apply LR algorithms onto the channel matrix $\boldsymbol{H}$ to obtain a new matrix $\tilde{\boldsymbol{H}}$, which is closer to orthogonality. However, as shown in (7), the covariance matrix of the colored noise $\boldsymbol{\eta}$ after equalization is $(\boldsymbol{H}^{\mathcal{H}}\boldsymbol{H})^{-1}$. Therefore, a more orthogonal $\boldsymbol{H}^{\dagger}$ ($(\boldsymbol{H}^{\mathcal{H}}\boldsymbol{H})^{-1}$ is more like a diagonal matrix) may lead to better performance than a more orthogonal $\boldsymbol{H}$. The dual LR-aided equalizers proposed in [52] aim to improve the orthogonality of $\boldsymbol{H}^{-1}$ and have been shown to achieve better performance than LR-aided equalizers.

Dual LR-aided equalizers apply LR algorithms onto the dual basis of the channel matrix $\left(\boldsymbol{H}^{\dagger}\right)^{\mathcal{H}}$ to obtain a new matrix $\hat{\boldsymbol{H}} = \left(\boldsymbol{H}^{\dagger}\right)^{\mathcal{H}}\boldsymbol{P}$, where $\boldsymbol{P}$ is also a unimodular matrix. Then, the linear system model in (1) can be rewritten as

$$\boldsymbol{y} = \boldsymbol{H}\left(\boldsymbol{P}^{\mathcal{H}}\right)^{-1}\boldsymbol{P}^{\mathcal{H}}\boldsymbol{s} + \boldsymbol{w} = \left(\hat{\boldsymbol{H}}^{\mathcal{H}}\right)^{\dagger}\boldsymbol{z} + \boldsymbol{w}, \tag{48}$$

Comparing to the system model of LR-aided equalizers in (65), it is straightforward to see that LR-aided equalizers can be applied onto (48) to obtain the estimate of $\boldsymbol{s}$ by replacing $\boldsymbol{T}$ with $\left(\boldsymbol{P}^{\mathcal{H}}\right)^{-1}$ and $\tilde{\boldsymbol{H}}$ with $\left(\hat{\boldsymbol{H}}^{\mathcal{H}}\right)^{\dagger}$. As shown in [52], the dual LLL (DLLL) aided equalizers achieve better performance than LLL-aided equalizers. Since the LLL algorithm focuses on the orthogonality of the input matrix, applying the LLL algorithm onto the dual basis makes $(\boldsymbol{H}^{\mathcal{H}}\boldsymbol{H})^{-1}$ more orthogonal than the one generated by applying LLL onto $\boldsymbol{H}$. However, this is not true for all LR algorithms. For example, applying SA onto the dual basis leads to the same performance as SA-aided equalizers, because SA balances the orthogonality between the original basis and the dual basis by adopting Seysen's metric as shown in (41). In the following, we compare the performance of the aforementioned (dual) LR-aided equalizers.

6.1.4 Performance Comparisons

With so many LR algorithms in the literature, it is difficult to justify which one is better in terms of performance and complexity. Therefore, it is difficult to position

SA among various LR algorithms. Here, we try to delineate the performance of the following well-known algorithms: the SA in [50], the CLLL algorithm in [66], the DLLL algorithm [53], and Brun's algorithm in [86]. We do not consider Gaussian reduction and KZ algorithms because the Gaussian reduction method is only for 2×2 matrices while the KZ algorithm has much higher complexity but only achieves a performance similar to that of the LLL algorithm [112]. Here, we need to note that the performance comparison of LR-aided equalizers with LLL and SA has been conducted in [49] and [118] for systems with small constellation (4-QAM) and small channel matrix size (e.g., 6×6). In the following, we put more emphasis on systems with large channel matrix and higher constellation (e.g., 64-QAM).

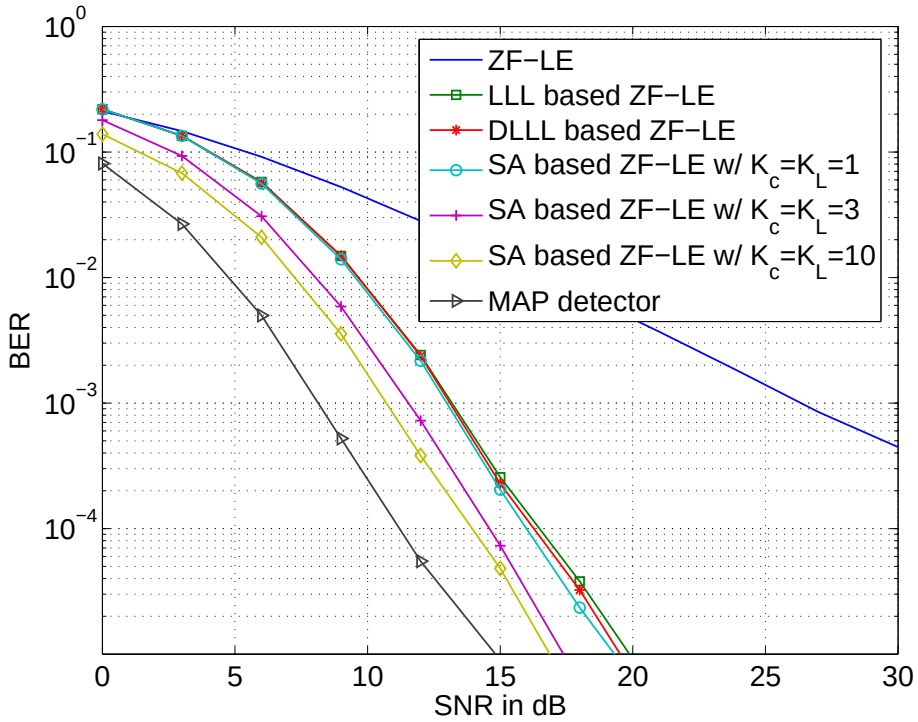

Figure 23: Performance comparisons for uncoded 4×4 systems with QPSK

Test case 6.1: In this example, we verify the performance of the proposed SA based detectors for i.i.d. channels with $M = N = 4$ and QPSK modulation. Here, we do not apply any error control codes. Seven detectors are employed on model (1): ZF,

LR-aided ZF hard detectors based on the CLLL algorithm, DLLL algorithm, and SA with $K_c = K_\ell = 1$, $K_c = K_\ell = 3$, and $K_c = K_\ell = 10$, and the MAP detector. The bit-error rate (BER) versus SNR performance is obtained by simulating 10^6 channels and is depicted in Fig. 23. It shows that all the LR-aided equalizers achieve diversity 4. Furthermore, we observe that, increasing $K_c = K_\ell$ from 1 to 10 also improves the performance at the cost of higher complexity.

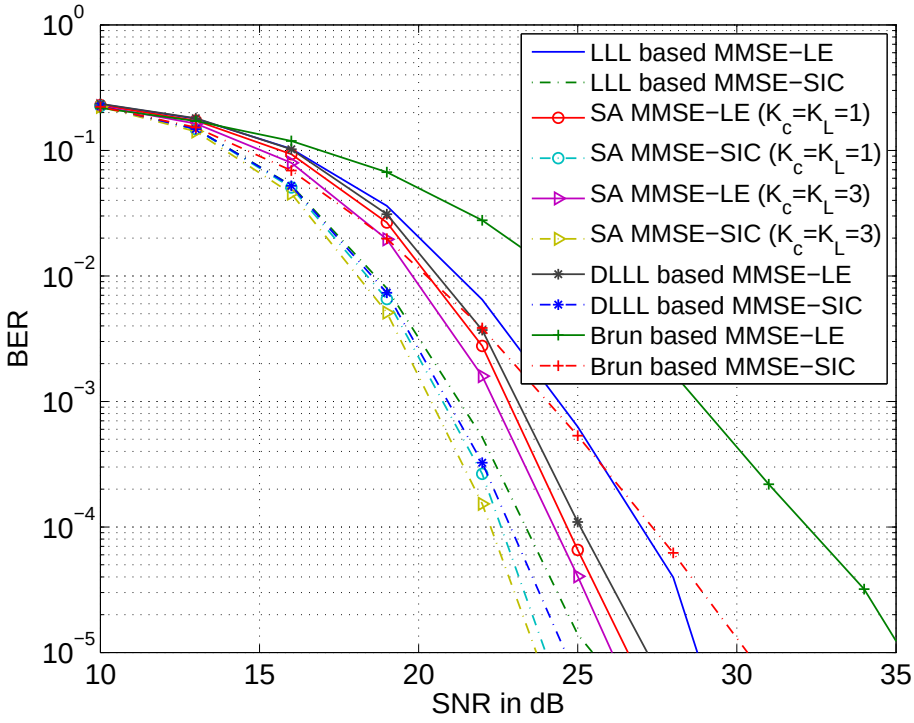

Figure 24: Performance comparisons for 8×8 systems with 64-QAM

Test case 6.2 (Performance comparison of LR-aided equalizers): We compare the BER performance of LR-aided MMSE and ordered MMSE-SIC equalizers with four different LR algorithms: the CLLL algorithm, DLLL algorithm, SA, and Brun's algorithm. SA is adopted with $K_c = K_\ell = 1$ (greedy SA) and $K_c = K_\ell = 3$. The 8×8 channel matrix $\boldsymbol{H}$ has i.i.d. zero-mean unit-variance Gaussian entries; the signal constellation was 64-QAM. Performance, averaged over 10^7 channel realizations,

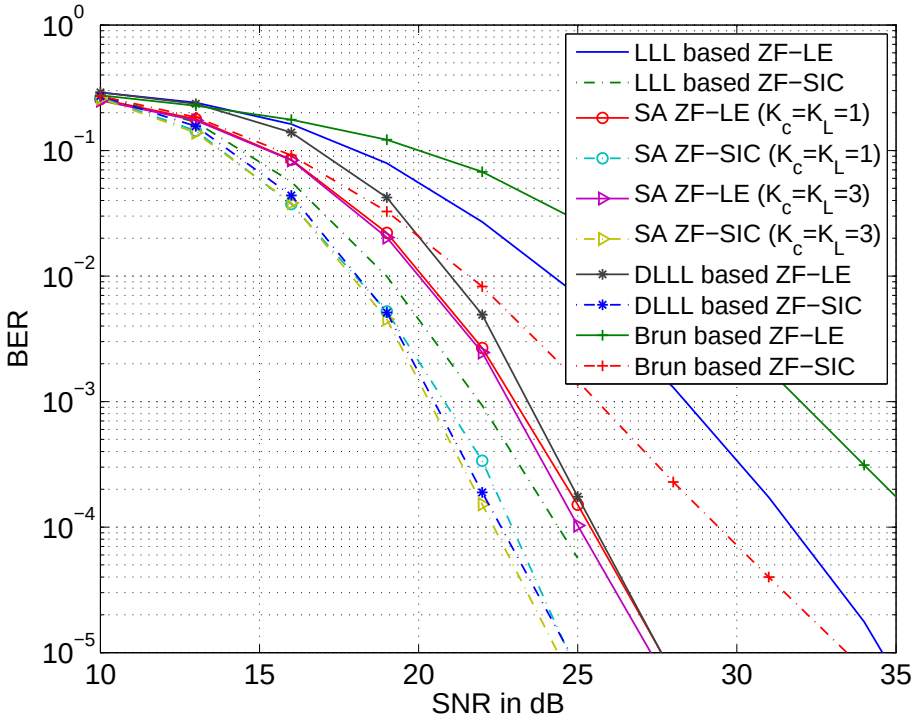

Figure 25: Performance comparisons for 50×50 systems with 64-QAM

is depicted in Fig. 24. We can see that Brun-aided equalizers have the worst performance while SA achieves the best performance among LR-aided MMSE-LEs. Among LR-aided equalizers, ordered MMSE-SICs, SA and LLL have similar performance. As stated in [49] and [118], the LLL algorithm can be easily combined with SIC ordering by employing the sorted QR decomposition (SQRD) given in [118]. Therefore, the LLL algorithm is preferable if successive interference cancelation is desired, whereas SA is preferable with direct LEs.

It has been mentioned that SA will fail if the matrix size is more than 35 [50]. However, this is based on the assumption that the lattice is an integer lattice, i.e., all the basis vectors are integer vectors. When the entries of the basis vectors are complex, such as the channel matrix $\boldsymbol{H}$ in our setup, the situation is not clear. Thus, we study the performance of SA for the challenging case of a 50×50 system with 64-QAM in Fig. 25 by simulating $50,000$ channel realizations. The figure shows

that SA-based LEs still work for high dimensional channels and achieve the best performance among the four different LR-aided LEs.

6.2 Lattice-Reduction-Aided Soft-Output Detectors

To enhance the information rate, error-control codes (ECC), e.g., Turbo codes [9] and low-density parity check (LDPC) codes [16], are concatenated in practical systems. The challenge to apply these concatenated systems is on designing a reliable but low-complexity receiver. A global optimal decoder is infeasible because of the long length of ECC. Decoupled hard detectors and decoders do not perform well (see e.g., [35]). The iterative receivers with joint detection and decoding have been well studied in the literature [35, 56, 94, 105, 134]. The key issue of iterative decoding is two-fold: i) generating a list of candidates with low complexity; ii) computing the soft information on the candidates.

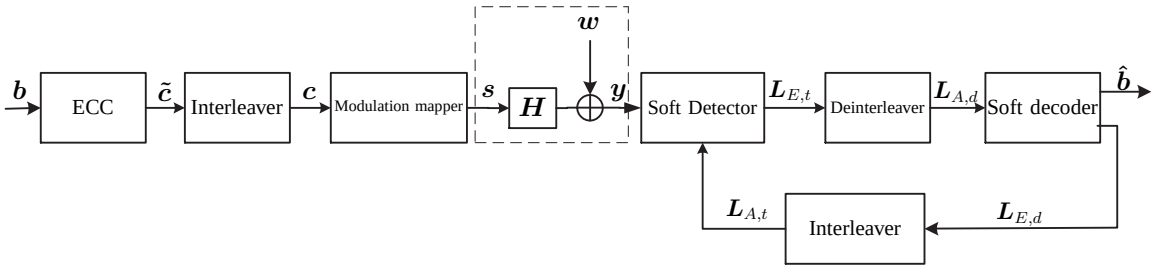

Figure 26: Block diagram of coded linear systems

Though these methods achieve near-optimal performance, their complexity is high especially when the constellation size and/or the channel dimension is high. Thus, we want to further reduce the complexity while maintaining the near-optimal performance. Similar to the case for hard detectors, we resort to the LR technique. The LR-aided soft-output detector is first proposed in [114], which consumes high complexity by applying LR on different submatrices of the channel matrix to obtain different candidates. Low complexity LR-aided soft-output detectors are developed independently by [72] and [91], and then improved in [79] by taking the covariance matrix of

the equivalent noise into consideration. [81] proposes another LR-aided soft-output detector by combining LR with the K-best method in [115]. It has also been shown that LR-aided linear equalizers with soft-decision have better coding gain [72, 79] than its hard-decoding counterpart, and can achieve near-optimal performance if the number of candidates is large enough [81, 91].

Consider a coded multiplexing transmission depicted in Fig. 26. A sequence of binary information bits $\boldsymbol{b}$ is drawn. After ECC and interleaving, the coded sequence $\boldsymbol{c}$ is mapped into a symbol sequence $\boldsymbol{s}$ where the constellation size is κ bits/symbol. Consider linear block transmissions during each channel use, the I/O relationship is the same as Eq. (1). At the receiver, iterative detection and decoding structure is adopted to exchange extrinsic information between the soft-output detector and the soft decoder of the ECC. Given the system model in (1), the extrinsic information is calculated by *a posteriori* probability (APP), which, for the i^{th} bit of $\boldsymbol{c}$, is approximated as [35, 72, 81, 91]

$$\begin{aligned} L_{E,t}(c_i \mid \boldsymbol{y}) \approx\ & \frac{1}{2} \max_{\boldsymbol{c} \in \mathcal{C}_s \bigcap \mathbb{S}_{i,+1}} \left\{ -\frac{2}{\sigma_w^2} \|\boldsymbol{y} - \boldsymbol{H}\boldsymbol{s}\|^2 + \boldsymbol{c}^T \boldsymbol{L}_{A,t} - L_{A,t}(c_i) \right\} \\ & - \frac{1}{2} \max_{\boldsymbol{c} \in \mathcal{C}_s \bigcap \mathbb{S}_{i,-1}} \left\{ -\frac{2}{\sigma_w^2} \|\boldsymbol{y} - \boldsymbol{H}\boldsymbol{s}\|^2 + \boldsymbol{c}^T \boldsymbol{L}_{A,t} + L_{A,t}(c_i) \right\}, \end{aligned} \tag{49}$$

where $\mathbb{S}_{i,+1}$ represents the set of all the κN-bit-long sequences with the i^{th} bit as $+1$ and similarly defined $\mathbb{S}_{i,-1}$. Then, this new APP is passed to the soft decoder of ECC, which takes it as the priori information. Now both complexity and performance depend on the size of the candidate list $\mathcal{C}_s$. If the list of candidates is too long, the complexity is too high (near the exhaustive search), but if the list is too short, the performance will be close to the one of hard detectors. In the following, we show low-complexity algorithms to generate the lists of candidates based on the CLLL algorithm and SA, respectively.

6.2.1 CLLL-aided Soft-Output Detectors

The CLLL algorithm finds a matrix $\tilde{\boldsymbol{H}} = \boldsymbol{HT}$ that is closer to orthogonality than the original channel matrix, and the system model in (1) is rewritten as Eq. (65) with respect to $\tilde{\boldsymbol{H}}$. Then we perform the ZF equalizer $\tilde{\boldsymbol{H}}^{\dagger}$ instead of $\boldsymbol{H}^{\dagger}$ to the observation vector as

$$\boldsymbol{x} = \tilde{\boldsymbol{H}}^{\dagger}\boldsymbol{y} = \boldsymbol{T}^{-1}\boldsymbol{s} + \tilde{\boldsymbol{H}}^{\dagger}\boldsymbol{w} := \boldsymbol{z} + \boldsymbol{n}, \tag{50}$$

where $\boldsymbol{n}$ is colored noise with zero mean and variance

$$\boldsymbol{C}_{nn} = E[\boldsymbol{n}\boldsymbol{n}^{\mathcal{H}}] = \sigma_w^2 \tilde{\boldsymbol{H}}^{\dagger}(\tilde{\boldsymbol{H}}^{\dagger})^{\mathcal{H}} = \sigma_w^2 \left(\tilde{\boldsymbol{H}}^{\mathcal{H}}\tilde{\boldsymbol{H}}\right)^{-1}. \tag{51}$$

For LR-aided hard detectors, the first step is to obtain an estimate of $\boldsymbol{z}$ in (83) and then $\boldsymbol{s}$ is estimated through one-to-one mapping. This implies that to have a soft-output detector, one needs to get a candidate list of $\boldsymbol{z}$. In the following, we introduce a method which constructs a sphere in z-domain and find the candidate list of $\boldsymbol{s}$.

6.2.1.1 Fixed radius algorithm (FRA)

For the soft input $\boldsymbol{x}$ in (83), we generate a list of candidates $\mathcal{C}_z$ by finding all possible $\boldsymbol{z}$ vectors which fall into the sphere centered at $\boldsymbol{x}$ with a radius r_z, i.e.,

$$\mathcal{C}_z = \{\tilde{\boldsymbol{z}} : \|\tilde{\boldsymbol{z}} - \boldsymbol{x}\|^2 < r_z\}. \tag{52}$$

Since for LR-aided hard-output equalizers, the estimate of $\boldsymbol{z}$ is obtained by applying element-wise rounding operation onto $\boldsymbol{x}$, the criterion in (52) leads to a list which includes all candidates around the LR-aided hard-decision result. One may argue that because of the colored noise $\boldsymbol{n}$ with variance matrix in (51), finding the optimal candidate set for $\boldsymbol{z}$ in ML sense in the z-domain should be

$$\mathcal{C}'_z = \left\{\tilde{\boldsymbol{z}} : \|\tilde{\boldsymbol{z}} - \boldsymbol{x}\|^2_{\tilde{H}^{\mathcal{H}}\tilde{H}} < r_z\right\} = \left\{\tilde{\boldsymbol{z}} : (\tilde{\boldsymbol{z}} - \boldsymbol{x})^{\mathcal{H}}\tilde{\boldsymbol{H}}^{\mathcal{H}}\tilde{\boldsymbol{H}}(\tilde{\boldsymbol{z}} - \boldsymbol{x}) < r_z\right\}. \tag{53}$$

However, searching for candidate set for $\boldsymbol{z}$ based on (53) is infeasible because of the high complexity (i.e., it becomes the same as the original ML search). Furthermore,

as we have explained, $\tilde{\boldsymbol{H}}$ is more like an orthogonal matrix than the original matrix $\boldsymbol{H}$, i.e., $\tilde{\boldsymbol{H}}^{\mathcal{H}}\tilde{\boldsymbol{H}}$ is close to a diagonal matrix after LR algorithms. Therefore, we can replace $\tilde{\boldsymbol{H}}^{\mathcal{H}}\tilde{\boldsymbol{H}}$ in (53) by an identity matrix, which leads to Eq. (52). This approximation has been adopted and justified by the analysis of LR algorithms as in [67, 86]. Thus, to reduce complexity, we adopt the search criterion in (52) to find the candidate set of $\boldsymbol{z}$ vectors.

Different from the SD method in [34], the sphere here is built in the z-domain centered at LR-aided estimate instead of the s-domain centered at ZF estimate or other estimate from pre-processing. However, because of matrix $\boldsymbol{T}$, the constellation of $\boldsymbol{z}$ is not ready. Some candidates $\tilde{\boldsymbol{z}}$ on integer lattice may not generate valid candidates in s-domain. One way is to find all possible $\boldsymbol{z}$'s and then perform searching [91]. This costs high computational complexity. Since our final goal is to obtain $\boldsymbol{s}$ not $\boldsymbol{z}$ and the alphabet of $\boldsymbol{s}$ is known, instead of building $\mathcal{C}_z$ in (52), it is equivalent to finding the list of candidates on $\boldsymbol{s}$, $\mathcal{C}_s$ as:

$$\mathcal{C}_s = \{\tilde{\boldsymbol{s}} : \|\boldsymbol{T}^{-1}\tilde{\boldsymbol{s}} - \boldsymbol{x}\|^2 < r_z\}. \tag{54}$$

To solve this problem, one obvious way is to calculate this Euclidean norm for all possible vectors $\boldsymbol{s}$. However, when the vector length or the constellation size is large, the complexity is still high.

To further reduce the complexity, we perform a low-complexity list searching method. Defining the QR-decomposition of $\boldsymbol{T}^{-1}$ as $\boldsymbol{T}^{-1} = \boldsymbol{Q}_T\boldsymbol{R}_T$, we obtain

$$\|\boldsymbol{T}^{-1}\tilde{\boldsymbol{s}} - \boldsymbol{x}\|^2 = \|\boldsymbol{Q}_T^{\mathcal{H}}\boldsymbol{x} - \boldsymbol{R}_T\tilde{\boldsymbol{s}}\|^2, \tag{55}$$

where $\boldsymbol{R}_T$ is an upper triangular matrix. Starting from the bottom layer, we implement a width-first tree-search method to obtain the list of candidates. The initial radius is controlled by the signal-to-noise ratio (SNR) and the average number of candidates which we will discuss later. The procedure of the FRA method is summarized in Table 10, where the detailed tree search algorithm (from S5 to S11) can refer to

[34]. Table 10 uses the MATLAB notation (e.g., $\boldsymbol{R}_T(n,n)$ denotes the $(n,n)^{\text{th}}$ element of matrix $\boldsymbol{R}_T$, $\boldsymbol{q}(n:N)$ consists of the n^{th} to the N^{th} elements of $\boldsymbol{q}$).

FRA searches all possible candidates in the sphere. In this case the number of candidates is random, i.e., there is no restriction on the number of candidates, which may cause difficulty on hardware implementation. In the following, we introduce another method which fixes the number of nodes (or tree leaves) on each detection layer.

Table 10: Fixed radius algorithm (FRA)

Input: $\boldsymbol{y}$, $\boldsymbol{H}$, r_z; Output: $\mathcal{C}_s$	
Initialize: $\mathcal{C}_s = \varnothing$	
(1)	$[\tilde{\boldsymbol{H}},\boldsymbol{T}]$ = CLLL $(\boldsymbol{H})$;
(2)	$[\boldsymbol{Q}_T,\boldsymbol{R}_T]$ = QR decomposition $(\boldsymbol{T}^{-1})$;
(3)	$\boldsymbol{x} = \tilde{\boldsymbol{H}}^{\dagger}\boldsymbol{y}$;
(4)	$\boldsymbol{q} = \boldsymbol{Q}_T^{\mathcal{H}}\boldsymbol{x}$;
(5)	For $n = N:(-1):1$
(6)	For each partial candidate vector $\tilde{\boldsymbol{s}} \in \mathcal{C}_s$
(7)	Find symbols $u \in \mathcal{S}$ that
(8)	$\|\boldsymbol{R}_T(n:N,n:N)[u;\tilde{\boldsymbol{s}}] - \boldsymbol{q}(n:N)\|^2 < r_z$
(9)	Replace $\tilde{\boldsymbol{s}} \in \mathcal{C}_s$ with $[u;\tilde{\boldsymbol{s}}]$;
(10)	end
(11)	end

6.2.1.2 Fixed points algorithm (FPA)

Instead of searching the whole vector with a fixed radius, one may apply an element-by-element searching with a fixed number of points on each layer. The idea here is similar to the K-best SD method in [115], but to guarantee diversity, we always include the LR-aided hard-decision in the candidate list.

First, we calculate the LR-aided hard-decision estimate. Then, for each detection layer, we calculate the partial Euclidean norm as in (55) for all the children nodes of each partial candidate, and then pick up the K_p best candidates with the smallest Euclidean norm (except the hard-decision point). Given these K_p-best candidates, one may move to the next layer and find another K_p-best candidates. The detailed

algorithm is provided in Table 11, where again the conventional MATLAB notation is adopted. To further improve the performance, the ordering of the detection layers with different criteria may be taken into consideration.

Table 11: Fixed points algorithm (FPA)

Input: $\boldsymbol{y}$, $\boldsymbol{H}$, K_p; Output: $\mathcal{C}_s$
Initialize: **Dist** = zeros $(1, K_p)$; and $\mathcal{C}_s = \varnothing$
Dist records the distance between $\boldsymbol{R}_T\tilde{\boldsymbol{s}}$ and $\boldsymbol{Q}_T^{\mathcal{H}}\boldsymbol{x}$, for $\tilde{\boldsymbol{s}} \in \mathcal{C}_s$

(1) $[\tilde{\boldsymbol{H}},\boldsymbol{T}]$ = CLLL $(\boldsymbol{H})$;
(2) Hard-decision solution: $\hat{\boldsymbol{s}}_{hd}$;
(3) $[\boldsymbol{Q}_T,\boldsymbol{R}_T]$ = QR decomposition $(\boldsymbol{T}^{-1})$;
(4) $\boldsymbol{x} = \tilde{\boldsymbol{H}}^{\dagger}\boldsymbol{y}$;
(5) $\boldsymbol{q} = \boldsymbol{Q}_T^{\mathcal{H}}\boldsymbol{x}$;
(6) For $n = N : (-1) : 1$
(7) For each partial candidate vector $\tilde{\boldsymbol{s}}_i \in \mathcal{C}_s$, $i \in [1, K_p]$
(8) For each symbol $u_l \in \mathcal{S}$, $l \in [1, |\mathcal{S}|]$ except the one in $\hat{\boldsymbol{s}}_{hd}$
(9) $\boldsymbol{D}_t(i,l) = \mathbf{Dist}(i) + |\boldsymbol{q}(n) - \boldsymbol{R}_T(n, n:N)[u_l; \tilde{\boldsymbol{s}}_i]^T|^2$;
(10) end
(11) end
(12) Find the K_p minimum values in $\boldsymbol{D}_t$ and save them as **Dist**;
(13) Save the corresponding vectors $[u_l; \tilde{\boldsymbol{s}}_i]$ as $\mathcal{C}_s$;
(14) end

Note that in our FPA method the candidate obtained from hard decision is also added to the candidate list after FPA finds K_p best candidates, if it is not in the list. This is the same as LRMAP in [91] and LRLSD in [72]. Thus, the average number of candidates on $\boldsymbol{s}$ is between K_p and $K_p + 1$. Note that, the number of candidates for FPA is fixed while the size of the candidate set for FRA is random given r_z. FPA reduces the complexity and saves memory relative to FRA. However, the performance of FPA is sacrificed compared with FRA due to the local optimization to each level. In terms of memory usage, FPA is too pessimistic while FRA is too optimistic. In the following, we introduce a method which combines these two algorithms while fixing the memory usage.

6.2.1.3 *Fixed memory-usage algorithm (FMA)*

In this approach, we assume the number of the allowable memory units for each detection layer is fixed. To perform the tree search, one starts with finding the nodes that fall into a sphere centered at $\boldsymbol{x}$ with radius r_z as in (54). If the number of candidates for the current detection layer is smaller than the number of memory units, all the partial candidates are kept and carried to next level. If the number of candidate points for the current detection layer is larger than the number of allowed memory units, say K_m, we pick the K_m best candidates among them. Thus, it can be seen that FMA is a combination of FRA and FPA with fixed memory cost. Furthermore, since we still find all the nodes as in (54) when the number of candidates on the current layer is less than K_m, the performance of FMA should be better than FPA. Because some tree branches may be pruned due to fixed memory cost, we also expect FMA has worse performance than FRA. The detailed algorithms can be found in Table 12, where again the conventional MATLAB notation is adopted. Note here, the number of candidates is also random given r_z and K_m.

After generating the list of candidates $\mathcal{C}_s$ using FRA, FPA, or FMA, we now need to obtain the reliability information of the estimate from the candidate list in (49). For uncoded systems, the proposed soft-output detectors are applied as hard detectors by finding estimate in the candidate list as

$$\hat{\boldsymbol{s}} = \arg\min_{\boldsymbol{s}\in\mathcal{C}_s} \|\boldsymbol{y} - \boldsymbol{H}\boldsymbol{s}\|^2. \tag{56}$$

Because of the multiple choices in the candidate list, the performance is improved relative to the original LR-aided equalizers, while we pay extra complexity to calculate this list. In the simulation part, we will show the performance improvement by (56) and illustrate how far these soft-output detectors's performance is from the optimal one.

Table 12: Fixed memory-usage algorithm (FMA)

Input: $\boldsymbol{y}$, $\boldsymbol{H}$, r_z, K_m; Output: $\mathcal{C}_s$
Initialize: $\mathcal{C}_s = \varnothing$

(1) $[\tilde{\boldsymbol{H}},\boldsymbol{T}]$ = CLLL $(\boldsymbol{H})$;
(2) $[\boldsymbol{Q}_T,\boldsymbol{R}_T]$ = QR decomposition $(\boldsymbol{T}^{-1})$;
(3) $\boldsymbol{x} = \tilde{\boldsymbol{H}}^{\dagger}\boldsymbol{y}$;
(4) $\boldsymbol{q} = \boldsymbol{Q}_T^{\mathcal{H}}\boldsymbol{x}$;
(5) For $n = N : (-1) : 1$
(6) For each partial candidate vector $\tilde{\boldsymbol{s}} \in \mathcal{C}_s$
(7) Find symbols $u \in \mathcal{S}$ that
(8) $\|\boldsymbol{R}_T(n:N, n:N)[u; \tilde{\boldsymbol{s}}] - \boldsymbol{q}(n:N)\|^2 < r_z$
(9) Replace $\tilde{\boldsymbol{s}} \in \mathcal{C}_s$ with $[u; \tilde{\boldsymbol{s}}]$;
(10) end
(11) If $|\mathcal{C}_s| > K_m$
(12) Choose the K_m points in $\mathcal{C}_s$ with shortest distance;
(13) end
(14) end

6.2.1.4 Comparisons with the existing methods

The LR-aided soft-output detector is first proposed in [114] with high complexity coming from executing LR on each $M \times (N-1)$ sub-matrix of $\boldsymbol{H}$. A low complexity LR-aided soft-output detector is then proposed in [91], which is named as LRMAP. For this method, the generation of the candidate list is based on listing all possible $\boldsymbol{z}$ vectors. Thus, the computational complexity of LRMAP is still high, and this method may be computationally infeasible to get all the candidates on $\boldsymbol{z}$ when N and κ are large. Compared with the LRMAP method in [91], it is not difficult to see that our FRA outperforms the LRMAP method in terms of both performance and complexity when we fix the number of candidates for $\boldsymbol{s}$. The reason is that the LRMAP method in [91] uses some local optimal criterion to find the list, and it needs to enumerate all possible vectors $\boldsymbol{z}$, which increases the complexity.

To reduce the complexity of the LRMAP method in [91], the so-called LRLSD method is proposed in [72]. By defining an integer matrix $\boldsymbol{D}$ whose columns are ordered nondecreasingly according to their Euclidean norms, the first L_{des} column

vectors in $\boldsymbol{T}(\hat{\boldsymbol{z}} + \boldsymbol{D})$ with all the entries belonging to the original constellation $\mathcal{S}$ are taken as the candidates. Since the LRLSD method does not need to generate $\boldsymbol{Z}$, the complexity is greatly reduced. The major problem of [72] is that the list of candidates for $\boldsymbol{z}$ may have a large size (depends on the maximum value of $\boldsymbol{T}$). Even if the desired set of candidates $\mathcal{C}_s$ is small, the size of $\mathcal{C}_z$ in [72] can be large (the worst case can be arbitrarily large). When the number of candidates on $\boldsymbol{s}$ is small, the performance improvement of LRLSD to hard-decision LR is marginal. Furthermore, when the number of candidates on $\boldsymbol{s}$ is small, to achieve better performance, we may consider ordering the columns of the $\boldsymbol{D}$ matrix in [72, Eq. (7)] according to the quantization error of each entry of $\boldsymbol{x}$ and the structure of matrix $\boldsymbol{T}$, instead of ordering them in nondecreasing Euclidean norm. However, this also sacrifices the low-complexity merit.

For the two LR-aided soft-output detectors in [79], the first one is similar to [72], and the second one considers the covariance matrix of the noise after LR equalization ($\boldsymbol{\eta}$ in (83)), which increases the complexity to search for the candidates. [81] also combines LR with K-best algorithm to search on the z-domain, which requires higher complexity than our FPA and may lose diversity over certain channels.

Our FPA method is similar to the K-best lattice decoding method in [115]. However, our method guarantees the same diversity as that of LR-aided equalizers (the same as ML equalizer enabled for i.i.d. channels), while K-best lattice decoding method in [115] cannot especially when K is small, because it starts from the original ZF, MMSE, or DFE solution. Therefore, with comparable complexity, our method achieves better performance.

6.2.1.5 Choosing the sphere radius

The sphere radius plays an important role for FRA. When the radius is small, only a few points can be found in the sphere and the probability that the optimal one is

included is small. On the other hand, if r_z is large, the optimal estimate falls into the candidate list with high probability, but the complexity is also high. Therefore, we want to delineate the relationship between the radius and the performance. Based on the decision rule in (54), we define the difference between $\boldsymbol{x}$ and the true $\boldsymbol{z}$ as

$$\|\boldsymbol{x}-\boldsymbol{z}\|^2 = \|\boldsymbol{n}\|^2 = \boldsymbol{w}^{\mathcal{H}}(\tilde{\boldsymbol{H}}^{\dagger})^{\mathcal{H}}\tilde{\boldsymbol{H}}^{\dagger}\boldsymbol{w} := r. \tag{57}$$

According to [92, p. 96], we obtain the pdf of r as

$$f(r) = \sum_{m=1}^{M} \frac{C_m}{\sigma_w^2 \lambda_m} \exp\left(-\frac{r}{\sigma_w^2 \lambda_m}\right), \tag{58}$$

where $\lambda_m, m \in [1, M]$ are the eigenvalues of the matrix $(\tilde{\boldsymbol{H}}^{\dagger})^{\mathcal{H}}\tilde{\boldsymbol{H}}^{\dagger}$, and

$$C_m = \prod_{i=1, i\neq m}^{M} \frac{\lambda_m}{\lambda_m - \lambda_i}.$$

Because $\boldsymbol{H}$ is random with i.i.d. entries, $\lambda_m = \lambda_i$, for $m \neq i$ is zero probability and (58) holds true with probability one. Obviously, the distribution of r depends on the channel matrix $\boldsymbol{H}$ and noise variance. Now, with the distribution of r, one can determine the search radius r_z based on the probability that the optimal solution is included in the candidate list by solving $P(r \leq r_z) = \epsilon$. On the other hand, r_z can also be determined by simple trial to achieve a certain average number of candidates based on the afforded complexity, and then by integrating Eq. (58) from 0 to r_z, we can find the probability that the optimal solution is in $\mathcal{C}_s$ to predict the reliability of the performance.

6.2.1.6 Complexity comparisons

For soft-output detectors, adjusting the number of candidates can achieve the tradeoff between performance and complexity. Generally, increasing the number of candidates improves the performance while also increasing the computational complexity. Thus, when comparing the complexity of different equalizers, we fix the number of candidates for $\boldsymbol{s}$. However, for some soft-output detectors, e.g., the FRA and FMA, the

number of candidates for $\boldsymbol{s}$ is random in a large range given the fixed searching radius. For these kinds of soft-output detectors (LRMAP, FRA and FMA), we fix the average number of candidates, while for other soft-output detectors like FPA and LRLSD in [72], the number of candidates on $\boldsymbol{s}$ is deterministic.

Table 13: Average numbers of operations for one transmission block with 4 symbols

Candidates	LR-ZF	FRA	FPA	FMA	LRMAP [91]	LRLSD [72]	MAP
3	2152	7396	6301	6745	29056	3809	98312
4	2152	8579	7561	8012	29995	4714	98312
5	2152	9876	8796	9236	30829	5384	98312

We list the numbers of arithmetic operations for different methods in Table 13, for which we take the complexity of LR operation into consideration and the complexity of the generation of $\boldsymbol{Z}$ if used. The results in Table 13 are found on a 4×4 i.i.d. Rayleigh fading channel with 20dB SNR and QPSK as the modulation scheme. We list the complexity by fixing the (average) number of candidates for $\boldsymbol{s}$ as $3, 4, 5$ respectively. From the table, we observe that, with the same number of candidates, among these soft-output detectors, the LRLSD method in [72] has the lowest complexity, while the performance is also low as we will confirm through the simulations in the next section. The complexity of MAP which is cited from [91], is the highest. All three proposed methods, FRA, FMA or FPA have lower complexity than LRMAP in [91]. Note that, for LRMAP in [91], the generation of the list of the candidates $\boldsymbol{Z}$ costs more complexity compared with the algorithm itself. Thus, our algorithms save a lot of complexity since they do not need to generate $\boldsymbol{Z}$. As we expected, FRA has higher complexity than FPA, and FMA has complexity in between. Furthermore, we notice, as the number of candidates increases, the complexity of all the soft-output detectors increases. Specifically, it is observed that FRA with 4 candidates has a complexity comparable with that of FPA with 5 candidates. Later, we will show that they also have similar performance. Considering the memory load of them, FPA is preferable

in this case.

6.2.2 SA-based Soft-Output Detectors

As shown in Section 5.2, SA is employed as one LR method that has been shown to have better performance than the well-documented LLL algorithm. Based on the tree-search implementation of SA in Section 5.2, we proposed following LR-aided soft-output detectors. The performance-complexity tradeoff of our proposed algorithms will also be studied.

[K-Best tree]: As we have explained, during the process of finding the optimal $\tilde{\boldsymbol{H}}$, many candidate $\tilde{\boldsymbol{H}}$'s are found, which have higher $S(\cdot)$ than the optimal one but lower than the original one. Thus, we can utilize these already generated candidate matrices to find candidates for $\boldsymbol{s}$. We keep the final K_c candidates for $\tilde{\boldsymbol{H}}$ generated by SA instead of just the one with the smallest $S(\cdot)$. Then, for each of them, we apply LE and thus obtain K_c estimates of $\boldsymbol{s}$. We choose the distinct estimates in these K_c candidates and build a candidate list. In this way, the generation of candidates for $\boldsymbol{s}$ does not consume much extra complexity compared with that of the hard detector. Furthermore, since it is based on the tree-search implementation of SA, K_c and K_ℓ can be adjusted to balance the trade-off between complexity and performance. In the last step (i.e., upon convergence, or when the maximum number of iterations has been exceeded), one could retain many more than the best K_c channels (up to $K_c K_\ell$ channels), potentially giving rise to more candidates, if needed.

[Greedy tree]: Another way to further reduce the complexity of this LR-aided soft-output detector is to adopt the greedy implementation of SA [50, 87], which means $K_c = K_\ell = 1$ for the general implementation depicted in Fig. 7. Though $K_c = 1$ means that in every step we only find one index pair that maximizes the reduction of $S(\boldsymbol{H})$, we could record K_g matrices that the search algorithm has already generated as candidates for the optimal $\tilde{\boldsymbol{H}}$. As with the K-best tree, this leads to additional

candidates for $\boldsymbol{s}$. The complexity is lower than that of the K-Best tree method, but the expected performance is also worse. These two algorithms are summarized in Fig. 27.

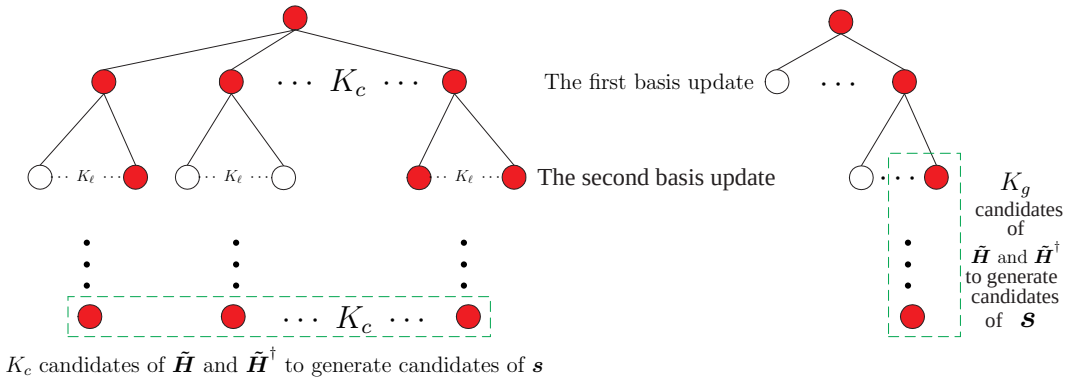

Figure 27: Diagrams of SA based soft-output detectors: (left)K-best tree (right) greedy tree

Compared with other LR-aided soft-output detectors, e.g., [72, 81, 91], our SA based soft-output detectors have several advantages. First, the extra complexity of the soft-output detectors is low, only slightly higher than that of the hard-output detector. Unlike the LR-aided maximum *a posteriori* (MAP) detector in [91], our LR-aided soft-output detector does not require generation of the $\boldsymbol{Z}$ matrix which contains all the possible points for $\boldsymbol{z}$ in (83). This leads to a large complexity advantage for our method over LR-aided MAP, though LR-aided MAP is claimed to have near-optimal performance when the number of candidates is large.

Compared with the LR-aided soft detectors in [72, 81], our proposed soft-output detector avoids the huge memory storage required for the predetermined matrix $\boldsymbol{D}$ as in [72, Eq. (7)]. Though the proposed soft-output detector may also need large memory storage to record the candidates for $\tilde{\boldsymbol{H}}$ and their pseudo-inverses, we can still control the size of the required memory by controlling the parameters K_c and K_ℓ. Second, the performance of our proposed detector is better than that of the soft-output detector in [72], especially when the number of candidates for $\boldsymbol{s}$ is small.

However, unlike the soft-output detectors in [72, 81, 91], our method may not

achieve optimal performance even when K_c, K_ℓ or K_g increase and approach infinity. This is mainly because the proposed soft detectors may not be able to list all possible candidates for the information symbols. However, the methods in [72, 81, 91] can achieve near-optimal performance only if a large number of candidates is available, which means really high complexity. Thus, for practical systems which cannot afford high complexity, our proposed soft-output detectors are preferable, since they have better performance and also lower complexity when the number of candidates is small.

6.2.3 Simulation Results

In this section, we use computer simulations to verify the performance of our proposed LR-aided soft-output detectors. In the following examples, QPSK modulation is used and SNR is defined as symbol energy versus noise power, i.e., $E[|s|^2]/\sigma_w^2$. For uncoded systems, SNR is calculated on each dimension, while for coded systems, the total transmit power is normalized to 1 as in [35]. Unless specifically stated, the linear mapper adopted here is spatial multiplexing, i.e., V-BLAST transmissions.

Test Case 6.3 (Performance comparisons of different detectors for uncoded systems): In this example, we verify the performance of FRA and FPA for i.i.d. channels with $M = N = 4$. The channel is time-invariant for one symbol period and changes independently from symbol to symbol. Here, we do not apply any ECC. Eight detectors are employed on model (1): ZF, LR-aided ZF hard detector, LR-aided soft-output detectors with FRA, FPA and FMA, LRMAP in [91], LRLSD in [72] and MAP detectors. When comparing the performance of different LR-aided soft-output detectors, we fix the (average) number of candidates of $\boldsymbol{s}$ as 3. By selecting the search radius of FRA as $r_z = 1$, and $(r_z, K_m) = (1.1, 4)$ for FMA, the average number of $\boldsymbol{s}$ candidates is approximately 3 for FRA and FMA given SNR at 18dB. $K_p = 2$ for FPA is to get almost 3 candidates including the one obtained by LR-aided

hard detector. The bit-error rate (BER) versus SNR performance is depicted in Fig. 28. It shows that all the LR-aided equalizers achieve diversity $M = 4$. However, the performance of LRLSD in [72] is quite close to the one of LR-aided hard detector since the number of total candidates for $\boldsymbol{s}$ is only 3. Furthermore, we observe that, among these soft decision methods, FRA reaches the near-optimal performance with only 7.5% complexity of MAP. If r_z, K_p and K_m are large enough, FRA, FPA and FMA reach the MAP decoder performance. An interesting observation is that FRA not only has better performance than LRMAP in [91], but also requires lower complexity as shown in Table 13.

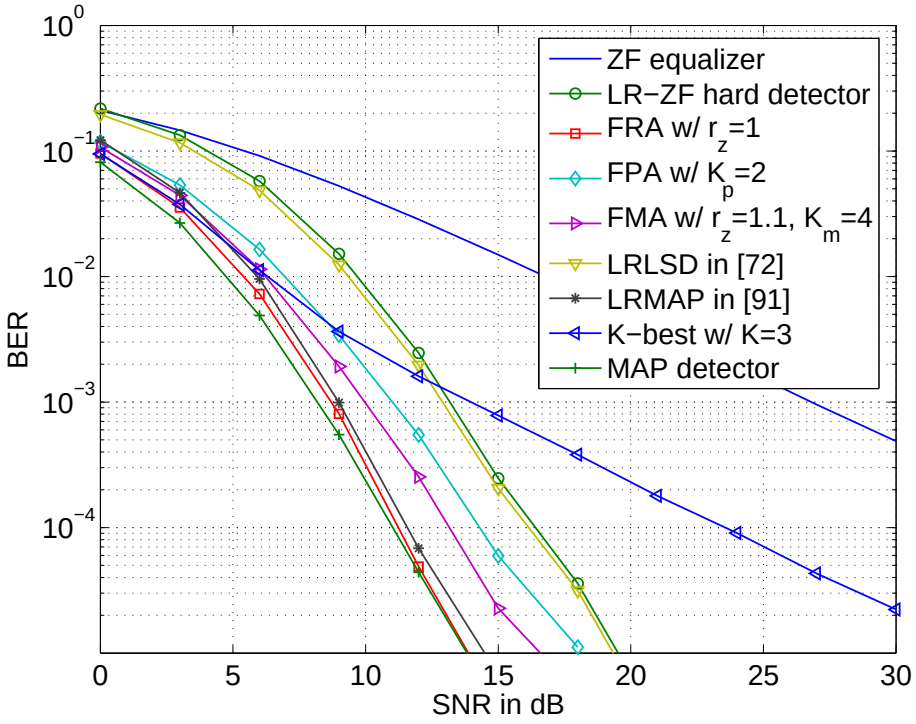

Figure 28: Performance comparisons with $M = N = 4$

One of FPA's advantages is easy to be implemented in VLSI. One natural competition for FPA is the K-Best algorithm in [115], which is a modification of the SD method to facilitate the hardware design. From Fig. 28, we notice that with 3 candidates K-best algorithm only collects diversity 1, the same as ZF equalizer. This is

because the K-Best algorithm uses the estimate of ZF as the initial point and also employs a width-first tree-search algorithm instead of the original depth-first algorithm of SD [34]. However, for our FPA, though the tree-search structure is like K-best algorithm, the diversity collected is 4, the same as the optimal one. This is because FPA includes the estimate of LR-aided ZF equalizer as one of the candidates. Thus, it guarantees the full diversity.

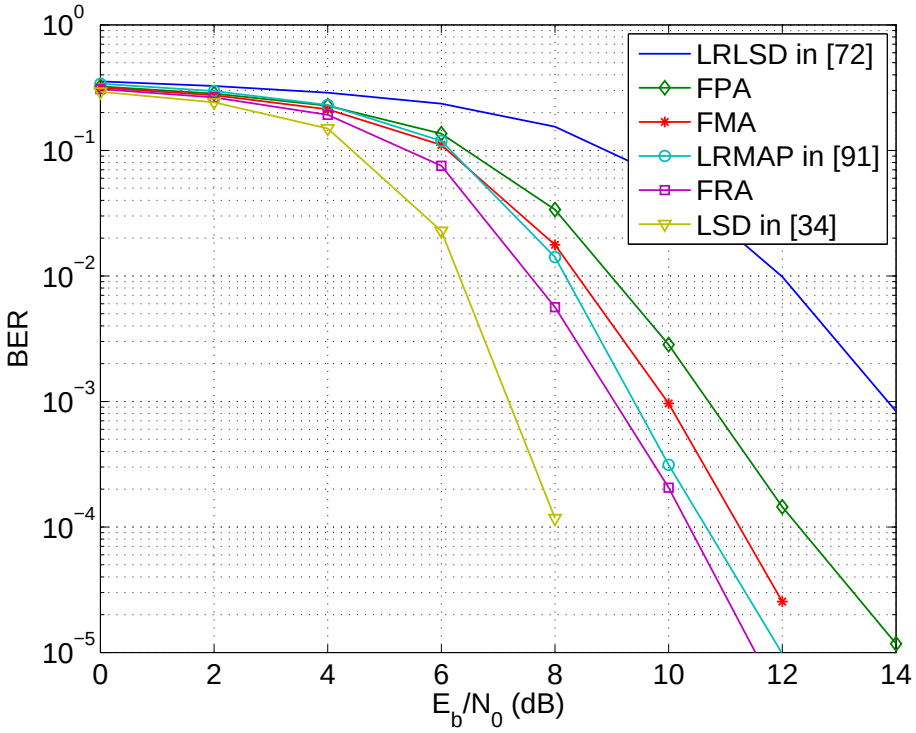

Figure 29: Performance comparisons for a coded system with $M = N = 4$

Test Case 6.4 (Performance comparisons of different detectors for coded systems): In this example, we verify the performance of FRA, FMA, and FPA with the same channel setup as the previous example but with Turbo codes. The parallel rate $\frac{1}{2}$ Turbo code is adopted with the generator $(1, \frac{1+D^2}{1+D+D^2})$. The information bit sequence is of length 1024. We employ the iterative decoder [9, 82] of Turbo code with 4 iterations as the soft decoder. Additionally, we use the method in [56] to constrain

the priori information transmitted between detector and decoder. Now we apply iterative receiver as shown in Fig. 26 with different soft-output detectors. Six detectors are employed respectively on model (1): LR-aided soft-output detectors with FRA, FPA and FMA, LRMAP in [91], LRLSD in [72] and LSD in [35]. From Fig. 29, we observe LRLSD in [72] still has the worst performance with only 3 candidates for the detector. Here we use LSD in [35] as a benchmark. The number of candidates for LSD is 3 for all SNR which requires adaptively changing the radius. We observe that among all LR-aided soft-output detectors FRA reaches the best performance with lower complexity. Compared with the performance shown in Fig. 28 for uncoded systems, the performance gap between FRA and LSD is enlarged when the Turbo code is applied onto the system. This is mainly because for FRA we fix the radius which results in the number of candidates smaller than 3 at low SNR. Adaptively adjusting the radius for FRA for different channel realizations is out of the scope of this paper.

Test Case 6.5 (Performance-complexity tradeoff for soft-output detectors): In this example, we compare the performance of FPA with different K_p in terms of performance for an uncoded 4×4 system. Here, as in many publications on tree-searching algorithms, we count the number of $\boldsymbol{s}$ candidates to represent the complexity. We plot the performance of FPA with $K_p = 2, 3, 4$ in Fig. 38, for which the number of candidates for $\boldsymbol{s}$ is 3, 4, and 5, respectively. From the figure, we observe that, as K_p increases, the performance becomes better and approaches the optimal one. Note that as shown in Table 13, when K_p is 4 (i.e., almost 5 candidates), the complexity of FPA is comparable with FRA with 4 candidates (in Fig. 28) and their performance is also comparable, but FPA is easier to be implemented by hardware with lower storage overhead.

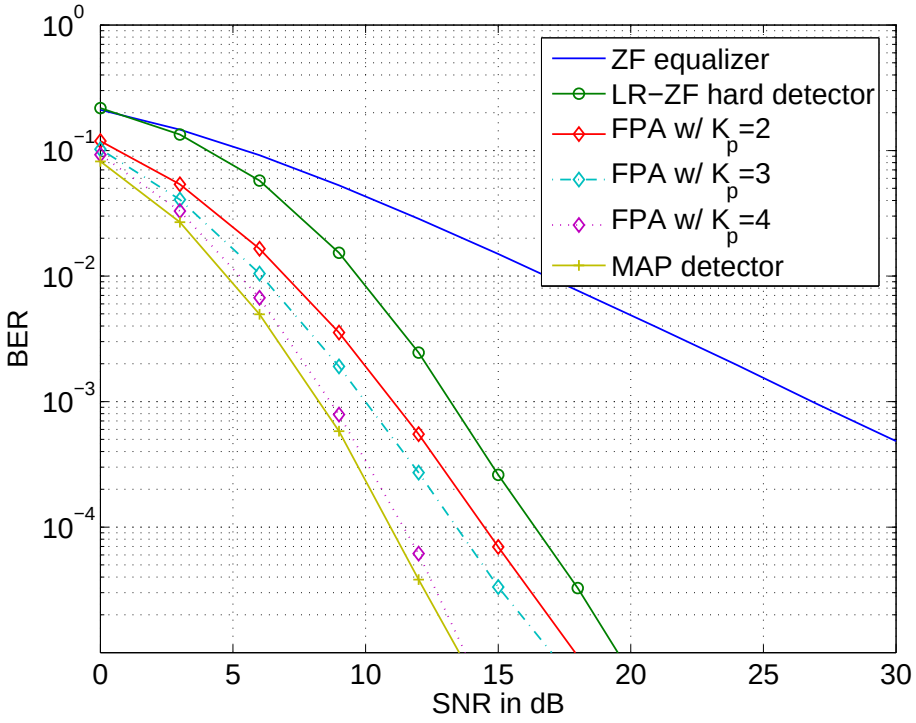

Figure 30: Performance comparison of FPA with different K_p

Test Case 6.6 (Performance comparison of different numbers of iterations for soft-output detectors): We adopt a Turbo coded 4×4 system with iterative receivers to show the effect of the number of iterations in the receiver. The performance of LR-aided soft-output detector with FRA algorithm is plotted in Fig. 31, with 1, 2, and 3 iterations at the receiver respectively. From the figure, we observe that, as the number of iterations increases, the performance becomes better. However, if we keep increasing the number of iterations, the performance improvement becomes marginal. We plot the performance of FRA, FPA, and FMA with 1 and 3 iterations respectively in Fig. 32. The performance improvement of FPA and FMA from one iteration to three iterations is not as big as that of FRA.

Test Case 6.7 (Performance comparisons of soft-output detectors for uncoded systems): Here, we verify the performance of the proposed SA based soft-output detectors for i.i.d. channels with $M = N = 4$. Here, we do not apply any

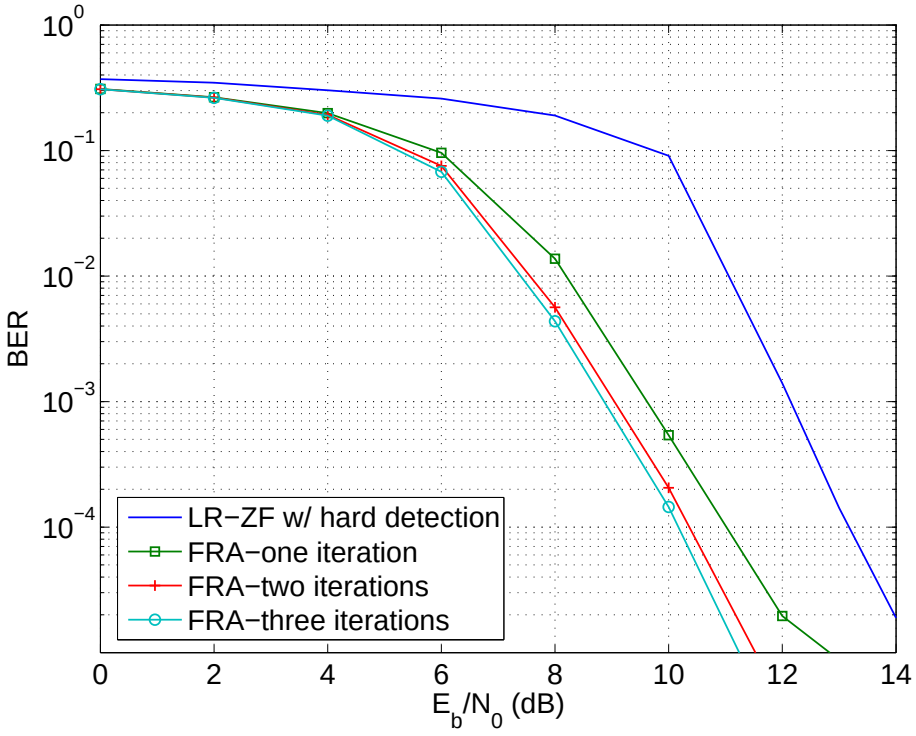

Figure 31: Performance of FRA with different numbers of iterations

error control codes. Thus, the soft-output detector output is

$$\hat{\boldsymbol{s}} = \arg \min_{\boldsymbol{s} \in \mathcal{C}_s} \|\boldsymbol{y} - \boldsymbol{H}\boldsymbol{s}\|^2. \tag{59}$$

Because of the multiple choices in the candidate list $\mathcal{C}_s$, the performance is improved relative to that of the original LR-aided hard detectors, while we pay extra complexity to calculate this list. Six detectors are employed on model (1): LR-aided ZF-LE based on SA with $K_c = K_\ell = 1$, LR-aided soft-output detectors based on greedy SA with $K_g = 3$, SA based soft-output detectors with $K_c = K_\ell = 3$ and $K_c = K_\ell = 10$, LRLSD in [72] and LRMAP in [91]. For the LRLSD detector in [72], we fix the average number of candidates of $\boldsymbol{s}$ at 3 when $SNR = 20$dB. The number of candidates generated for the SA based soft-output detectors is small. For example, the average number of candidates is approximately 1.5 for greedy soft SA with $K_g = 3$. The bit-error rate (BER) versus SNR performance was obtained by simulating more than 10^6 channels

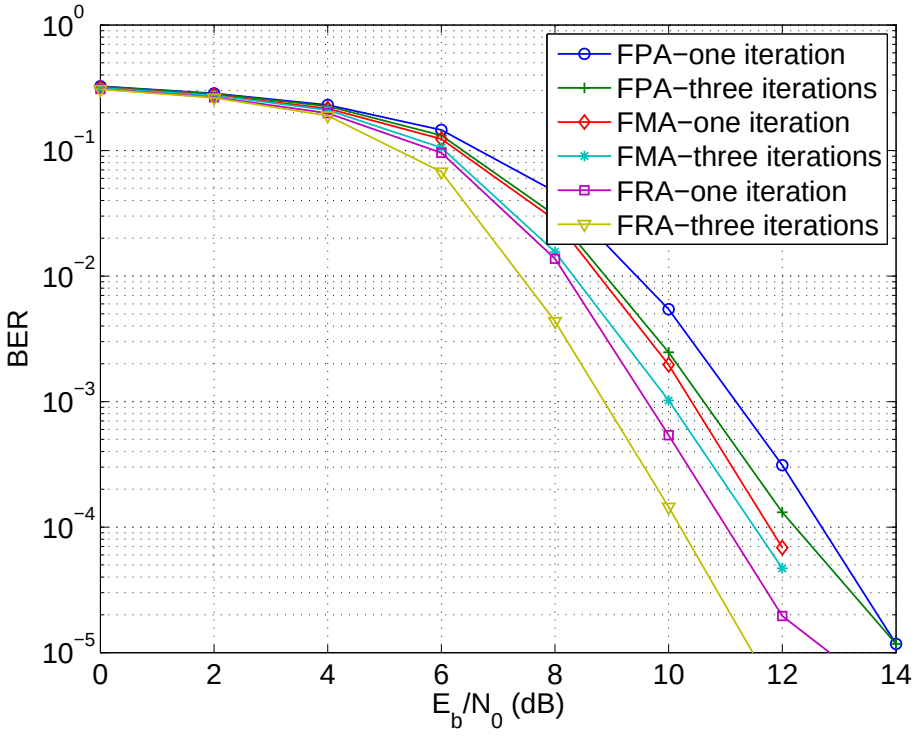

Figure 32: Performance comparisons of FRA, FPA, and FMA with different numbers of iterations

and is depicted in Fig. 33 for 4×4 systems. It shows that all the LR-aided soft-output detectors achieve the maximum possible diversity order $M = 4$. The performance of LRLSD in [72] is quite close to that of the SA based hard detector, while LRMAP in [91] has the best performance.

Test Case 6.8 (Performance comparisons of soft-output detectors for coded systems): In this example, we verify the performance of the proposed LR-aided soft-output detectors based on SA for 4×4 systems. The channel setup is the same as in the previous example but with Turbo codes. The parallel Turbo code is rate $\frac{1}{2}$ with the generator $(1, \frac{1+D^2}{1+D+D^2})$. The information bit sequence is of length 1024. We employ the iterative decoder of Turbo code with 4 iterations as the soft decoder. The extrinsic information is calculated as in (49) at the detector during each iteration.

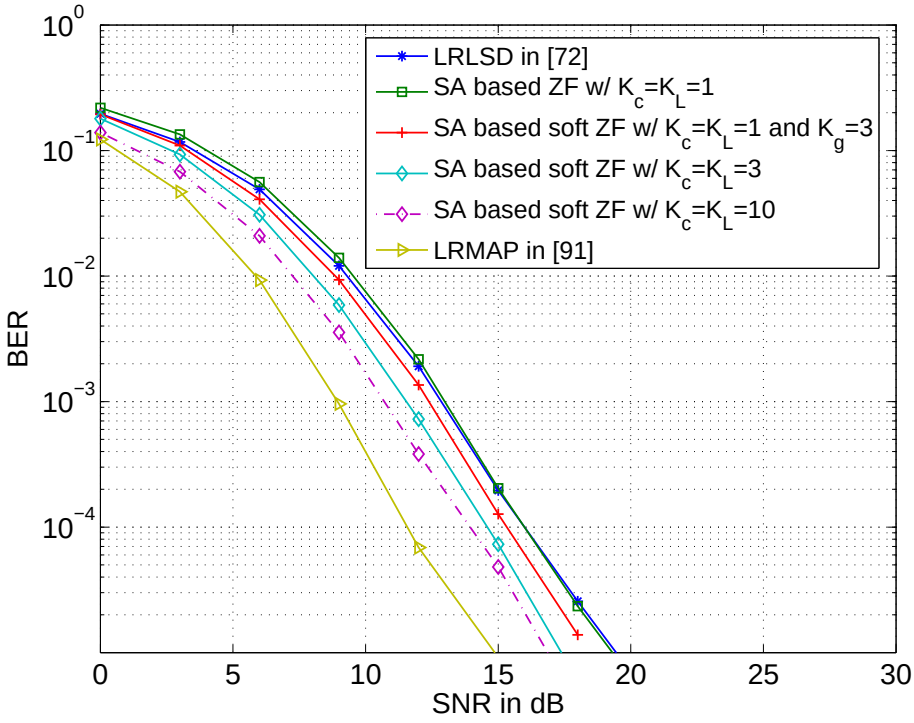

Figure 33: Performance comparisons for soft-output detectors for uncoded 4×4 systems with QPSK

Four detectors are employed on model (1): linear ZF equalizer, LRLSD in [72], LR-aided soft-output detectors based on greedy SA with $K_g = 3$, and LRMAP in [91]. We also fix the average number of candidates of $\boldsymbol{s}$ at 3 for LRLSD and LRMAP, while the average number of candidates for greedy SA soft-output detector is less than 3. As shown in Fig. 34, LRLSD in [72] still has the worst performance, the same as that for uncoded systems. Furthermore, we observe that, with fewer number of basis updates and fewer candidates, the LR-aided soft-output detector based on greedy SA is better than LRLSD in [72], while LRMAP in [91] has the best performance and much higher complexity.

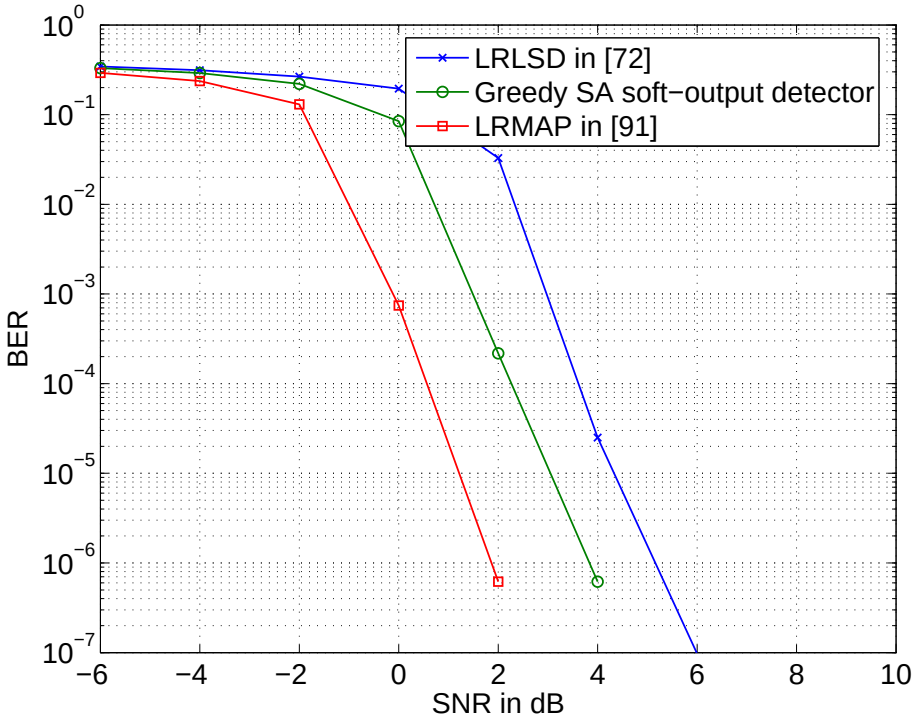

Figure 34: Performance comparisons for coded systems with $M = N = 4$

6.3 Performance Analysis of Lattice-Reduction-Aided Detectors

In this section, we analyze the performance of the proposed LR-aided equalizers in terms of error probability, mutual information, and complexity.

6.3.1 Probability of Errors

To our best knowledge, the performance of LR-aided equalizers has been analyzed only when the LLL algorithm is adopted as the LR method. SA-aided equalizers have also been discussed following similar procedures of LLL-aided low-complexity equalizers. The performance of LR-aided equalizers with other LR methods, e.g., the KZ and Brun's algorithms, has not been studied theoretically, since the property of output matrices of these LR methods has not been quantified yet. In the following, we give the results on the performance analysis of LR-aided equalizers with the LLL

algorithm and SA as LR methods.

6.3.1.1 LR-aided hard-output detectors

With the result in Proposition 5, we analyze the performance of LLL-aided equalizers for different transmission systems. We summarize the results for i.i.d. channels in the following proposition.

Proposition 8 *Given the model in* (1)*, if the channels are i.i.d. complex Gaussian distributed, the diversity order collected by an LR-aided LE (LR-aided ZF or LR-aided MMSE) is N, which is the same as that achieved by the ML detector.*

Proof: See Appendix J.

Similarly, for LR-aided MMSE equalizer, we can show that it also collects diversity M. As we have shown in [67], the linear equalizers can only collect diversity $M-N+1$ for V-BLAST transmissions. However, after introducing LR technique into the linear equalization process, the maximum diversity is recovered for V-BLAST systems. This confirms that the LR technique brings the performance curves of the linear equalizers parallel to that of MLE.

The performance of LLL-aided equalizers for LP-OFDM system in [57] is given in the following proposition.

Proposition 9 *For the LP-OFDM system in [57] with group size K and frequency-selective channel order L with channel correlation matrix with rank ($\rho_h \leq L+1$), the diversity order collected by the LR-aided LEs is* $\min(K, \rho_h)$ *which is the same as that obtained by the (near-) MLEs.*

Proof: See Appendix K.

As we have shown in [69], LEs cannot exploit any multipath diversity for LP-OFDM systems. However, after introducing the LR technique into the linear equalization process, multipath diversity is collected. Similarly, one can show that the

LR-aided MMSE equalizer also collects full multipath diversity. Furthermore, since DFEs (SICs) achieve better performance than that of LEs, LR-aided DFEs are expected to achieve the same diversity as (near-) MLEs for these two transmission systems.

Example 6.1 (LR-aided equalizers for i.i.d. channels): We verify Proposition 8 by plotting BER curves of different equalizers for i.i.d. channels with $(M, N) = (4, 3)$ and QPSK in Figure 35. We notice that the linear detectors can only achieve diversity order $M - N + 1$, which is 2 in this case. The MLE collects diversity $M = 4$. As expected, the LR-aided linear detectors achieve the same diversity order as the MLE does. However, there still exist performance gaps between LR-aided equalizers and the MLE.

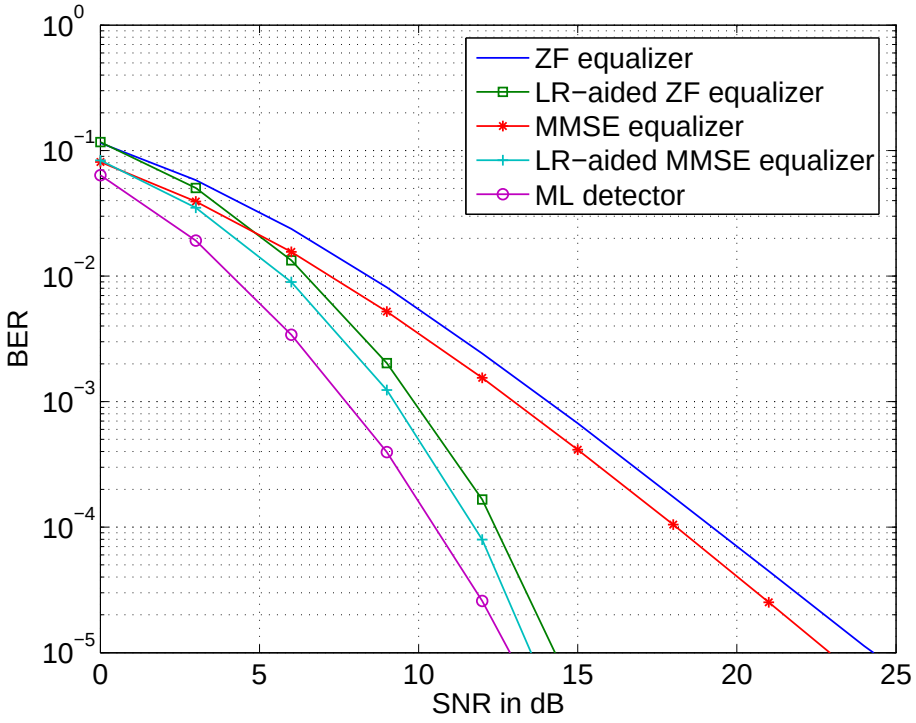

Figure 35: Performance of i.i.d. channels with $(M, N) = (4, 3)$ and QPSK modulation

Example 6.2 (LR-aided equalizers for LP-OFDM): To verify the performance for LP-OFDM systems, we fix the channel order of frequency-selective channel as $L =$

3, and the number of subcarriers $N_c = 64$. The channel taps are independent complex Gaussian random variables with zero mean and variance $\frac{1}{L+1}$. The subcarriers are split into $N_g = 16$ groups with size $K = 4$. Figure 36 shows the BER performance of LR-aided ZF, MMSE, ZF-DFE, MMSE-DFE, and MLE. From this figure, we observe that LR-aided equalizers collect diversity order $L + 1$, as does the MLE, although there still exists a gap between the performance of the LR-aided equalizers and the MLE. The performance of the LR-aided MMSE-DFE equalizer is better than that of the LR-aided ZF equalizer, ZF-DFE, and MMSE.

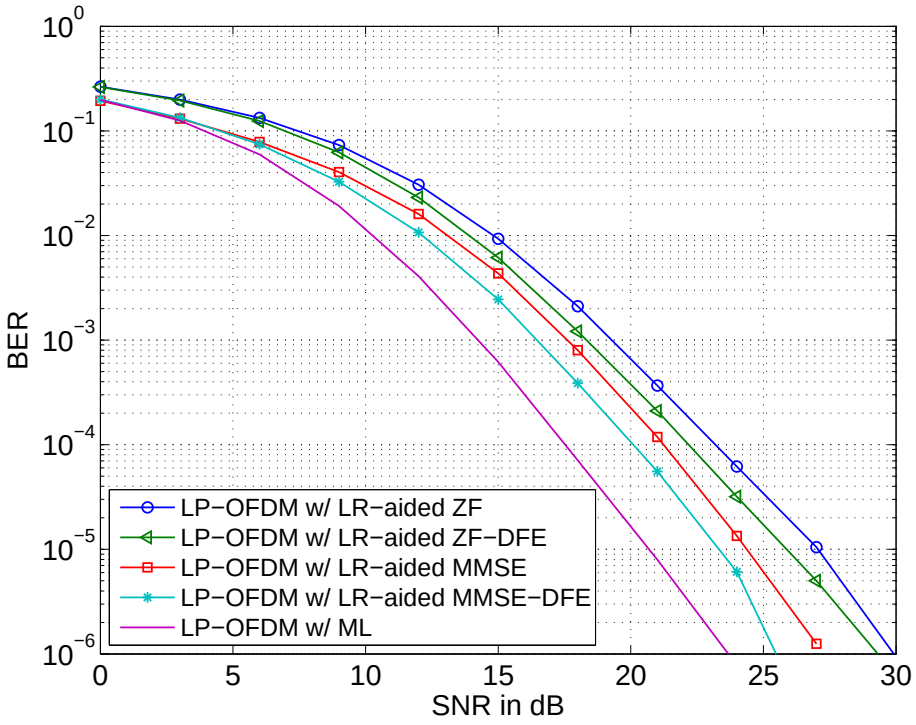

Figure 36: Comparisons among different LR-aided equalizers for LP-OFDM with QPSK modulation

Similar to the LLL algorithm, if SA upper bounds the output $S(\tilde{\boldsymbol{H}})$ by a finite constant, it can be easily proved that SA-aided low-complexity equalizers collect the same diversity as MLE does as Propositions 12 and 9. For 2×2 systems, Proposition 7 shows that SA upper bounds the Seysen's metric of the output matrix $\tilde{\boldsymbol{H}}$ by a finite number. For an N-D lattice, the simulation results show the existence of a

finite upper bound, but it is not theoretically proved yet. However, according to the simulation results in [87] and our own simulation experience, SA-aided equalizers collect the same diversity as LLL-aided equalizers for many transmission systems.

6.3.1.2 LR-aided soft-output detectors

We now analyze the BER performance of our three LR-aided soft-output detectors in a coded system. Suppose $\boldsymbol{c}^{(1)}$ is the transmitted codeword generated by the original information bits. At the receiver, it is erroneously detected and decoded to a different information sequence. These two bit sequences are different in d_e positions. Because of the interleaver between ECC and linear mapping, which is random for every codeword, these d_e errors are sufficiently far from each other. Furthermore, usually an interleaver is added just before the transmission to decorrelate the channels and make the channel vary fast enough. Based on these assumptions, we suppose that for each transmitted symbol vector of this codeword $\boldsymbol{c}^{(1)}$, i.e., $\boldsymbol{s}^{(1)}(k)$, has at most one entry different from the detected block, where $k \in [1, M_c]$ with M_c being the number of transmission blocks for one codeword.

Without loss of generality, we assume the blocks that have an error are $\boldsymbol{s}^{(1)}(i)$ for $i \in [1, d_e]$. For each transmitted block, we use the LR-aided linear equalizer to detect the transmitted symbol vector $\boldsymbol{s}^{(1)}(i)$. Suppose $\boldsymbol{s}^{(1)}(i)$ is estimated as $\boldsymbol{s}^{(s)}(i)$ through LR-aided soft-output detectors or $\boldsymbol{s}^{(h)}(i)$ by LR-aided hard detectors. For FRA, since the hard estimate is adopted as the center point of the tree search algorithm, $\boldsymbol{s}^{(h)}(i)$ is always included in the candidate list. Furthermore, as we mentioned, for FPA and FMA algorithms, the estimate from the LR-aided hard detector is manually added to the candidates set. Thus, for the three proposed LR-aided soft-output detectors, we have

$$\|\boldsymbol{y} - \boldsymbol{H}\boldsymbol{s}^{(s)}\| \leq \|\boldsymbol{y} - \boldsymbol{H}\boldsymbol{s}^{(h)}\|. \tag{60}$$

If the ML solution is $\boldsymbol{s}^{ML}$, then

$$\|\boldsymbol{y} - \boldsymbol{H}\boldsymbol{s}^{ML}\| \leq \|\boldsymbol{y} - \boldsymbol{H}\boldsymbol{s}^{(s)}\|. \tag{61}$$

These mean that

$$P_e^{ML} \leq P_e^{(s)} \leq P_e^{(h)},$$

where P_e denotes bit error probability depending on different equalizers. Thus, the diversity order of soft-output detectors is greater than or equal to that of hard detectors but less than or equal to that of the ML detector. Furthermore, as shown in [67] and [96], the diversity order of LR-aided hard detectors for V-BLAST MIMO transmission systems is the same as that of the ML detector. Thus, for V-BLAST transmission over i.i.d. channels, the diversity order of the proposed LR-aided soft-output detectors is the same as that of the ML detector.

In summary, if the diversity of LR-aided soft-output detectors is G_d, at high SNR regime, we have

$$P\left(\boldsymbol{s}^{(1)}(i) \to \boldsymbol{s}^{(s)}(i)\right) = E_{H(i)}\{P(\boldsymbol{s}^{(1)}(i) \to \boldsymbol{s}^{(s)}(i) \mid \boldsymbol{H}(i))\} \approx c\left(\frac{1}{\sigma_w^2}\right)^{-G_d}, \tag{62}$$

where c is a constant that depends on the size and the distribution of the channel matrix $\boldsymbol{H}$. For coded case, suppose the channel matrix for each transmitted symbol vector is independent, which is enabled by the interleaver before transmission. We have the following expression on the probability that $\boldsymbol{c}^{(1)}$ is erroneously decoded as $\boldsymbol{c}^{(s)}$

$$\begin{aligned} P(\boldsymbol{c}^{(1)} \to \boldsymbol{c}^{(s)}) &= E_{H(1),H(2),\ldots,H(d_e)}\{P(\boldsymbol{c}^{(1)} \to \boldsymbol{c}^{(s)} \mid \boldsymbol{H}(1), \boldsymbol{H}(2), \ldots \boldsymbol{H}(d_e))\} \\ &= \prod_{i=1}^{d_e} E_{H(i)}\{P(\boldsymbol{s}^{(1)}(i) \to \boldsymbol{s}^{(s)}(i) \mid \boldsymbol{H}(i))\} \approx c^{d_e}\left(\frac{1}{\sigma_w^2}\right)^{-G_d d_e}. \end{aligned} \tag{63}$$

This is for the d_e errors case. Applying the union bound to all error events, we can get the average BER as (see e.g., [8, p. 514])

$$P_e \approx \sum_{d_e=d_{min}}^{M_c} c_{d_e}\left(\frac{1}{\sigma_w^2}\right)^{-G_d d_e}, \quad \text{where} \quad c_{d_e} = c^{d_e}\sum_{w=1}^{K_c}\frac{w}{K_c}B_{w,d_e}, \tag{64}$$

B_{w,d_e} is the number of error events with input sequence weight w and d_e output weight, and K_c is the number of information bits per input sequence. Define d_{min} the minimum Hamming distance of ECC. Thus, the diversity of the coded transmissions through i.i.d. channels with LR-aided soft-output detectors is at most $d_{min}G_d$. Here, we assume the channel varies fast enough. However, this is not necessarily true even when the interleaver is added before transmission. This means usually the diversity of a practical system is less than $d_{min}G_d$. One extreme case is that the channel remains the same for one codeword (M_c transmitted symbol vectors). In this case, the diversity order of this coded system is G_d, which is between that of the ML detector and that of LR-aided hard detectors. The analysis here is consistent with the one for ML detectors in [23, Chapter 10].

6.3.2 Mutual Information

Now let us analyze the effect of LR on mutual information. Since $\tilde{\boldsymbol{H}}$ is obtained after applying LR algorithms onto the channel matrix $\boldsymbol{H}$, we can rewrite the system model in (1) as

$$\boldsymbol{y} = \boldsymbol{H}\boldsymbol{T}(\boldsymbol{T}^{-1}\boldsymbol{s}) + \boldsymbol{w} = \tilde{\boldsymbol{H}}\boldsymbol{z} + \boldsymbol{w}.$$

Following the same procedure as in Section 3.2, when MLE is applied on (65) in two steps (first estimate $\boldsymbol{z}$ and then estimate $\boldsymbol{s}$), it is ready to show that

$$C_{ML}^{LR}(\boldsymbol{H}) = \log_2\left[\det\left(\boldsymbol{I}_M + \frac{1}{\sigma_w^2}\tilde{\boldsymbol{H}}\boldsymbol{R}_z\tilde{\boldsymbol{H}}^{\mathcal{H}}\right)\right] = \log_2\left[\det\left(\boldsymbol{I}_N + \frac{1}{\sigma_w^2}\boldsymbol{H}^{\mathcal{H}}\boldsymbol{H}\right)\right], \quad (65)$$

where $\boldsymbol{R}_z = E[\boldsymbol{z}\boldsymbol{z}^{\mathcal{H}}] = \boldsymbol{T}^{-1}\boldsymbol{R}_s(\boldsymbol{T}^{-1})^{\mathcal{H}}$. From this equation, we know the capacity of MLE after LR preprocessing is the same as using MLE directly. This is not surprising because LR process does not change the system model. Now let us focus on the capacity of LR-aided LEs.

Although $\mathcal{H}(\boldsymbol{s}|\boldsymbol{H})$ is the same as in (15), $\mathcal{H}(\boldsymbol{s}|\boldsymbol{x};\boldsymbol{H})$ now changes since $\hat{\boldsymbol{z}}$ is estimated from $\boldsymbol{x}$ in (83) first, and then $\boldsymbol{s}$ is decoded by mapping $\boldsymbol{T}\hat{\boldsymbol{z}}$ to the original

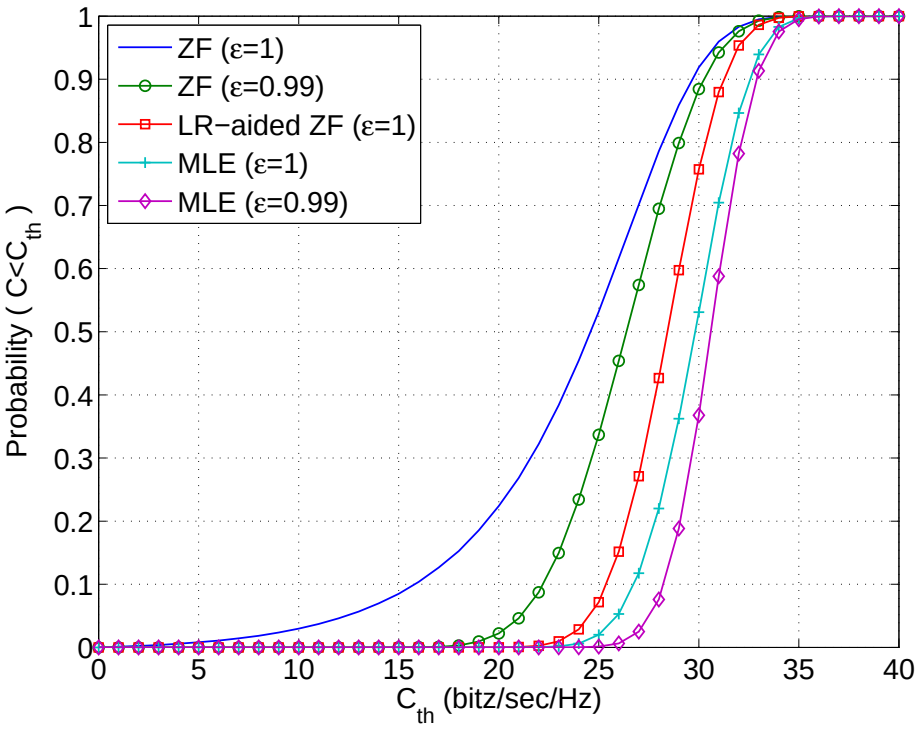

Figure 37: CDF of the capacity based on different equalizers

constellation. Thus, the covariance matrix of $\boldsymbol{s}$ given $\boldsymbol{H}$ and $\boldsymbol{x}$ in (83) is expressed as

$$\begin{aligned}\boldsymbol{R}_{s|x;H} &= \boldsymbol{T}\boldsymbol{R}_{z|x;H}\boldsymbol{T}^{\mathcal{H}} = \boldsymbol{T}\left(\boldsymbol{R}_z^{-1} + \frac{1}{\sigma_w^2}\boldsymbol{R}_\xi^{-1}\right)^{-1}\boldsymbol{T}^{\mathcal{H}} \\ &= \left((\boldsymbol{T}^{\mathcal{H}})^{-1}\boldsymbol{T}^{\mathcal{H}}\boldsymbol{R}_s^{-1}\boldsymbol{T}\boldsymbol{T}^{-1} + \frac{1}{\sigma_w^2}(\boldsymbol{T}^{\mathcal{H}})^{-1}\boldsymbol{R}_\xi^{-1}\boldsymbol{T}^{-1}\right)^{-1} \\ &= \left(\boldsymbol{R}_s^{-1} + \frac{1}{\sigma_w^2}(\boldsymbol{T}^{\mathcal{H}})^{-1}\boldsymbol{R}_\xi^{-1}\boldsymbol{T}^{-1}\right)^{-1}, \end{aligned} \tag{66}$$

where $\boldsymbol{R}_\xi = \mathrm{diag}[\tilde{C}_{1,1}, \tilde{C}_{2,2}, \ldots, \tilde{C}_{N,N}]$ is the covariance matrix of the equivalent noise vector $\boldsymbol{\xi}$ in (83), with $\tilde{C}_{i,i}$ being the $(i,i)^{\text{th}}$ entry of the matrix $\tilde{\boldsymbol{C}} = (\tilde{\boldsymbol{H}}^{\mathcal{H}}\tilde{\boldsymbol{H}})^{-1}$. As we have assumed for MLE and LEs, the information symbols $\boldsymbol{s}$ are Gaussian distributed with $\boldsymbol{R}_s = \boldsymbol{I}_N$. Thus, we obtain the instantaneous capacity of the LR-aided ZF equalizer as

$$C_{ZF}^{LR}(\boldsymbol{H}) = \log_2\left[\det\left(\boldsymbol{I}_N + \frac{1}{\sigma_w^2}(\boldsymbol{T}^{\mathcal{H}})^{-1}\boldsymbol{R}_\xi^{-1}\boldsymbol{T}^{-1}\right)\right]. \tag{67}$$

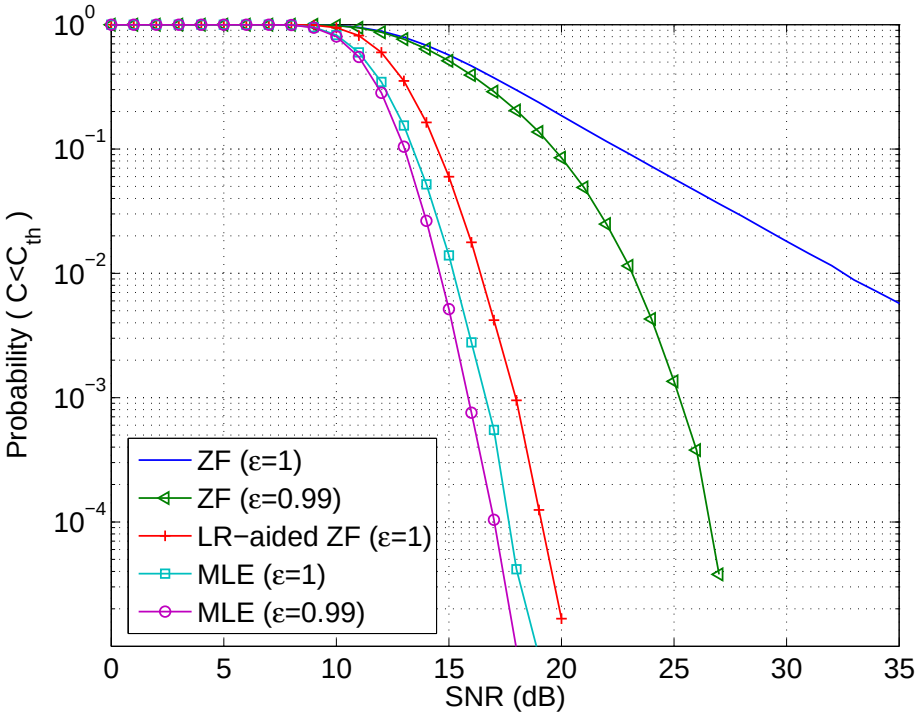

Figure 38: Outage probability vs. SNR

Similar to (20), when SNR is high, the expression in (67) can be approximated as

$$C_{ZF}^{LR}(\boldsymbol{H}) \approx \log_2 \left[\det\left(\boldsymbol{R}_{\xi}^{-1}\right)\right] - N \log_2 \sigma_w^2, \tag{68}$$

because $\det(\boldsymbol{T}^{\mathcal{H}}\boldsymbol{T}) = 1$. Since we have shown that LR preprocessing does not change the capacity when MLE is adopted at the receiver [cf. (65)], similar to (22), we have

$$C_{ZF}^{LR}(\boldsymbol{H}) \leq C_{ML}^{LR}(\boldsymbol{H}) = C_{ML}(\boldsymbol{H}). \tag{69}$$

According to Proposition 5, we know $od(\tilde{\boldsymbol{H}})$ has an upper bound $1-c_\delta^2 < 1$. With Lemma 2, Proposition 5, and Theorem 2, the outage probability of the capacity of the LR-aided ZF equalizer $P(C_{ZF}^{LR} < C_{th})$ is parallel to that of MLE. However, the original ZF equalizer does not have this property.

Example 6.3 (Mutual information of LR-aided LEs): The CDFs of the capacity with these equalizers are depicted in Fig. 37 with SNR = 20 dB for i.i.d. channels with $M = N = 4$ and different equalizers: ZF ($\epsilon = 1$ and 0.99), LR-aided ZF

and MLEs. Outage probabilities of the capacity versus SNR are plotted in Fig. 38 with $C_{th} = 20$ bits/sec/Hz. Comparing Figs. 37 and 38, we notice that (i) when $\sup(od((\boldsymbol{H}^{\dagger})^{\mathcal{H}})) = 1$ (ZF with $\epsilon = 1$ case) LE loses outage diversity (i.e., the curve of LE is not parallel with the one of MLE); this is different from the average capacity in Fig. 28; and (ii) when $od((\boldsymbol{H}^{\dagger})^{\mathcal{H}})$ has an upper bound which is less than 1 (LR-aided ZF case and ZF with $\epsilon = 0.99$ case), the outage probability curves of LEs become parallel with those of MLEs. This is consistent with Theorem 2 and our analysis in Section 3.3.

6.3.3 System Design Issues

For iterative algorithms such as the SA and the LLL algorithms, a common approach for hardware implementation is to fix the maximum number of iterations so that the algorithms are forced to stop when the number of iterations reaches this threshold. However, to make efficient usage of the hardware components, this limit cannot be too large. Thus, with a certain probability, the algorithms will be terminated before they end normally, which means performance degradation compared with the fully executed algorithms. Obviously, the number of iterations needed for the algorithms is an important criterion to quantify implementation complexity. On the other hand, the total number of arithmetic operations (real additions and real multiplications) needed for the algorithms is another important criterion to quantify algorithm complexity. After comparing the performance of different LR-aided equalizers, we focus on the complexity comparison of different LR algorithms in terms of the number of basis updates and the number of arithmetic operations in this section.

We start the comparison by considering the number of arithmetic operations per basis update. During one basis update iteration, the basis is updated as $\boldsymbol{h}_m \leftarrow \boldsymbol{h}_m + c\boldsymbol{h}_n$, where c is an integer. For SA, we keep finding index pairs (m, n) and integers $\lambda_{m,n}$ to reduce $S(\tilde{\boldsymbol{H}})$. In each iteration, we need to update $\tilde{\boldsymbol{H}}$, $\tilde{\boldsymbol{H}}^{\dagger}$, and $\boldsymbol{B}$ as

in (42), which takes $24N$ arithmetic operations. Furthermore, updating the entries of $\boldsymbol{\lambda}$ and $\boldsymbol{\Delta}$ matrices as in (43) and (44) is more complex. Here, we adopt the method in [87] to simplify the computation. However, it still needs $(104N - 18)$ operations. Thus, in total, SA needs $(128N - 18)$ arithmetic operations in each basis update.

For the complex LLL algorithm, the number of arithmetic operations for each basis update is random. The basis updates of the LLL algorithm are composed of size reduction process and δ condition updating process [19, 66]. In the n^{th} basis update, size reduction requires at most $(16N + 2)$ arithmetic operations. In addition, the δ condition updating process needs $28(M + N) \cdot p_u$ operations, where p_u is the probability that the δ condition fails and thus updating is necessary. Thus, the LLL algorithm needs $(16N + 2) + 28(M + N) \cdot p_u$ operations in each basis update, which is less than that of SA (unless $M >> N$). Furthermore, the probability p_u is small according to simulations [19, 66], which means the actual complexity of each basis update is even lower. Similar bounds on the worst-case complexity per iteration can be found in [49].

Here, we need to note that though SA needs more arithmetic operations per basis update than the LLL algorithm, the number of arithmetic operations is fixed given the channel size, while the number of arithmetic operations for each basis update is random for the LLL algorithm. This leads to a more efficient usage of the hardware components for SA. Considering the less average number of basis updates SA needed, the choice of fixed maximum number of iterations is more flexible.

Example 6.4 (Complexity comparisons for i.i.d. channels): We verify the complexity by plotting the average number of arithmetic operations (including real additions and real multiplications) per channel realization for $M = N = 2$ to 16 in Figure 39. Five equalizers are adopted: ZF-LE, ZF-DFE, LR-aided ZF-LE, LR-aided ZF-DFE, and SD method. For LR-aided equalizers, the CLLL algorithm is adopted. Here, the complexity of ZF-LE is obtained by adopting the Gaussian elimination for

matrix inversion, while ZF-DFE adopts the QR decomposition implemented through Householder transformation. The SD method is implemented as in [34]. From the figure, we can see that the complexity gap between LR-aided equalizers and traditional low-complexity equalizers is much smaller than that between SD and LEs/DFEs. The difference becomes larger as the dimension increases. Provided the significant performance improvement by the LR-aided equalizers, the complexity of LR-aided equalizers is really low. Furthermore, the complexity of LR-aided ZF-LE is slightly smaller than that of LR-aided ZF-DFE. Comparing the operations in Tables 8 and 9, we can see LR-aided ZF-DFE only requires an extra matrix-vector multiplication.

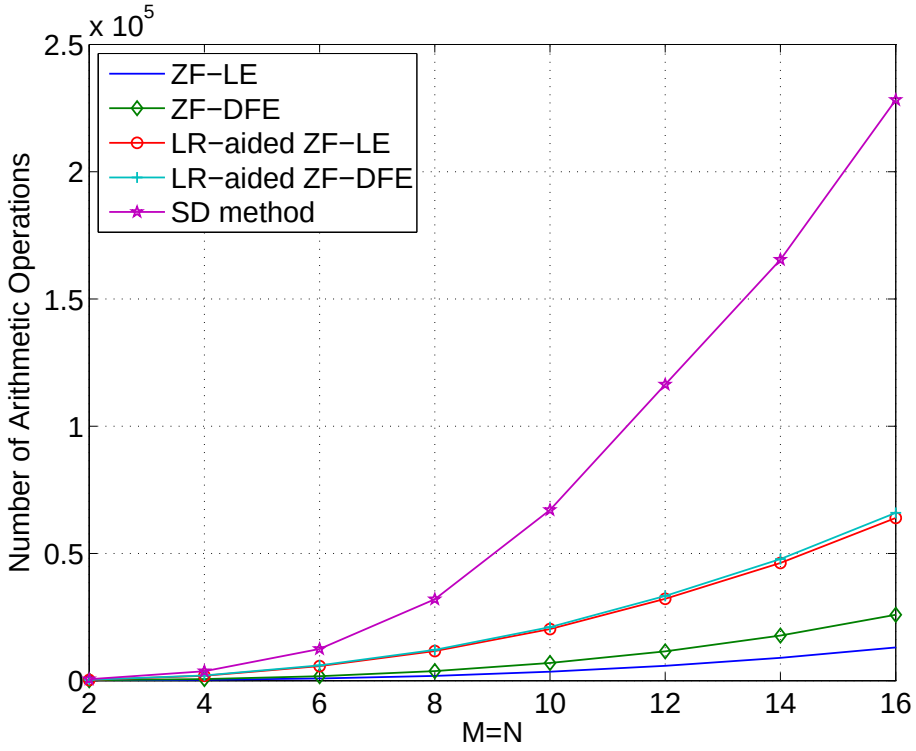

Figure 39: Complexity comparison of different equalizers with QPSK modulation.

In Fig. 40, we plot the average number of arithmetic operations for SA and the complex LLL algorithm (dual LLL algorithm has the same complexity as LLL), SA-aided ZF and LLL-aided ZF equalizers. For reference, we also plot the complexity of ZF equalizer and QR decomposition. From the figure, we can see that SA needs

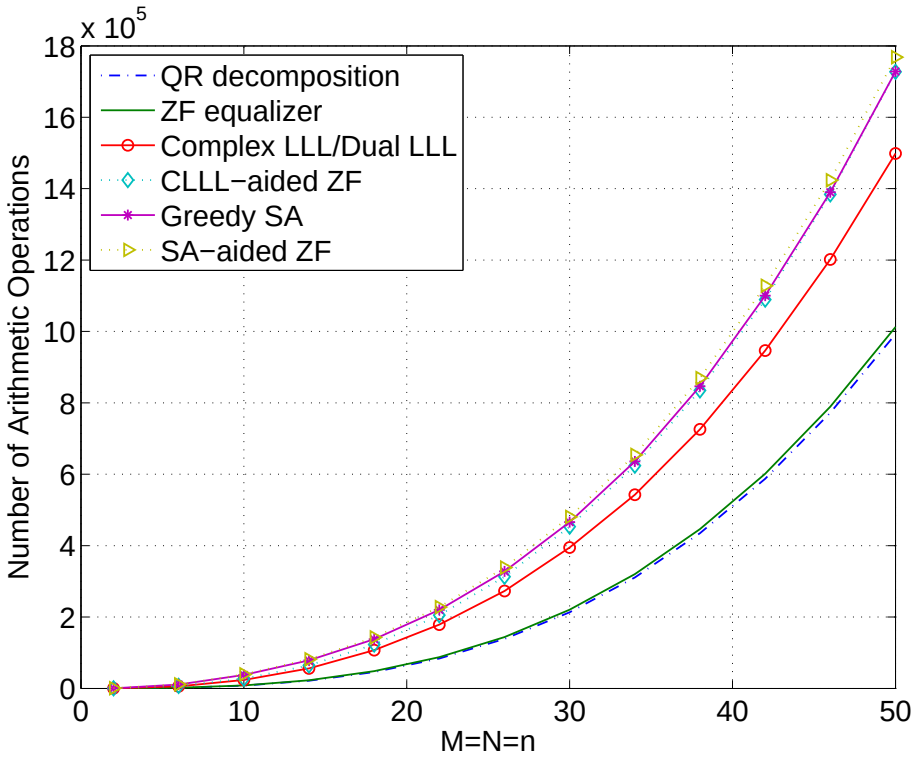

Figure 40: Complexity comparisons for uncoded systems with $N = M = n$

more arithmetic operations than LLL does. This verifies our analysis. Though SA needs less number of basis updates, the larger number of arithmetic operations per iteration makes the complexity of SA higher than that of LLL. Furthermore, the gap between the SA-aided ZF and LLL-aided ZF equalizers is smaller than that between SA and LLL. The complexity of the LLL-aided ZF equalizer is quite close to that of SA-aided ZF. This is because even more extra complexity is needed to implement the LLL-aided ZF equalizer than that with SA. Recalling the performance comparison in Fig. 25, we can see that, with comparable complexity, SA-aided ZF equalizer has better performance than dual LLL-aided ZF equalizer. Thus, SA is preferred to for use with LR-aided LEs, where the inverse of matrices is involved. However, when it comes to SICs, it is favorable to adopt LLL from an implementation point of view since LLL is based on QR decomposition.

As we have mentioned, one major advantage of SA over LLL is that SA reduces

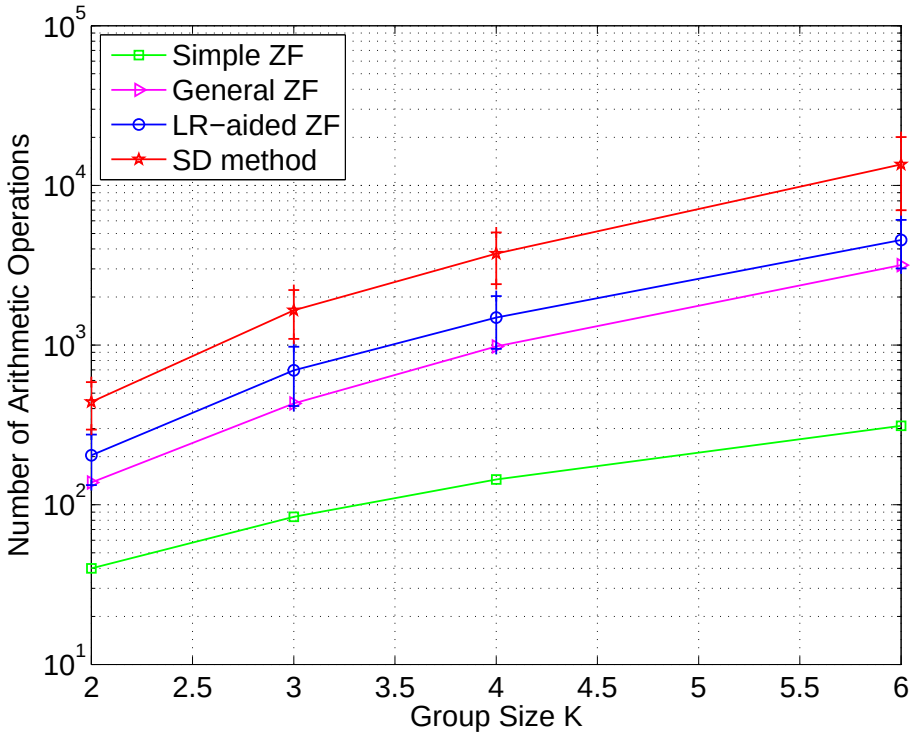

Figure 41: Average complexity and standard deviation comparison of SD method and LR-aided ZF equalizer at SNR = 30dB

$S(\boldsymbol{H})$ in every basis update, while LLL does not even guarantee to reduce $od(\boldsymbol{H})$ for each realization of $\boldsymbol{H}$. This advantage becomes especially important when it comes to hardware implementation since we need to set an upper bound on the number of iterations for these iterative algorithms. We use the following test case to demonstrate the performance when we have fixed number of iterations.

Example 6.5 (Complexity comparison of decoding schemes for LP-OFDM): We set the number of sub-carriers to $N_c = 120$ and the channel order to $L = 5$. Hence, the maximum multipath diversity order is 6. To compare the complexity of different decoding methods, we fix SNR at 30 dB and count the number of arithmetic operations (real additions and real multiplications). In Fig. 41, we plot four curves to represent: the SD method [34], the LR-aided ZF equalizer, a general ZF equalizer and a simplified ZF detector for LP-OFDM . Here, the general ZF equalizer inverts

$\boldsymbol{H}_{equ}$ directly (i.e., $(\boldsymbol{D}_H\boldsymbol{\Theta})^{-1}$) and the simplified ZF detector is $\boldsymbol{\Theta}^{\mathcal{H}}\boldsymbol{D}_H^{-1}$ based on the knowledge that $\boldsymbol{\Theta}$ is unitary. The SD method chosen here may not be up-to-date [34], but it is representative. The standard deviations of the complexity are also plotted for LR-aided ZF and SD method on each group size. From Fig. 41, we notice that, the curve of the LR-aided ZF equalizer is much closer to that of the general ZF detector than to that of the SD method. This means that the decoding complexity of the LR-aided ZF is very close to that of general ZF equalizers (about twice), and much lower than that of the SD method. Furthermore, the standard deviation of the complexity of LR-aided ZF is smaller than that of the SD method. Note that the complexity shown in Fig. 41 is in the high SNR regime. When SNR is low, SD has much higher complexity (it is exponential for the worst case), while LR-aided ZF equalizer still keeps the same complexity shown in Fig. 41. In the same figure, we also observe that the complexity of the simplified ZF equalizer is quite low thanks to the unitary property of $\boldsymbol{\Theta}$. However, it can only collect diversity 1. With a complexity that is a little bit higher than that of the general ZF equalizer, the LR-aided ZF equalizer can guarantee the diversity order of the ML detector.

Example 6.6 (Performance comparisons of LR algorithms with fixed-complexity): In Fig. 42, we plot the performance of SA, LLL and dual LLL-aided ZF equalizers with a fixed number of iterations N_i for a 6×6 V-BLAST system. We fix the maximum number of iterations as $N_i = 8, 10$, and 12, respectively. From the figure, we can see that SA-aided ZF equalizer has the best performance among these three equalizers with fixed number of iterations, and the performance gap becomes larger as N_i increases. Thus, once again we confirm that SA is more friendly to hardware implementation than LLL algorithm.

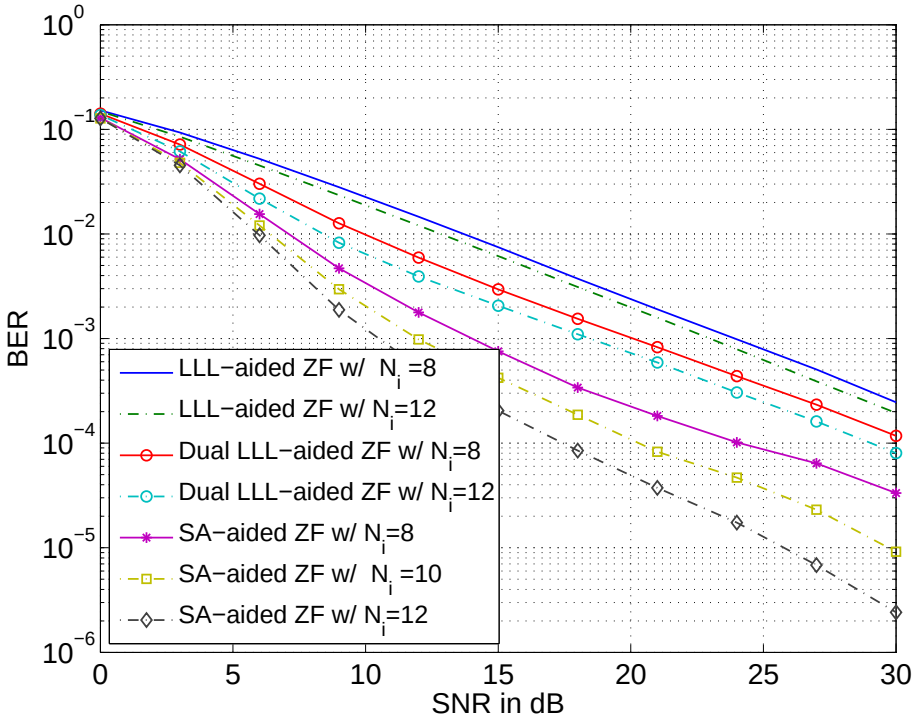

Figure 42: Performance comparisons with fixed complexity for $N = M = 6$

CHAPTER VII

DIVERSITY WITH FINITE-BIT REPRESENTATION

So far, all existing results on diversity and also our previous analysis are based on the mathematical derivation in real or complex field, which assumes the numbers are represented in infinite accuracy. However, in practical systems and even simulation tools (including MATLAB), only finite bits are afforded to represent real/complex numbers. Surely, this will affect the performance of the communication systems [55]. Therefore, the diversity has to be revisited and quantified for systems with finite-bit representation.

Suppose that signal $\boldsymbol{s}$ is transmitted while vector $\tilde{\boldsymbol{s}} \neq \boldsymbol{s}$ is detected at the receiver. The pairwise error probability (PEP) of MLE in (5) is quantified as [7, 57, 123]

$$P_e(\boldsymbol{s} \to \tilde{\boldsymbol{s}}|\boldsymbol{H}) = Q\left(\frac{1}{\sigma_w^2}\|\boldsymbol{H}(\tilde{\boldsymbol{s}} - \boldsymbol{s})\|^2\right) := Q\left(\frac{1}{\sigma_w^2}\|\boldsymbol{H}\boldsymbol{e}\|^2\right), \tag{70}$$

where $\boldsymbol{e} = \tilde{\boldsymbol{s}} - \boldsymbol{s}$ is the error vector, and $Q(\cdot)$ is the Gaussian tail function. By defining an $MN \times 1$ vector $\boldsymbol{h} = [\boldsymbol{h}_1^T, \ldots, \boldsymbol{h}_N^T]^T$, where $\boldsymbol{h}_n$ is the n^{th} column of $\boldsymbol{H}$, we have

$$\|\boldsymbol{H}\boldsymbol{e}\|^2 = \boldsymbol{h}^{\mathcal{H}}\boldsymbol{E}\boldsymbol{h} \sim \tilde{\boldsymbol{h}}^{\mathcal{H}}\boldsymbol{A}_e\tilde{\boldsymbol{h}}, \tag{71}$$

where $\boldsymbol{E} = \boldsymbol{I}_M \otimes \left((\boldsymbol{e}^T)^{\mathcal{H}}\boldsymbol{e}^T\right)$, the correlation matrix of $\boldsymbol{h}$ is $\boldsymbol{R}_h = E[\boldsymbol{h}^{\mathcal{H}}\boldsymbol{h}]$ with rank ρ_h, for which the SVD is $\boldsymbol{U}_h^{\mathcal{H}}\boldsymbol{\Lambda}_h\boldsymbol{U}_h$, an $\rho_h \times 1$ vector $\tilde{\boldsymbol{h}}$ has i.i.d. complex Gaussian entries, $\boldsymbol{A}_e = \boldsymbol{\Lambda}_h^{\frac{1}{2}}\boldsymbol{U}_h^{\mathcal{H}}\boldsymbol{E}\boldsymbol{U}_h\boldsymbol{\Lambda}_h^{\frac{1}{2}}$ is determined by the error vector $\boldsymbol{e}$ and $\boldsymbol{R}_h$, and "$\sim$" denotes the identical distributions. Since each entry of the signal $\boldsymbol{s}$ is drawn from the constellation $\mathcal{S}$, the error signal $\boldsymbol{e}$ belongs to a set $\mathcal{S}_e = \{\boldsymbol{e} := \tilde{\boldsymbol{s}} - \boldsymbol{s}|\tilde{\boldsymbol{s}} \neq \boldsymbol{s}, \tilde{\boldsymbol{s}}, \boldsymbol{s} \in \mathcal{S}^N\}$. With infinite bits representation, the diversity order $G_d^{(i)}$ collected by the MLE is defined as (see e.g., [7, 57, 123])

$$G_d^{(i)} = \min_{\boldsymbol{e} \in \mathcal{S}_e} \text{rank}(\boldsymbol{A}_e). \tag{72}$$

In this paper, instead of assuming each number (the real or complex numbers) is represented by infinite bits, we consider the situation where finite-bit representation is adopted, e.g., fixed-point or floating-point number representation. In this case, a small real number may be quantified to zero. Thus, the performance of MLE in (5) is affected because the rank of $\boldsymbol{A}_e$ in (71) may be different due to the following two cases:

S1) The statistical property of $\boldsymbol{H}$ is changed when the number of bits adopted is too small;

S2) $\boldsymbol{H}$ is still well approximated as a complex Gaussian random matrix, but the constellation $\mathcal{S}$ spans a wide range and thus the rank of finite-bit represented $\boldsymbol{A}_e$ is smaller than the rank of original $\boldsymbol{A}_e$.

In the following, we analyze the diversity order for these two cases with finite-bit representation.

7.1 Finite Bit Represented Channels

A Gaussian random variable h is represented by finite bits as (using fixed-point with two's complement arithmetic)

$$\mathcal{F}(h, G, F) = -b_{G-1}2^{G-1} + \sum_{i=0}^{G-2} b_i 2^i + \sum_{i=1}^{F} a_i 2^{-i}, \tag{73}$$

where G and F are the number of integer and fractional bits, and a_i and b_i are binary bits. When the number of bits is not enough, the Gaussian variable can not be well approximated, and thus the diversity may be lost. Here, we use one example to show how the number of bits adopted will affect the diversity.

Example 7.1 (Finite bit represented Gaussian channel): We assume 4-QAM constellation and $M = N = 1$ in (1). We plot the bit-error-rate (BER) curves in Fig. 43 with fixed-point arithmetic, and the numbers of integer and fractional bits (G, F)

are $(10, 10), (8, 8), (6, 6)$, and $(4, 4)$, respectively. We also plot one curve for the same system with 15 digits scaled fixed-point format in MATLAB as a benchmark. From the figure we can see, the diversity is either one or zero (error floor), since H now is a complex Gaussian random variable.

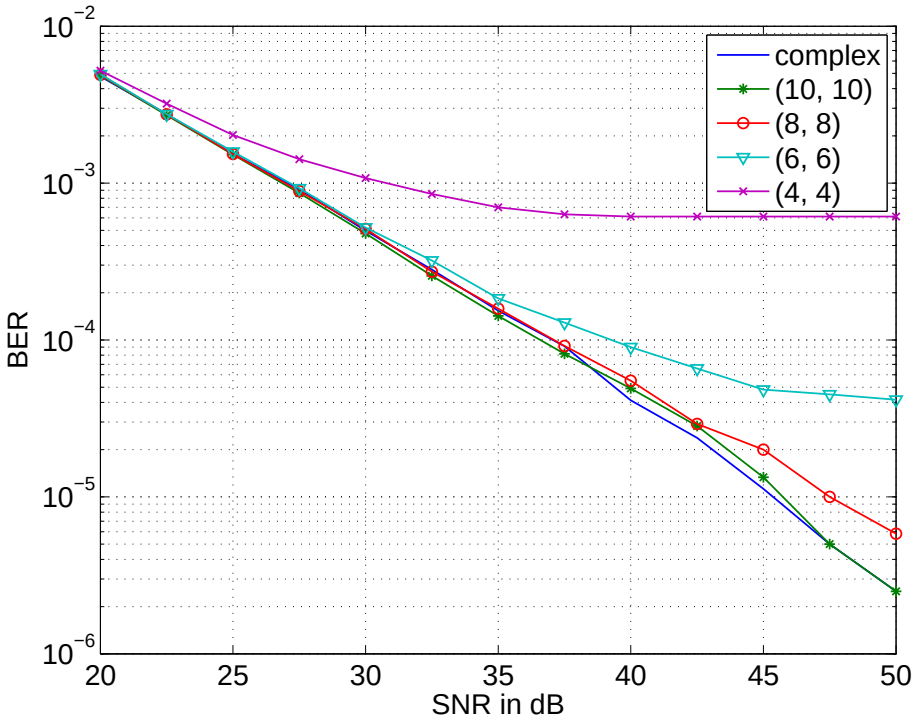

Figure 43: Effects of finite-bit representation on diversity

Given finite-bit representation, when SNR is high enough, error floor of the BER curves shows up because finite bits cannot differentiate large numbers above a certain bound. How many bits are adopted determines when the error floor (zero diversity) appears. Approximately, based on (73), the error floor appears at:

$$\text{SNR} = (G + F)10 \log_{10} 2 \approx 3(G + F)\text{dB}.$$

Thus, in practical systems, the number of bits is chosen large enough ($>$ (8, 8)) so that within a reasonable SNR range ($<$ 50 dB), the channel will not lose its diversity.

7.2 Diversity with Different Transmitters

To analyze the diversity for **ANY** QAM constellation with finite-bit representation, we need to focus on the structure of $\boldsymbol{A}_e$. Suppose that the SVD of $\boldsymbol{A}_e$ in (71) is $\boldsymbol{U}_e^{\mathcal{H}}\boldsymbol{\Lambda}_e\boldsymbol{U}_e$, where $\boldsymbol{\Lambda}_e$ is a diagonal matrix with the diagonal entries $\alpha_1, \alpha_2, \ldots, \alpha_{\rho_e}$ as the eigenvalues of $\boldsymbol{A}_e$ and ρ_e is the rank of $\boldsymbol{A}_e$. Thus, we have $\tilde{\boldsymbol{h}}^{\mathcal{H}}\boldsymbol{A}_e\tilde{\boldsymbol{h}} = \sum_{n=1}^{\rho_e}\alpha_n|\bar{h}_n|^2$, where $\bar{h}_n$ is the n^{th} entry of $\bar{\boldsymbol{h}} = \boldsymbol{U}_e\tilde{\boldsymbol{h}}$. Since $\boldsymbol{U}_e$ is a unitary matrix, we know $\bar{\boldsymbol{h}}$ is a vector with i.i.d. complex Gaussian distributed entries. For systems with finite-bit representation, if α_n is less than ϵ_{th} which is the lower bound of the finite-bit representation, it will be quantified to zero. Thus, for systems with finite-bit representation, the rank of $\boldsymbol{A}_e$ needs to be revisited. The result is summarized as follows.

Proposition 10 *Suppose the transmission system is based on finite-bit representation. Given the specific constellation, the diversity order collected by the MLE in* (5) *is*

$$G_d^{(f)} = \min_{\boldsymbol{e}\in\mathcal{S}_e} \text{rank}(\mathcal{F}(\boldsymbol{A}_e, G, F)), \tag{74}$$

where $\mathcal{F}(a, G, F)$ *is defined in* (73) *and* $\boldsymbol{A}_e$ *is expressed as in* (71).

Obviously, the system diversity with finite-bit representation in (74) depends on two terms: i) the range of the values in $\boldsymbol{A}_e$; ii) the number of bits adopted to represent the numbers. For fixed number of bits, the diversity is determined by the rank of quantized $\boldsymbol{A}_e$, i.e., the non-zero eigenvalues of $\boldsymbol{A}_e$. In general, the eigenvalues of $\boldsymbol{A}_e$ depend on the constellation size and the transmitter structure. To find the non-zero eigenvalues for any constellation is equivalent to finding non-vanishing eigenvalues which are defined as follows.

Definition 6 *Suppose* $\alpha_1 \leq \alpha_2 \leq \cdots \leq \alpha_{\rho_e}$ *are the ordered nonzero eigenvalues of*

$\boldsymbol{A}_e$ *in* (71). *If there exists a constant* $\epsilon > 0$ *such that*

$$\inf_{|\mathcal{S}|\to\infty} |\alpha_n| > \epsilon, \tag{75}$$

then α_n *is called a non-vanishing eigenvalue as the constellation size increases to infinity.*

If the eigenvalue α_n is vanishing, then given a finite number of bits (no matter how many bits are adopted), α_n will be smaller than ϵ_{th} and quantified to zero when the constellation size is large enough. Furthermore, with some constraints of the transmitter, e.g., the fixed norm of $\boldsymbol{e}$ or the determinant is nonzero, not all eigenvalues of $\boldsymbol{A}_e$ vanish simultaneously. Thus, we can see, the asymptotic diversity as the constellation size increases to infinity is the smallest number of non-vanishing eigenvalues of $\boldsymbol{A}_e$. Now we summarize our results as follows.

Proposition 11 *The asymptotic diversity collected by MLE as the constellation size increases to infinity is defined as*

$$G_d^{(a)} = \lim_{|\mathcal{S}|\to\infty,\forall\mathcal{F}} \min_{\boldsymbol{e}\in\mathcal{S}_e} \operatorname{rank}(\mathcal{F}(\boldsymbol{A}_e, G, F)). \tag{76}$$

In other words, the asymptotic diversity equals the number of non-vanishing eigenvalues of $\boldsymbol{A}_e$.

Proposition 11 shows that given finite-bit representation, when the constellation size keeps increasing, even MLE may lose diversity. A natural question now is how fast the schemes lose diversity. In the following, we use three examples [7, 27, 57, 123] to illustrate this phenomenon.

Example 7.2 (V-BLAST systems): For V-BLAST system in [27], the error pattern $\boldsymbol{e}$ is an $N \times 1$ vector. Suppose the channel coefficients are i.i.d. complex Gaussian distributed. Eq. (71) can be rewritten as

$$\|\boldsymbol{H}\boldsymbol{e}\|^2 = \boldsymbol{h}^{\mathcal{H}} \left(\boldsymbol{I}_M \otimes \left((\boldsymbol{e}^T)^{\mathcal{H}} \boldsymbol{e}^T\right)\right) \boldsymbol{h}, \tag{77}$$

where $\boldsymbol{h}$ is an $MN \times 1$ column vector by stacking all columns of $\boldsymbol{H}$ into one column. Thus, according to [27], the maximum diversity is M. Specifically, in this case, the M nonzero eigenvalues of $\boldsymbol{I}_M \otimes ((\boldsymbol{e}^T)^{\mathcal{H}} \boldsymbol{e}^T)$ are the same as $\|\boldsymbol{e}\|^2$, which is lower bounded by the minimum Euclidean distance ($d_{\min}$) of the constellation. Thus, if the minimum value ϵ_{th} that the finite bits can represent is smaller than $d_{\min}$, then the diversity is M. Otherwise, the diversity is zero. All eigenvalues vanish simultaneously when we reduce the number of bits.

Example 7.3 (Precoded OFDM systems): The LCFC-OFDM system [57] is designed to collect multipath diversity of frequency-selective channels. The equivalent channel matrix for LCFC-OFDM systems is $\boldsymbol{H} = \boldsymbol{D}_H \boldsymbol{\Theta}$, where $\boldsymbol{D}_H = \text{diag}[H(0), H(1), \ldots, H(N-1)]$ with $H(n)$ as the channel response at subcarrier n, and $\boldsymbol{\Theta}$ is an $N \times N$ full-rank square unitary precoder. By stacking $H(n)$ into one $N \times 1$ column $\boldsymbol{h}$, we can rewrite (71) as

$$\|\boldsymbol{H}\boldsymbol{e}\|^2 = \boldsymbol{h}^{\mathcal{H}} \left(\text{diag}[\boldsymbol{u}]^{\mathcal{H}} \text{diag}[\boldsymbol{u}]\right) \boldsymbol{h}, \tag{78}$$

where $\boldsymbol{u} = \boldsymbol{\Theta}(\tilde{\boldsymbol{s}} - \boldsymbol{s})$. The eigenvalues of $\boldsymbol{A}_e$ are the norm of the entries of $\boldsymbol{u}$. As shown in [57], the minimum entry of $|\boldsymbol{u}|$ only depends on the minimum distance $d_{\min}$ of the constellation adopted. Thus, the minimum eigenvalue will not approach zero as the constellation size increases to infinity. Neither will other eigenvalues. As the number of bits decreases, not like V-BLAST, LCFC-OFDM loses diversity gradually since the eigenvalues are not all equal.

Example 7.4 (Golden code for 2×2 systems): The golden code is a full-diversity-full-rate space-time coding scheme for 2×2 i.i.d. channels [7, 123]. Since golden code is implemented in two time slots, the error pattern $\boldsymbol{e}$ now is a 2×2 matrix. Thus, (71) can be expressed as

$$\|\boldsymbol{H}\boldsymbol{e}\|^2 = \boldsymbol{h}^{\mathcal{H}} \left(\boldsymbol{I}_2 \otimes \boldsymbol{A}^{\mathcal{H}} \boldsymbol{A}\right) \boldsymbol{h}, \tag{79}$$

where $\boldsymbol{h}$ is a 4×1 vector by stacking all four channel coefficients into one column, and

$$\boldsymbol{A} = \begin{bmatrix} e_{11}\cos\theta_1 - e_{22}\sin\theta_1 & e_{12}\cos\theta_2 - e_{21}\sin\theta_2 \\ e_{12}\sin\theta_2 + e_{21}\cos\theta_2 & e_{11}\sin\theta_1 + e_{22}\cos\theta_1 \end{bmatrix}, \tag{80}$$

where e_{mn} is the $(m,n)^{\text{th}}$ entry of $\boldsymbol{e}$. In [123], it has been shown that $|\det(\boldsymbol{A})| \geq \frac{1}{2\sqrt{5}}$ with the optimal $(\theta_1,\theta_2) = (\frac{1}{2}\arctan\frac{1}{2}, \frac{1}{2}\arctan 2)$. The two eigenvalues of $\boldsymbol{A}^{\mathcal{H}}\boldsymbol{A}$ are

$$\alpha_{1,2} = \|\boldsymbol{e}\|^2 \left(1 \pm \sqrt{1 - \frac{4\det(\boldsymbol{A}^{\mathcal{H}}\boldsymbol{A})}{\|\boldsymbol{e}\|^4}}\right). \tag{81}$$

If the error pattern is $e_{12} = e_{22} = 0$, and e_{11}, e_{21} are real integers such that

$$|e_{11} - \sqrt{2}e_{21}| < \epsilon\sqrt{e_{21}}\ , \quad \forall\ \epsilon > 0, \tag{82}$$

then it can be verified that $\det(\boldsymbol{A}^{\mathcal{H}}\boldsymbol{A}) = (e_{11}^2 - 2e_{21}^2)^2 < (\epsilon^2 e_{21} + 2\sqrt{2}\epsilon e_{21}^{\frac{3}{2}})^2$. Thus, it is ready to show that when e_{11} and e_{21} go to infinity, one of the eigenvalues in (81) approaches zero. Different from V-BLAST and LCFC-OFDM, as the constellation size increases, the minimum eigenvalue of $\boldsymbol{A}$ decreases for golden code. To maintain the determinant non-zero, at most one eigenvalue of $\boldsymbol{A}^{\mathcal{H}}\boldsymbol{A}$ could approach zero as the constellation size increases. Because there are two groups of identical eigenvalues in $\boldsymbol{A}_e$, the number of non-vanishing eigenvalues is 2. It is not difficult to find such an error pattern that makes one of the eigenvalues be quantized to zero. For example, using MATLAB with 15 digits scaled fixed point format, when $\boldsymbol{e} = [65780, 85786; 59796, 69848]$, one eigenvalue of $\boldsymbol{A}^{\mathcal{H}}\boldsymbol{A}$ is quantified to zero, while the determinant of $\boldsymbol{A}^{\mathcal{H}}\boldsymbol{A}$ is 2.2×10^4 and $\text{rank}(\boldsymbol{A}^{\mathcal{H}}\boldsymbol{A}) = 1$. Although an extremely large constellation is needed to reach this error pattern, the diversity for this particular constellation is 2, according to the code design in [123].

Example 7.5 (Diversity of systems with finite-bit representation): We plot the performance of LCFC-OFDM [57] for frequency-selective channels with channel order 3 (multipath diversity is 4), V-BLAST systems [27] for 4×4 i.i.d. channels,

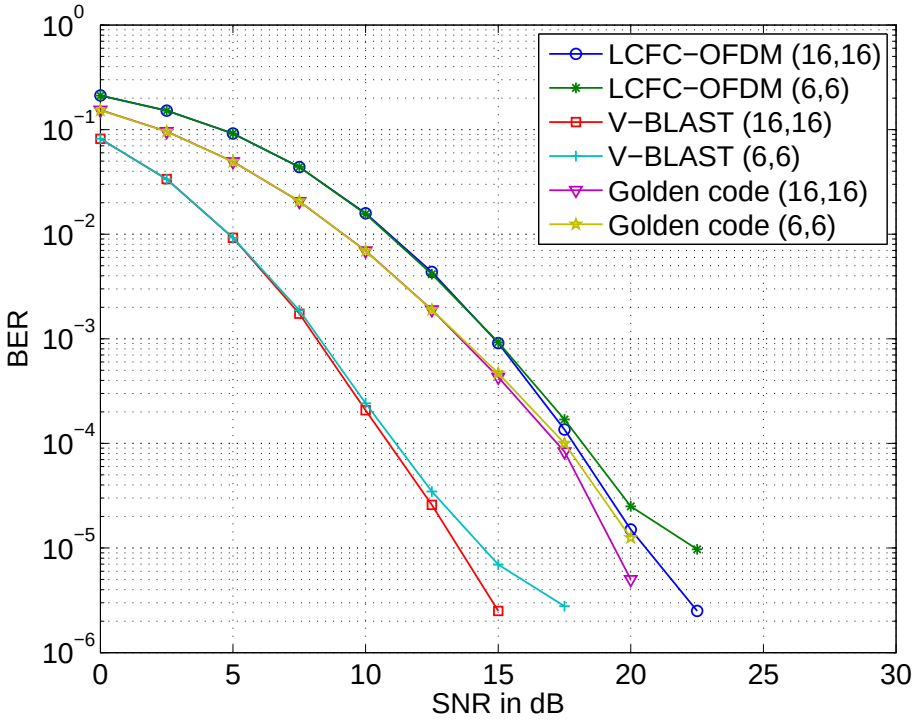

Figure 44: Performance with finite-bit representation

and golden code [123] for 2×2 i.i.d. channels. We adopt 4-QAM and fix the number of integer bits G and number of fractional bits F as $(16, 16)$ and $(6, 6)$, respectively. From Fig. 44 we observe that diversity 4 is collected by all these three systems when the number of bits is high enough. However, when the number of bits is low, diversity is lost when SNR is high.

7.3 Diversity Collected by Different Receivers

In this section, we illustrate that finite-bit representation also affects the diversity that a receiver can collect. Instead of MLE, we consider LRAEs, which are proposed in [19, 67, 111, 122] to improve the performance of LEs without increasing complexity much. We adopt the complex LLL (CLLL) algorithm [19, 67] to perform LRAE on the channel matrix $\boldsymbol{H}$. A reduced lattice basis $\tilde{\boldsymbol{H}} = \boldsymbol{HT}$ is obtained by the CLLL algorithm, where $\boldsymbol{T}$ is a unimodular matrix with all the entries being Gaussian integers

and the determinant of $\boldsymbol{T}$ being ± 1 or $\pm j$. Then we perform the ZF equalizer $\tilde{\boldsymbol{H}}^{\dagger}$ instead of $\boldsymbol{H}^{\dagger}$ to the observation vector as

$$\boldsymbol{x} = \tilde{\boldsymbol{H}}^{\dagger}\boldsymbol{y} = \boldsymbol{T}^{-1}\boldsymbol{s} + \tilde{\boldsymbol{H}}^{\dagger}\boldsymbol{w} := \boldsymbol{z} + \boldsymbol{n}. \tag{83}$$

Since all the entries of $\boldsymbol{T}^{-1}$ and the signal constellation belong to Gaussian integer ring, the entries of $\boldsymbol{z}$ are also Gaussian integers. Thus, we perform the first hard-decoding step by rounding $\boldsymbol{x}$ to the nearest Gaussian integers to get $\hat{\boldsymbol{z}}$. The second hard-decoding step is to quantize $\boldsymbol{T}\hat{\boldsymbol{z}}$ to the signal constellation $\mathcal{S}$ to obtain the estimated symbols $\hat{\boldsymbol{s}}$. The detailed algorithm can be found in [19, 67].

Note that the constellation size of $\boldsymbol{z}$ is infinite because the entries of $\boldsymbol{T}$ can be arbitrarily large. Furthermore, as stated in [19, 67], the CLLL algorithm upper bounds the orthogonality deficiency of $\tilde{\boldsymbol{H}}$. Thus, according to the results in [66], LEs based on $\tilde{\boldsymbol{H}}$ have the same diversity as that of MLE based on $\tilde{\boldsymbol{H}}$. For the MLE based on $\tilde{\boldsymbol{H}}$, we can express the PEP as in (70)

$$P_e(\boldsymbol{z} \to \tilde{\boldsymbol{z}}|\tilde{\boldsymbol{H}}, \{\tilde{\boldsymbol{z}}, \boldsymbol{z}\} \in \mathbb{Z}[j]^{N\times 1}) = Q\left(\frac{1}{\sigma_w^2}\|\tilde{\boldsymbol{H}}(\tilde{\boldsymbol{z}} - \boldsymbol{z})\|^2\right),$$

where $\mathbb{Z}[j]$ denotes the complex integer set whose elements have the form $\mathbb{Z} + j\mathbb{Z}$, with $j = \sqrt{-1}$. Then, in the first quantization step, LRAEs achieve the same diversity as MLE based on infinite constellation under finite-bit representation. Now, we summarize the result as follows.

Proposition 12 *Given finite-bit representation, the diversity collected by LRAEs is the same as the asymptotic diversity enabled by the transmitter with infinite constellation.*

With Proposition 12, we can then quantify the diversity collected by LRAEs for general systems. For example, for V-BLAST and LCFC-OFDM systems, LRAEs collect the same diversity as MLEs, because the minimum eigenvalue is non-vanishing as constellation size increases. This is consistent with the theoretical results in [67, 68].

In general, we claim that to design a coding scheme which could achieve full diversity with LRAEs at fairly low complexity, the matrix $\boldsymbol{A}_e$ in (71) needs to be designed so that the minimum eigenvalue is non-vanishing when constellation size increases to infinity.

Example 7.6 (Diversity of golden code): In this example, we implement the

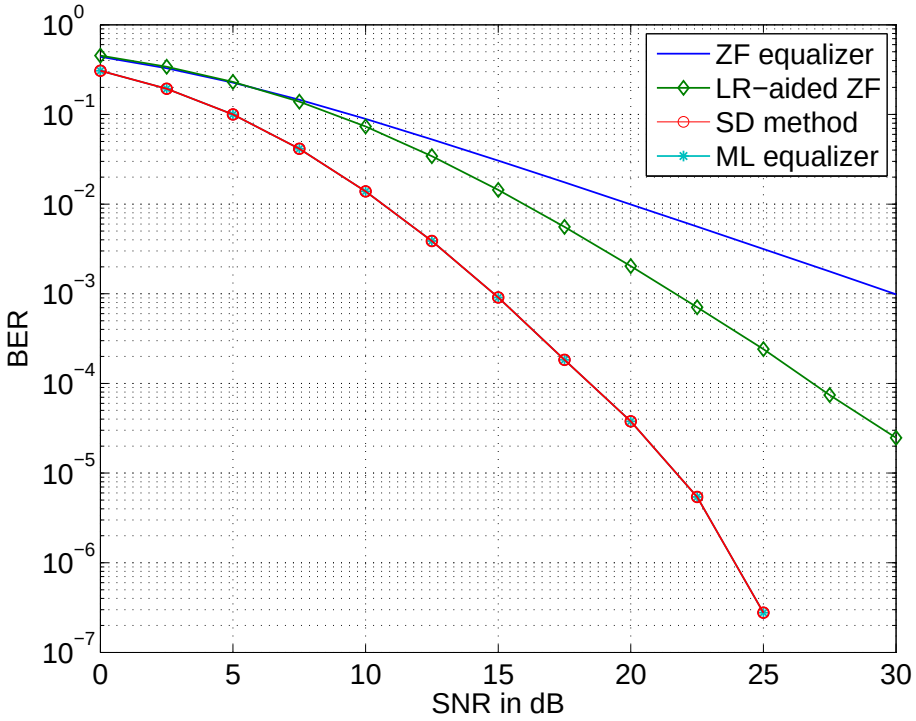

Figure 45: Performance of Golden code

golden code in [123] for a 2×2 system in MATLAB. The channel coefficients are assumed to be i.i.d. complex Gaussian random variables. Four detectors are adopted to recover the signal: ZF, LR-aided ZF, sphere decoding (SD) and ML detectors. It can be observed from Fig. 45 that both SD and ML detectors exploit full diversity 4. ZF equalizer collects diversity 1 [68] while LR-aided ZF equalizer only has diversity 2. LRAE loses diversity 2 because of the finite-bit representation of MATLAB, which verifies our analysis in Proposition 12.

CHAPTER VIII

HARDWARE IMPLEMENTATION

After analyzing the performance, we are well motivated to implement LR-aided equalizers on hardware to verify the performance. The first LR VLSI silicon implementation for MIMO systems reported in literature is the channel precoder described in [11]. The implemented algorithm achieves lower algorithm complexity than the CLLL algorithm at the cost of simplifications and approximations that greatly reduce the performance [85] compared to the LLL algorithm. In the interest of closing this nearly 5 dB performance gap and implementing an algorithm that has been proven to collect full diversity, we explore the datapath and scheduling aspects of a VLSI implementation of the CLLL algorithm for 4×4 MIMO systems in [22]. Below we summarize our initial contributions.

The major hardware complexity of the CLLL process (operations on the $\tilde{Q}$ and $\tilde{R}$ matrix after the QR decomposition of the H matrix) comes from the iterative checking of the condition in (39) and basis update if this condition fails. Since $\tilde{R}_{k,k}$ is a real diagonal element and $\tilde{R}_{k-1,k}$ is a complex off-diagonal element of $\tilde{\boldsymbol{R}}$, if we group these elements into a real vector as

$$\boldsymbol{v} = \left[\tilde{R}_{k,k}, \Re[\tilde{R}_{k-1,k}], \Im[\tilde{R}_{k-1,k}]\right]^T, \tag{84}$$

then the right side of the inequality in (39) becomes the norm of a 3D vector. A well understood and numerically stable algorithm, Householder CORDIC [36], exists that employs low hardware complexity shift and addition iterations to compute arbitrary 3D rotations. In our existing work we use vectoring operations on $\boldsymbol{v}$ to determine the right side of the inequality in (39) within a constant Householder CORDIC gain factor. Furthermore, by checking the "early exit" condition, $\sqrt{\delta}|\tilde{R}_{k-1,k-1}| < |\tilde{R}_{k,k}|$, we can

often avoid computing this vector norm. The reverse application of these vectoring operations (rotation) can then be used to compute the unitary matrix required for a basis update.

Division operations in the CLLL algorithm function to force the condition in (38) true. Full precision division, however, is not required because only integer-rounded quotients are used in the CLLL algorithm. In addition, divisors are reused during the algorithm, suggesting the utility of a reciprocation-based approach. In [20] we develop a single Newton-Raphson iteration-based integer-rounded divider that reduces FPGA resource usage by 40% and improves average divider latency when compared to a straightforward SRT division architecture.

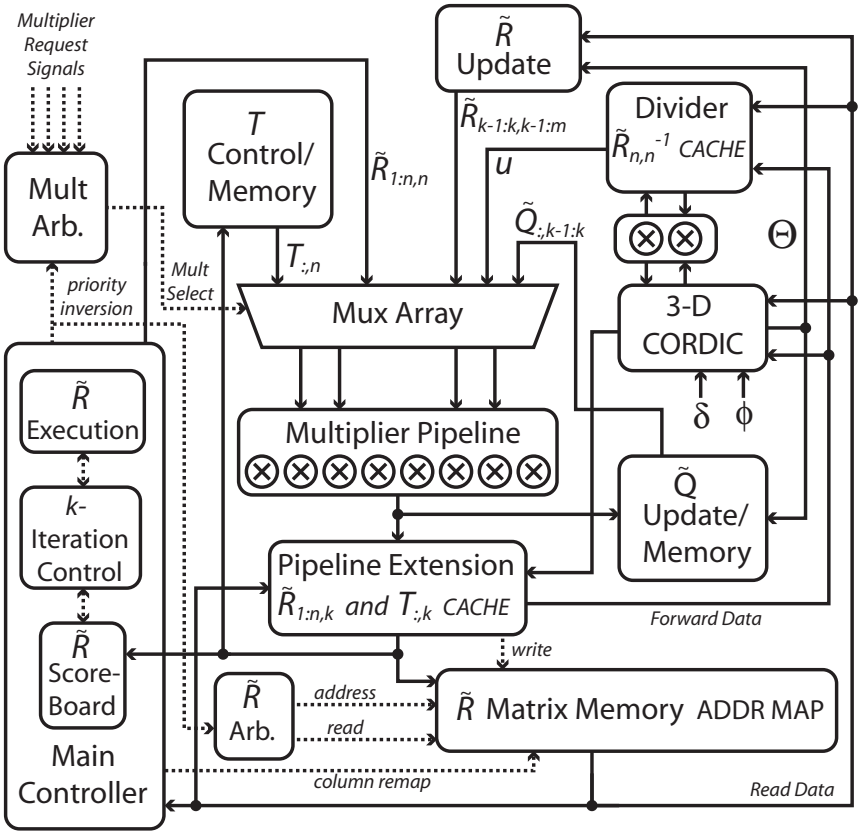

Figure 46: Simplified block diagram of CLLL processor

The remaining operations of the CLLL algorithm consist of a varying number and

varying sequence of complex-valued multiplications. The 4×4 architecture of our existing work (Figure 46) accommodates this dynamic dataflow by employing a time-multiplexed complex multiplier pipeline and separate control modules that handle data fetching for and operations on the $\tilde{T}$, $\tilde{R}$, and $\tilde{Q}$ matrices in addition to the 3D CORDIC modules and integer-rounded divider modules described earlier. Contention among these modules for the shared complex multiplier and matrix memory is handled by arbitration modules that use priority-inversion to prevent deadlocks because of data dependencies. A top-level control module tracks the overall progress of the algorithm and issues start and stop commands to the various modules. These techniques allow the architecture to take advantage of both within-iteration (size-reduction and (39) condition checking) and across-iteration (basis updates) parallelism inherent in the CLLL algorithm.

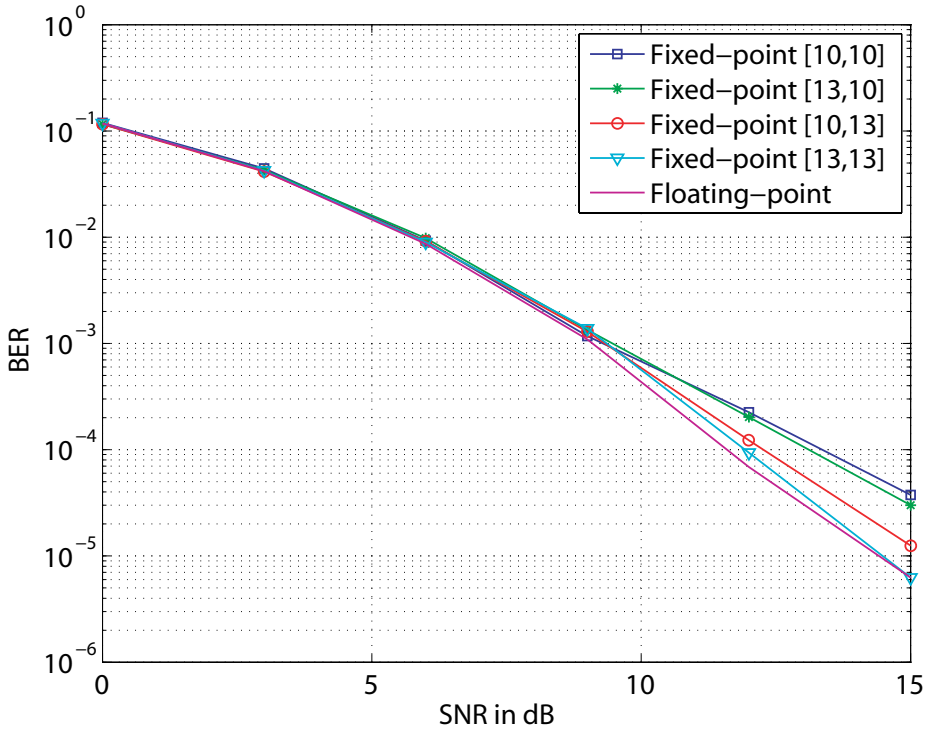

Figure 47: Hardware fixed-point simulations of an LR-aided ZF-DFE for a 4×4 V-BLAST transmission using a variety of bit precisions

Table 14: VLSI implementation results

	Virtex4	**Virtex5**
Area		
Real Multipliers	10/96	10/64
Gate Equivalents	88,308	78,683
Slices	3,617/67,584	1,712/17,280
Clock frequency	140 MHz	163 MHz
Avg. cycles per matrix	130	130

Fixed-point CLLL processor simulation results of a 4×4 V-BLAST transmission with LR-aided nulling canceling equalizer (LRNC) for a variety of $\tilde{R}$ number representations are shown in Figure 47. We choose the [13.13] $\tilde{R}$ representation because this implementation achieves a BER of 10^{-5} at an SNR that is only 0.1 dB higher than the SNR required by the floating-point implementation. The hardware realization results obtained from a Synplify Pro synthesis and Xilinx ISE P/R implementation flow are shown in Table 14. The modest FPGA resources and $1.25M$ matrices/s average throughput of this architecture are encouraging given that this architecture is not optimized for a particular channel model or equalizer.

CHAPTER IX

CONCLUDING REMARKS

The objective of the proposed research is to present efficient receiver designs that can achieve low bit-error-rate (BER), high capacity, and low decoding complexity. We focuses on the design of low-complexity receivers for wireless systems based on a generic linear system model. We first revealed the fundamental condition to achieve full diversity with LEs by investigating the error performance and mutual information of existing low-complexity equalizers. To meet the fundamental condition and then achieve the diversity, we propose a hybrid equalizer framework, for which the performance-complexity trade-off is quantified by providing the distribution of channel quality. Another approach we proposed is to apply different LR algorithms to achieve full diversity with LR-aided detectors. Both LR-aided hard-output detectors and LR-aided soft-output detectors are proposed and analyzed in terms of diversity, mutual information, and complexity, respectively. The effect of finite-bit precision in simulations and practical systems has also been investigated. Furthermore, the results of hardware implementation verify the practicality of our proposed receiver designs. Throughout this research, the theoretical analysis is corroborated by computer simulations.

9.1 Contributions

We summarize below primary contributions of this dissertation:

- Revealed the fundamental limits of linear equalizers on diversity, capacity, and complexity;
- Proposed a hybrid equalizer framework to achieve full diversity for which the

performance-complexity trade-off is quantified by deriving the distribution of od;

- Investigated different metrics to quantify the distance to orthogonality for matrices;
- Investigated the performance and complexity of different lattice reduction algorithms;
- Proposed complex LLL-aided and SA-aided equalizers and analyzed the performance in terms of diversity, mutual information, and complexity;
- Proposed tree-search implementation for SA and designed SA-aided soft-output detectors based on the tree-search implementation;
- Analyzed the performance for general systems when finite-bit representation is adopted;
- Verified the practicality of the proposed designs through hardware implementation.

9.2 Suggestions for Future Research

The following is a list of interesting research topics that can be pursued as extensions of this dissertation:

- Diversity of LEs for general systems when the fundamental condition is not satisfied;
- The diversity-multiplexing trade-off of LR-aided detectors;
- Outage diversity with finite-bit representation;
- High speed hardware implementation.

APPENDIX A

PROOF OF LEMMA 1

According to the definition of $od(\boldsymbol{H})$ in (10) and the extended system in (9), we have

$$\begin{aligned}\sup_{\sigma_w^2,\boldsymbol{H}}(od(\bar{\boldsymbol{H}})) &= 1-\inf_{\sigma_w^2,\boldsymbol{H}}\left(\frac{\det(\boldsymbol{H}^{\mathcal{H}}\boldsymbol{H}+\sigma_w^2\boldsymbol{I}_N)}{\prod_{n=1}^{N}(\|\boldsymbol{h}_n\|^2+\sigma_w^2)}\right)\\ &\geq 1-\inf_{\boldsymbol{H}}\left(\frac{\det(\boldsymbol{H}^{\mathcal{H}}\boldsymbol{H})}{\prod_{n=1}^{N}\|\boldsymbol{h}_n\|^2}\right)=\sup_{\boldsymbol{H}}(od(\boldsymbol{H})).\end{aligned}$$

If $\sup(od(\boldsymbol{H}))=\epsilon=1$, it is ready to obtain that $1=\sup(od(\boldsymbol{H}))\leq\sup(od(\bar{\boldsymbol{H}}))\leq 1$, which means $\sup(od(\bar{\boldsymbol{H}}))=\epsilon'=1$.

Next, we want to show that ϵ' is less than 1 when $\epsilon<1$. Suppose $\epsilon'=1$, and then we have

$$\inf_{\sigma_w^2,\boldsymbol{H}}\left(\frac{\det(\boldsymbol{H}^{\mathcal{H}}\boldsymbol{H}+\sigma_w^2\boldsymbol{I}_N)}{\prod_{n=1}^{N}(\|\boldsymbol{h}_n\|^2+\sigma_w^2)}\right)=1-\sup_{\sigma_w^2,\boldsymbol{H}}(od(\bar{\boldsymbol{H}}))=0. \tag{85}$$

Furthermore, since

$$\begin{aligned}&\text{when } \sigma_{\mathrm{w}}^2=0,\quad \inf\left(\frac{\det(\boldsymbol{H}^{\mathcal{H}}\boldsymbol{H}+\sigma_w^2\boldsymbol{I}_N)}{\prod_{n=1}^{N}(\|\boldsymbol{h}_n\|^2+\sigma_w^2)}\right)=1-\epsilon\neq 0\\ &\text{when}\|\boldsymbol{h}_{\mathrm{n}}\|\to\infty \text{ or } \sigma_{\mathrm{w}}^2\to\infty,\ \frac{\det(\boldsymbol{H}^{\mathcal{H}}\boldsymbol{H}+\sigma_w^2\boldsymbol{I}_N)}{\prod_{n=1}^{N}(\|\boldsymbol{h}_n\|^2+\sigma_w^2)}\to 1\neq 0,\end{aligned}$$

to have (85) hold true, we need $\inf(\det(\boldsymbol{H}^{\mathcal{H}}\boldsymbol{H}+\sigma_w^2\boldsymbol{I}))=0$, where $\|\boldsymbol{h}_n\|$ and σ_w^2 are finite but non-zero. However, because $\det(\boldsymbol{H}^{\mathcal{H}}\boldsymbol{H}+\sigma_w^2\boldsymbol{I})>\det(\boldsymbol{H}^{\mathcal{H}}\boldsymbol{H})$, we will have $\inf(\det(\boldsymbol{H}^{\mathcal{H}}\boldsymbol{H}))=0$, which contradicts the assumption that $\sup(od(\boldsymbol{H}))<\epsilon<1$. Therefore, we have $\epsilon'<1$ when $\epsilon<1$. ■

APPENDIX B

PROOF OF THEOREM 1

For the system given in (1), ZF detector is given in (7). Here, it is straightforward to see that the quantization step amounts to make a hard decision on every single entry of $\hat{\boldsymbol{s}}$ into alphabet $\mathcal{S}$.

Since all the entries of $\boldsymbol{s}$ belong to the Gaussian integer ring, it is straightforward to see that if the real and imaginary parts of the n^{th} entry of $\boldsymbol{\eta} = \boldsymbol{H}^{\dagger}\boldsymbol{w}$ are in the interval $(-\frac{1}{2}, \frac{1}{2})$, we will definitely decode the n^{th} symbol of $\boldsymbol{s}$ correctly. Let us define $\boldsymbol{H}^{\dagger} = [\boldsymbol{a}_1, \boldsymbol{a}_2, \ldots, \boldsymbol{a}_N]^T$, where $\boldsymbol{a}_n^T, n \in [1, N]$ is the n^{th} row of $\boldsymbol{H}^{\dagger}$. Hence, if $|\boldsymbol{a}_n^T\boldsymbol{w}|$ is less than $\frac{1}{2}$, that means both $|\Re[\eta_n]|$ and $|\Im[\eta_n]|$ are less than $\frac{1}{2}$, we will definitely decode the n^{th} symbol of $\boldsymbol{s}$ correctly. Thus, the error probability of the n^{th} symbol for a given $\boldsymbol{H}$, $P_{e,n|H}$ is upper-bounded by

$$P_{e,n|H} \leq P\left(|\boldsymbol{a}_n^T\boldsymbol{w}| \geq \frac{1}{2}\middle| \boldsymbol{H}\right). \tag{86}$$

From [96, Lemma 1], we obtain the following inequality:

$$\|\boldsymbol{a}_n^T\| \leq \frac{1}{\sqrt{1 - od(\boldsymbol{H})} \cdot \|\boldsymbol{h}_n\|} \tag{87}$$

where $\boldsymbol{h}_n, n \in [1, N]$ represents the n^{th} column of $\boldsymbol{H}$. Because

$$|\boldsymbol{a}_n^T\boldsymbol{w}| \leq \|\boldsymbol{a}_n^T\| \cdot \|\boldsymbol{w}\| \leq \frac{1}{\sqrt{1 - od(\boldsymbol{H})} \cdot \|\boldsymbol{h}_n\|}\|\boldsymbol{w}\|, \tag{88}$$

$P_{e,n|H}$ is further bounded by

$$P_{e,n|H} \leq P\left(\frac{\|\boldsymbol{w}\|}{\sqrt{1 - od(\boldsymbol{H})} \cdot \|\boldsymbol{h}_n\|} \geq \frac{1}{2}\middle| \boldsymbol{H}\right). \tag{89}$$

Furthermore, as we have assumed, if there exists $\epsilon \in (0, 1)$ such that $\forall \boldsymbol{H}$, $od(\boldsymbol{H}) \leq \epsilon$, we obtain the following inequality:

$$P_{e,n|H} \leq P\left(\|\boldsymbol{w}\| \geq \frac{\sqrt{1-\epsilon}}{2}\|\boldsymbol{h}_n\|\middle| \boldsymbol{H}\right). \tag{90}$$

Here, we notice that ϵ is a constant independent of $\boldsymbol{H}$.

Thus, by averaging (133) with respect to the random matrix $\boldsymbol{H}$, the average error probability can be further simplified as

$$\begin{aligned} P_{e,n} = E_H\left[P_{e,n|H}\right] &\leq E_H\left[P\left(\|\boldsymbol{w}\|^2 \geq \frac{1-\epsilon}{4}\|\boldsymbol{h}_n\|^2 \middle| \boldsymbol{H}\right)\right] \\ &= E_w\left[P\left(\|\boldsymbol{h}_n\|^2 \leq \frac{4\|\boldsymbol{w}\|^2}{1-\epsilon} \middle| \boldsymbol{w}\right)\right]. \end{aligned} \tag{91}$$

Suppose that the rank of the covariance matrix $\boldsymbol{R} = E[\boldsymbol{h}_n\boldsymbol{h}_n^{\mathcal{H}}]$ is D_n and $D_n \leq M$. Using the eigenvalue decomposition, we have $\boldsymbol{R} = \boldsymbol{U}\boldsymbol{\Lambda}\boldsymbol{U}^{\mathcal{H}}$, where $\boldsymbol{U}$ is an $M \times D_n$ unitary matrix and $\boldsymbol{\Lambda}$ is a $D_n \times D_n$ diagonal matrix. Define $\tilde{\boldsymbol{h}}_n$ as a $D_n \times 1$ vector, whose entries are independent Gaussian random variables with zero mean and variance $\sigma_{n,d}^2$. Since $\boldsymbol{h}_n$ has identical distribution with $\boldsymbol{U}\tilde{\boldsymbol{h}}_n$, for any $\beta > 0$ we have:

$$P\left(\|\boldsymbol{h}_n\|^2 \leq \beta\right) = P\left(\|\tilde{\boldsymbol{h}}_n\|^2 \leq \beta\right) \leq \prod_{d=1}^{D_n} P(|\tilde{h}_{n,d}|^2 \leq \beta), \tag{92}$$

where $\tilde{h}_{n,d}$ is the d^{th} entry of $\tilde{\boldsymbol{h}}_n$. Because $\tilde{h}_{n,d}$ is Gaussian distributed, $2|\tilde{h}_{n,d}|^2/\sigma_{n,d}^2$ is Chi-square distributed with degrees of freedom 2. Therefore, we have

$$\begin{aligned} P\left(\frac{2|\tilde{h}_{n,d}|^2}{\sigma_{n,d}^2} \leq \frac{2\beta}{\sigma_{n,d}^2}\right) &= 1 - e^{-\gamma_{n,d}} \\ &= e^{-\gamma_{n,d}} \sum_{k=1}^{\infty} \frac{(\gamma_{n,d})^{k-1}}{k!}\gamma_{n,d}, \end{aligned} \tag{93}$$

where $\gamma_{n,d} = \frac{\beta}{\sigma_{n,d}^2}$. Plugging (93) into (92), we obtain the upper bound

$$P\left(\|\boldsymbol{h}_n\|^2 \leq \beta\right) \leq c_n \beta^{D_n}, \tag{94}$$

where c_n is defined and bounded as

$$c_n = \prod_{d=1}^{D_n} \frac{e^{-\gamma_{n,d}}}{\sigma_{n,d}^2} \sum_{k=1}^{\infty} \frac{(\gamma_{n,d})^{k-1}}{k!} \leq \prod_{d=1}^{D_n} \frac{1}{\sigma_{n,d}^2}.$$

Consequently, the probability term in (134) is bounded as

$$\begin{aligned} P_{e,n} &\leq E_w \left[P\left(\|\boldsymbol{h}_n\|^2 \leq \frac{4\|\boldsymbol{w}\|^2}{1-\epsilon} \middle| \boldsymbol{w} \right) \right] \\ &\leq E_w \left[c_n \left(\frac{4}{1-\epsilon} \right)^{D_n} \|\boldsymbol{w}\|^{2D_n} \right] \\ &= c_n \left(\frac{4}{1-\epsilon} \right)^{D_n} \frac{(2D_n-1)!}{(D_n-1)!} \left(\frac{1}{\sigma_w^2} \right)^{-D_n}, \end{aligned} \tag{95}$$

where the last equality is based on the pdf of the Chi-square distribution [43, p. 25]. Therefore, the diversity order of the ZF equalizer for the n^{th} symbol is greater than or equal to $D_n = \text{rank}(E[\boldsymbol{h}_n \boldsymbol{h}_n^{\mathcal{H}}])$, if there exists $\epsilon \in (0,1)$ such that $\forall \boldsymbol{H}$, $od(\boldsymbol{H}) \leq \epsilon$. In general, for the system in (1), the diversity order of the ZF equalizer is greater than or equal to $\min_n\{\text{rank}(E[\boldsymbol{h}_n \boldsymbol{h}_n^{\mathcal{H}}])\}$.

Now, let us revisit the diversity order of MLE. According to [101, p. 66], we know that for MLE, the pairwise error probability for an error pattern $\boldsymbol{e} = \boldsymbol{s} - \boldsymbol{s}'$ $(\boldsymbol{s} \neq \boldsymbol{s}')$ is bounded as

$$P(\boldsymbol{s} \to \boldsymbol{s}' \mid \boldsymbol{H}) \leq \exp\left(-\frac{\|\boldsymbol{H}\boldsymbol{e}\|^2}{4\sigma_w^2} \right) = \exp\left(-\frac{\|\boldsymbol{h}_e\|^2}{4\sigma_w^2} \right), \tag{96}$$

where $\boldsymbol{h}_e = \boldsymbol{H}\boldsymbol{e}$, which is a linear combination of $\boldsymbol{h}_n$'s, $n \in [1, N]$, with coefficients $\boldsymbol{e}$ drawn from Gaussian integer ring. Furthermore, by averaging (96) with respect to $\boldsymbol{H}$, we obtain the error probability as [80, Chp. 14]

$$P(\boldsymbol{s} \to \boldsymbol{s}') \leq C_e \left(\frac{1}{\sigma_w^2} \right)^{-G_{d,e}}, \tag{97}$$

where C_e is a finite constant and $G_{d,e} = \text{rank}(E[\boldsymbol{h}_e \boldsymbol{h}_e^{\mathcal{H}}])$. Thus, the diversity order that MLE can collect is

$$G_d^{ML} = \min_{e \neq 0} G_{d,e} = \min_{e \neq 0} \text{rank}(E[\boldsymbol{h}_e \boldsymbol{h}_e^{\mathcal{H}}]). \tag{98}$$

Compared with the diversity of the ZF equalizer, it is straightforward to obtain

$$G_d^{ML} = \min_{e \neq 0} \text{rank}(E[\boldsymbol{h}_e \boldsymbol{h}_e^{\mathcal{H}}]) \leq \min_n \text{rank}(E[\boldsymbol{h}_n \boldsymbol{h}_n^{\mathcal{H}}]) \leq G_d^{ZF}.$$

Thus, we conclude that, if $od(\boldsymbol{H}) < \epsilon$ and $\epsilon < 1$, the ZF equalizer collects the same diversity as that exploited by MLE ■

APPENDIX C

PROOF OF THEOREM 2

Given the instantaneous capacity difference in (23) and the condition $od(\boldsymbol{H}(\boldsymbol{H}^{\mathcal{H}}\boldsymbol{H})^{-1}) \leq \epsilon$, we have

$$C_{ML}(\boldsymbol{H}) - C_{ZF}(\boldsymbol{H}) \leq -\log_2(1-\epsilon) := C_\epsilon, \tag{99}$$

where C_ϵ is finite. Therefore, the outage probability of the capacity of ZF equalizer is upper-bounded by

$$P(C_{ZF}(\boldsymbol{H}) < C_{th}) \leq P\left(C_{ML}(\boldsymbol{H}) < (C_{th} + C_\epsilon)\right). \tag{100}$$

Because $C_{ZF}(\boldsymbol{H}) \leq C_{ML}(\boldsymbol{H})$ in (22), we have that the outage capacity of the ZF equalizer is lower bounded by

$$P(C_{ML}(\boldsymbol{H}) < C_{th}) \leq P(C_{ZF}(\boldsymbol{H}) < C_{th}). \tag{101}$$

Combining (100) with (101), we claim that when at high SNR, $od(\boldsymbol{H}(\boldsymbol{H}^{\mathcal{H}}\boldsymbol{H})^{-1}) \leq \epsilon$, and $\epsilon \in (0,1)$, the outage probability of the ZF capacity is parallel with the one of MLE. ■

APPENDIX D

PROOF OF LEMMA 2

Suppose that $od(\boldsymbol{H}) < \epsilon < 1$ but $od((\boldsymbol{H}^\dagger)^{\mathcal{H}})$ does not have an upper bound less than 1. That means $\sup(od((\boldsymbol{H}^\dagger)^{\mathcal{H}})) = 1$. Thus, for any constant $\epsilon' \in (0, 1)$, there exists a non-empty set $\mathcal{P} = \{\boldsymbol{H} : od((\boldsymbol{H}^\dagger)^{\mathcal{H}}) > \epsilon'\}$. Furthermore, $\forall \boldsymbol{H} \in \mathcal{P}$, based on the definition of od in (10), we have

$$\frac{\det\left((\boldsymbol{H}^{\mathcal{H}}\boldsymbol{H})^{-1}\right)}{\prod_{n=0}^{N}\|\boldsymbol{a}_n\|^2} < 1 - \epsilon', \tag{102}$$

where $\boldsymbol{a}_n$ is the n^{th} column of $(\boldsymbol{H}^\dagger)^{\mathcal{H}}$. Based on (87), we have

$$\frac{(\sqrt{1 - od(\boldsymbol{H})})^{2N}\prod_{n=0}^{N}\|\boldsymbol{h}_n\|^2}{\det(\boldsymbol{H}^{\mathcal{H}}\boldsymbol{H})} < 1 - \epsilon'.$$

Then, according to the definition of od in (10) again, it is straightforward to obtain

$$(1 - od(\boldsymbol{H}))^{N-1} < 1 - \epsilon',$$

Therefore, we obtain the lower bound of $od(\boldsymbol{H})$ as

$$od(\boldsymbol{H}) > 1 - (1 - \epsilon')^{\frac{1}{N-1}}. \tag{103}$$

Thus, we can see as ϵ' approaches 1, $od(\boldsymbol{H})$ for $\boldsymbol{H} \in \mathcal{P}$ also approaches 1, which means there is no upper bound for $od(\boldsymbol{H})$ that is strictly less than 1. This contradicts with the condition that $od(\boldsymbol{H}) < \epsilon$. Hence, $od((\boldsymbol{H}^\dagger)^{\mathcal{H}})$ has an upper bound which is strict less than 1. ■

APPENDIX E

PROOF OF THEOREM 3

For the $M \times N$ channel matrix $\boldsymbol{H} = [\boldsymbol{h}_1, \boldsymbol{h}_2, \ldots, \boldsymbol{h}_N]$ in (1), with the QR decomposition, we rewrite $od(\boldsymbol{H})$ in (10) as

$$\begin{aligned} od(\boldsymbol{H}) &= 1 - \frac{\det(\boldsymbol{H}^{\mathcal{H}}\boldsymbol{H})}{\prod_{n=1}^{N} |\boldsymbol{h}_n|^2} = 1 - \frac{\prod_{n=1}^{N} R_{n,n}^2}{\prod_{n=1}^{N} |\boldsymbol{r}_n|^2} \\ &= 1 - \prod_{n=1}^{N} \frac{R_{n,n}^2}{R_{n,n}^2 + \sum_{m=1}^{n-1} |R_{m,n}|^2}, \end{aligned} \tag{104}$$

where $\boldsymbol{r}_n$ is the n^{th} column of $\boldsymbol{R}$. From Lemma 3, we know that $2R_{n,n}^2$ is Chi-square distributed with $2(M - n + 1)$ DOF. Since the off-diagonal entries $R_{m,n}$ are i.i.d. complex Gaussian random variables with zero mean and unit variance, $2\sum_{m=1}^{n-1} |R_{m,n}|^2$ is also Chi-square distributed with $2(n-1)$ DOF [78]. As we know, a Chi-square random variable with $2n$ DOF can also be considered as Gamma distributed with parameters $(n, 2)$. Thus, according to [78, p. 188], $\frac{R_{n,n}^2}{R_{n,n}^2 + \sum_{m=1}^{n-1} |R_{m,n}|^2}$ is a Beta random variable with parameters $(M - n + 1, n - 1)$. Then we can rewrite (104) as

$$1 - od(\boldsymbol{H}) = \prod_{n=1}^{N} \frac{R_{n,n}^2}{R_{n,n}^2 + \sum_{m=1}^{n-1} |R_{m,n}|^2} = \prod_{n=1}^{N} X_n, \tag{105}$$

where $X_n \sim \boldsymbol{\beta}(M-n+1, n-1)$ and $\beta(a, b)$ denotes Beta distribution with parameters a and b. Now to find the distribution of od becomes to find the distribution of the product of N independent Beta random variables. The distribution of the product of N independent Beta random variables can be computed by induction from the distribution of the product of $N - 1$ Beta variables. The exact distribution of the product of independent Beta random variables can be found by following the approach in [31, p. 58]. Here, we correct and simplify the expression according to our specific problem. Specifically, the PDF of the od of the i.i.d. Gaussian channel matrix $\boldsymbol{H}$ is

expressed as

$$f(x) = \left(\prod_{n=1}^{N} \frac{(M-1)!}{(M-n)!} \right) \sum_{k=1}^{N-1} \sum_{\ell=0}^{k-1} \frac{\rho_{k,\ell}(1-x)^{M-N+k-1}(-\ln(1-x))^{k-1-\ell}}{(k-1-\ell)!\ell!} \tag{106}$$

where

$$\rho_{k,0} = \prod_{q=1, q\neq k}^{N-1} (q-k)^{-q} \qquad \text{and}$$

$$\rho_{k,\ell} = \sum_{r=0}^{\ell-1} \prod_{q=1, q\ \neq k}^{N-1} (-1)^{r+1} \binom{\ell-1}{r} \frac{r! \cdot q \cdot \rho_{k,\ell-1-r}}{(q-k)^{r+1}}. \tag{107}$$

■

APPENDIX F

PROOF OF PROPOSITION 5

According to the CLLL reduction criterion in (39), for a reduced basis $\tilde{\boldsymbol{H}}$, we have

$$|\tilde{R}_{i,i}|^2 \geq \delta|\tilde{R}_{i-1,i-1}|^2 - |\tilde{R}_{i-1,i}|^2 \geq \left(\delta - \frac{1}{2}\right)|\tilde{R}_{i-1,i-1}|^2,$$

which can be generalized as $|\tilde{R}_{i,i}|^2 \leq (\delta - \frac{1}{2})^{i-k}|\tilde{R}_{k,k}|^2$, for $1 \leq i < k \leq N$. Furthermore, we have

$$\begin{aligned}\|\tilde{\boldsymbol{r}}_k\|^2 &= |\tilde{R}_{k,k}|^2 + \sum_{i=1}^{k-1}|\tilde{R}_{i,k}|^2 \leq |\tilde{R}_{k,k}|^2 + \sum_{i=1}^{k-1}\frac{1}{2}|\tilde{R}_{i,i}|^2 \\ &\leq |\tilde{R}_{k,k}|^2 + \sum_{i=1}^{k-1}\frac{1}{2}\left(\delta - \frac{1}{2}\right)^{i-k}|\tilde{R}_{k,k}|^2, \end{aligned} \tag{108}$$

where $\tilde{\boldsymbol{r}}_k$ is the k^{th} column of $\tilde{\boldsymbol{R}}$. Defining $\xi = \frac{2}{2\delta-1}$, since $\delta \in (\frac{1}{2}, 1)$, $\xi \in (2, \infty)$. Eq. (108) can be simplified as

$$\|\tilde{\boldsymbol{r}}_k\|^2 \leq \left(\frac{1}{2} + \frac{1-\xi^k}{2(1-\xi)}\right)|\tilde{R}_{k,k}|^2 \leq \frac{1}{2}\xi^k|\tilde{R}_{k,k}|^2. \tag{109}$$

Thus, for the reduced basis $\tilde{\boldsymbol{H}}$, the orthogonality deficiency $od(\tilde{\boldsymbol{H}})$ satisfies

$$\begin{aligned} od(\tilde{\boldsymbol{H}}) &= 1 - \frac{\det(\tilde{\boldsymbol{H}}^{\mathcal{H}}\tilde{\boldsymbol{H}})}{\prod_{k=1}^{N}\|\tilde{\boldsymbol{h}}_k\|^2} = 1 - \frac{\prod_{k=1}^{N}|\tilde{R}_{k,k}|^2}{\prod_{k=1}^{N}\|\tilde{\boldsymbol{r}}_k\|^2} \\ &\leq 1 - \frac{\prod_{k=1}^{N}|\tilde{R}_{k,k}|^2}{\prod_{k=1}^{N}\frac{1}{2}\xi^k|\tilde{R}_{k,k}|^2} \\ &= 1 - 2^N\xi^{-\frac{N(N+1)}{2}} = 1 - 2^N\left(\frac{2}{2\delta-1}\right)^{-\frac{N(N+1)}{2}}. \end{aligned} \tag{110}$$

Therefore, we have

$$\sqrt{1 - od(\tilde{\boldsymbol{H}})} \geq 2^{\frac{N}{2}}\left(\frac{2}{2\delta-1}\right)^{-\frac{N(N+1)}{4}} := c_\delta.$$

Similar proof for RLLL can be found in [51]. ■

APPENDIX G

PROOF OF THEOREM 4

If the $S(\boldsymbol{H})$ is bounded by a finite number ξ, $\forall \boldsymbol{H}$, it is ready to see that

$$\|\boldsymbol{h}_m\|^2 \|\boldsymbol{a}_m^T\|^2 \leq \sum_{n=1}^{N} \|\boldsymbol{h}_n\|^2 \|\boldsymbol{a}_n^T\|^2 = S(\boldsymbol{H}) \leq \xi, \quad \text{for} \quad m = 1, 2, \ldots, N, \tag{111}$$

where $\boldsymbol{a}_m^T$ is the m^{th} row of $\boldsymbol{H}^\dagger$. Furthermore, we obtain that

$$\|\boldsymbol{a}_m^T\| \leq \frac{\xi}{\|\boldsymbol{h}_m\|}, \tag{112}$$

which is different from Eq. (87) in Appendix B by only a constant factor on the right side of the inequality. Thus, following the procedures in Eqs. (87)-(141) in Appendix B, we arrive the following upper bound on the average error probability

$$P_{e,n} \leq c_n \; \xi^M \; \frac{(2D_n - 1)!}{(D_n - 1)!} \left(\frac{1}{\sigma_w^2} \right)^{-D_n}, \tag{113}$$

where c_n is a finite constant, the same as in Eq. (141). Therefore, the diversity order of ZF-LE is greater than or equal to $D_n = \text{rank}(E[\boldsymbol{h}_n \boldsymbol{h}_n^{\mathcal{H}}])$. Therefore, as shown in Appendix B, ZF-LE collects the same diversity as that of the MLE.

APPENDIX H

PROOF OF PROPOSITION 6

The Gaussian reduction algorithm is an LR algorithm for lattices in two dimensions [32]. It has been applied onto linear equalizers to improve their performance for 2x2 MIMO communication systems by Yao and Wornell [122]. The pseudo code of this algorithm is given in Table 15, where the basis vectors are $\boldsymbol{b}_1$ and $\boldsymbol{b}_2$. When the iterative procedure stops, the resulting basis will have the following properties

$$\|\boldsymbol{b}_1\| \leq \|\boldsymbol{b}_2\|, \tag{114}$$

$$|\mathrm{Re}(\langle \boldsymbol{b}_1, \boldsymbol{b}_2 \rangle)| \leq \frac{1}{2}\|\boldsymbol{b}_1\|^2 \text{ and } |\mathrm{Im}(\langle \boldsymbol{b}_1, \boldsymbol{b}_2 \rangle)| \leq \frac{1}{2}\|\boldsymbol{b}_1\|^2. \tag{115}$$

Bases satisfying (114) and (115) are called Gaussian reduced bases. These two properties imply that: i) For a Gaussian reduced basis, $\boldsymbol{b}_1$ is the shortest vector in the lattice and $\boldsymbol{b}_2$ is the shortest vector not a multiple of $\boldsymbol{b}_1$ [122]; ii) A Gaussian reduced basis of a particular lattice is unique (up to signs) [124, p. 244].

For a real lattice, define the angle between $\boldsymbol{b}_1$ and $\boldsymbol{b}_2$ as β and the angle between $\boldsymbol{b}_1$ and $\boldsymbol{b}_1'$ as α, as shown in Figure 18. It is ready to see that $\boldsymbol{b}_1'$ and $\boldsymbol{b}_2'$ are also β (or $2\alpha + \beta$) angle apart from each other, because $\boldsymbol{b}_1'$ is orthogonal to $\boldsymbol{b}_2$ and so is $\boldsymbol{b}_2'$ to $\boldsymbol{b}_1$. Thus, we can rewrite the inner products (see Figure 18) as

$$\langle \boldsymbol{b}_1, \boldsymbol{b}_2 \rangle = \|\boldsymbol{b}_1\| \, \|\boldsymbol{b}_2\| \cos(\beta) \qquad \text{and} \qquad \langle \boldsymbol{b}_1', \boldsymbol{b}_2' \rangle = -\|\boldsymbol{b}_1'\| \, \|\boldsymbol{b}_2'\| \cos(\beta), \tag{116}$$

This algebraic argument also holds for complex case. As shown in [124, Eq. (7)], the complex angle β between $\boldsymbol{b}_1$ and $\boldsymbol{b}_2$ is expressed as

$$\cos(\beta) = \cos[\angle(\tilde{\boldsymbol{b}}_1, \tilde{\boldsymbol{b}}_2)] + \sqrt{-1}\cos[\angle(\bar{\boldsymbol{b}}_1, \tilde{\boldsymbol{b}}_2)], \tag{117}$$

Table 15: The Gaussian Reduction Algorithm

Do
  If $\|\boldsymbol{b}_2\| < \|\boldsymbol{b}_1\|$ swap $(\boldsymbol{b}_1, \boldsymbol{b}_2)$
  $\mu \leftarrow \left\lfloor \frac{\langle \boldsymbol{b}_1, \boldsymbol{b}_2 \rangle}{\|\boldsymbol{b}_1\|^2} \right\rceil$
  $\boldsymbol{b}_2 \leftarrow \boldsymbol{b}_2 - \mu \boldsymbol{b}_1$
While $\|\boldsymbol{b}_2\| < \|\boldsymbol{b}_1\|$

where

$$\tilde{\boldsymbol{b}}_1 = [\mathrm{Re}(\boldsymbol{b}_1(1)); \mathrm{Im}(\boldsymbol{b}_1(1)); \mathrm{Re}(\boldsymbol{b}_1(2)); \mathrm{Im}(\boldsymbol{b}_1(2))]$$

$$\text{and } \bar{\boldsymbol{b}}_1 = [-\mathrm{Im}(\boldsymbol{b}_1(1)); \mathrm{Re}(\boldsymbol{b}_1(1)); -\mathrm{Im}(\boldsymbol{b}_1(2)); \mathrm{Re}(\boldsymbol{b}_1(2))]$$

are obtained by extending $\boldsymbol{b}_1$ to real vectors. Similarly, the complex angle β' between $\boldsymbol{b}_1'$ and $\boldsymbol{b}_2'$, can be expressed as $\cos(\beta') = \cos[\angle(\tilde{\boldsymbol{b}}_1', \tilde{\boldsymbol{b}}_2')] + \sqrt{-1}\cos[\angle(\bar{\boldsymbol{b}}_1', \tilde{\boldsymbol{b}}_2')]$ by extending $\boldsymbol{b}_1'$ and $\boldsymbol{b}_2'$ to real vectors. Because the real lattice $(\tilde{\boldsymbol{b}}_1', \tilde{\boldsymbol{b}}_2')$ is still the dual lattice of $(\tilde{\boldsymbol{b}}_1, \tilde{\boldsymbol{b}}_2)$ and the same for $(\bar{\boldsymbol{b}}_1', \tilde{\boldsymbol{b}}_2')$ and $(\bar{\boldsymbol{b}}_1, \tilde{\boldsymbol{b}}_2)$, we have $\cos(\beta) = -\cos(\beta')$. Thus, Eq. (116) also holds true for complex case.

Furthermore, according to the definition of the dual basis, we obtain

$$\begin{cases} 1 = \langle \boldsymbol{b}_1', \boldsymbol{b}_1 \rangle = \|\boldsymbol{b}_1'\| \, \|\boldsymbol{b}_1\| \cos(\alpha) \\ 1 = \langle \boldsymbol{b}_2, \boldsymbol{b}_2' \rangle = \|\boldsymbol{b}_2\| \, \|\boldsymbol{b}_2'\| \cos(\alpha) \end{cases} \Rightarrow \frac{\|\boldsymbol{b}_1\|}{\|\boldsymbol{b}_2\|} = \frac{\|\boldsymbol{b}_2'\|}{\|\boldsymbol{b}_1'\|}. \tag{118}$$

Furthermore, the parameter λ_{ij} is calculated as

$$\lambda_{ij} = \left\lfloor \tilde{\lambda}_{ij} \right\rceil = \left\lfloor \frac{1}{2} \left(\frac{\langle \boldsymbol{b}_i', \boldsymbol{b}_j' \rangle}{\left\|\boldsymbol{b}_j'\right\|^2} - \frac{\langle \boldsymbol{b}_i, \boldsymbol{b}_j \rangle}{\left\|\boldsymbol{b}_i\right\|^2} \right) \right\rceil. \tag{119}$$

Plugging (116) and (118) into (119) for $i \neq j$, we have

$$\lambda_{ij} = \left\lfloor \frac{1}{2} \left(-\frac{\|\boldsymbol{b}_i'\| \cos(\beta)}{\left\|\boldsymbol{b}_j'\right\|} - \frac{\|\boldsymbol{b}_j\| \cos(\beta)}{\left\|\boldsymbol{b}_i\right\|} \right) \right\rceil = \left\lfloor -\frac{\|\boldsymbol{b}_j\| \cos(\beta)}{\left\|\boldsymbol{b}_i\right\|} \right\rceil = -\left\lfloor \frac{\langle \boldsymbol{b}_i, \boldsymbol{b}_j \rangle}{\left\|\boldsymbol{b}_i\right\|^2} \right\rceil.$$

Specifically, λ_{12} and λ_{21} for 2-D lattices can be simply expressed as

$$\lambda_{12} = -\left\lfloor \frac{\langle \boldsymbol{b}_1, \boldsymbol{b}_2 \rangle}{\left\|\boldsymbol{b}_1\right\|^2} \right\rceil, \quad \lambda_{21} = -\left\lfloor \frac{\langle \boldsymbol{b}_2, \boldsymbol{b}_1 \rangle}{\left\|\boldsymbol{b}_2\right\|^2} \right\rceil. \tag{120}$$

When the algorithm stops, we have the resulting basis satisfying $\lambda_{12} = \lambda_{21} = 0$ [50]. If $\|\boldsymbol{b}_1\| \leq \|\boldsymbol{b}_2\|$, we note that $-\mu = \lambda_{12}$, where μ is defined in Table 15. Therefore we have $\mu = 0$. Thus, the Seysen reduced basis satisfies both properties of a Gaussian reduced basis stated in Eqs. (114) and (115). If $\|\boldsymbol{b}_2\| < \|\boldsymbol{b}_1\|$, we can just interchange $\boldsymbol{b}_1$ and $\boldsymbol{b}_2$ by multiplying $\boldsymbol{B}$ with a permutation matrix. Then, we still have $-\mu = \lambda_{21} = 0$. This means, the Seysen reduced basis $\boldsymbol{B}$ is the same as the Gaussian reduced basis (up to signs). ■

APPENDIX I

PROOF OF PROPOSITION 7

We first define the angle between two vectors either in a real or a complex vector space as follows.

Definition 7 *The angle between two vectors* $\boldsymbol{a}$ *and* $\boldsymbol{b}$ *is defined as*

$$\cos(\theta) = \frac{\langle \boldsymbol{a}, \boldsymbol{b} \rangle}{\|\boldsymbol{a}\| \|\boldsymbol{b}\|}. \tag{121}$$

If $\{\boldsymbol{a}, \boldsymbol{b}\} \in \mathbb{R}$ *the angle is real, and if* $\{\boldsymbol{a}, \boldsymbol{b}\} \in \mathbb{C}$*, the angle is generally complex. Furthermore, for the complex case we define the real Hermitian angle* $\theta_H \in [0, \frac{\pi}{2}]$ *as in [83]*

$$\cos(\theta_H) = \frac{|\langle \boldsymbol{a}, \boldsymbol{b} \rangle|}{\|\boldsymbol{a}\| \|\boldsymbol{b}\|}. \tag{122}$$

We give the analysis for real lattices (i.e. $\boldsymbol{b}_i \in \mathbb{R}^N$) and complex lattices (i.e. $\boldsymbol{b}_i \in \mathbb{C}^N$) respectively.

a) Real lattices: When SA stops $\lambda_{12} = \lambda_{21} = 0$. Thus, $\widetilde{\lambda}_{ij}$'s in (119) are bounded as follows

$$\begin{cases} -\frac{1}{2} \leq \widetilde{\lambda}_{12} \leq \frac{1}{2} \\ -\frac{1}{2} \leq \widetilde{\lambda}_{21} \leq \frac{1}{2} \end{cases} \Leftrightarrow \begin{cases} -\frac{1}{2} \leq \frac{\|\boldsymbol{b}_2\|}{\|\boldsymbol{b}_1\|} \cos(\beta) \leq \frac{1}{2} \\ -\frac{1}{2} \leq \frac{\|\boldsymbol{b}_1\|}{\|\boldsymbol{b}_2\|} \cos(\beta) \leq \frac{1}{2} \end{cases}.$$

Multiplying these two equations yields $\cos^2(\beta) \leq \frac{1}{4}$ which leads to $\sin^2(\beta) = 1 - \cos^2(\beta) \geq \frac{3}{4}$. Thus, with the expression of $S(\boldsymbol{B})$ in (34) for $N = 2$, we obtain

$$S(\boldsymbol{B}) = \frac{2}{\cos^2(\alpha)} = \frac{2}{\sin^2(\beta)} \leq \frac{8}{3}. \tag{123}$$

b) Complex lattices: When SA stops, the real and imaginary parts of $\widetilde{\lambda}_{ij}$ are bounded as follows

$$\begin{cases} -\frac{1}{2} \le \{\mathrm{Re}(\widetilde{\lambda}_{12}), \mathrm{Im}(\widetilde{\lambda}_{12})\} \le \frac{1}{2} \\ -\frac{1}{2} \le \{\mathrm{Re}(\widetilde{\lambda}_{21}), \mathrm{Im}(\widetilde{\lambda}_{21})\} \le \frac{1}{2} \end{cases} \Leftrightarrow \begin{cases} -\frac{1}{2} \le \frac{\|\boldsymbol{b}_2\|}{\|\boldsymbol{b}_1\|}\{\mathrm{Re}(\cos(\beta)), \mathrm{Im}(\cos(\beta))\} \le \frac{1}{2} \\ -\frac{1}{2} \le \frac{\|\boldsymbol{b}_1\|}{\|\boldsymbol{b}_2\|}\{\mathrm{Re}(\cos(\beta)), \mathrm{Im}(\cos(\beta))\} \le \frac{1}{2} \end{cases}$$

Multiplying the inequalities for real and imaginary parts respectively, we get $(\mathrm{Re}(\cos(\beta)))^2 \le \frac{1}{4}$ and $(\mathrm{Im}(\cos(\beta)))^2 \le \frac{1}{4}$. Furthermore, we can bound the Hermitian angle β_H defined in (122) as

$$\cos^2(\beta_H) = |\cos(\beta)|^2 = (\mathrm{Re}(\cos(\beta)))^2 + (\mathrm{Im}(\cos(\beta)))^2 \le \frac{1}{2}. \tag{124}$$

To continue our proof we need the following lemma.

Lemma 4 *Suppose that* $\boldsymbol{u}$ *and* $\boldsymbol{v}$ *are two orthogonal complex vectors (i.e.* $\langle \boldsymbol{u}, \boldsymbol{v} \rangle = 0$*) and* $\boldsymbol{w}$ *is a complex vector that lies in the vector space spanned by* $\boldsymbol{u}$ *and* $\boldsymbol{v}$*. Denote the Hermitian angle between* $\boldsymbol{u}$ *and* $\boldsymbol{w}$ *as* θ_H *and the Hermitian angle between* $\boldsymbol{v}$ *and* $\boldsymbol{w}$ *as* γ_H*. Then we have*
$\theta_H + \gamma_H = \frac{\pi}{2}$.

Proof: Since $\boldsymbol{w}$ belongs to the vector space spanned by $\boldsymbol{u}$ and $\boldsymbol{v}$, we can express $\boldsymbol{w}$ as a linear combination of $\boldsymbol{u}$ and $\boldsymbol{v}$

$$\boldsymbol{w} = \frac{\langle \boldsymbol{w}, \boldsymbol{u} \rangle \boldsymbol{u}}{\|\boldsymbol{u}\|^2} + \frac{\langle \boldsymbol{w}, \boldsymbol{v} \rangle \boldsymbol{v}}{\|\boldsymbol{v}\|^2} \tag{125}$$

Because $\boldsymbol{u}$ and $\boldsymbol{v}$ are orthogonal, we get

$$\|\boldsymbol{w}\|^2 = \frac{|\langle \boldsymbol{w}, \boldsymbol{u} \rangle|^2 \|\boldsymbol{u}\|^2}{\|\boldsymbol{u}\|^4} + \frac{|\langle \boldsymbol{w}, \boldsymbol{v} \rangle|^2 \|\boldsymbol{v}\|^2}{\|\boldsymbol{v}\|^4} \tag{126}$$

With some simple mathematical derivations, we can rewrite (126) as

$$\frac{|\langle \boldsymbol{w}, \boldsymbol{u} \rangle|^2}{\|\boldsymbol{u}\|^2 \|\boldsymbol{w}\|^2} = 1 - \frac{|\langle \boldsymbol{w}, \boldsymbol{v} \rangle|^2}{\|\boldsymbol{v}\|^2 \|\boldsymbol{w}\|^2} \tag{127}$$

With the definition of the Hermitian angle, (127) can be rewritten as $\cos^2(\theta_H) = 1 - \cos^2(\gamma_H) = \sin^2(\gamma_H)$. Since θ_H and γ_H are real angles in $[0, \frac{\pi}{2}]$, we have $\theta_H + \gamma_H = \frac{\pi}{2}$.

From (34) we know that Seysen's metric $S(\boldsymbol{B})$ in two dimensions can be written as $S(\boldsymbol{B}) = \frac{2}{\cos^2(\alpha)}$. Because $\cos(\alpha) = \frac{1}{\|\boldsymbol{b}_1\|\|\boldsymbol{b}_1'\|} \in \mathbb{R}$, with Lemma 4 it is ready to see that $\cos(\alpha) = \cos(\alpha_H) = \sin(\beta_H)$. Thus, with the inequality in (124) we are now able to upper bound $S(\boldsymbol{B})$ by

$$S(\boldsymbol{B}) = \frac{2}{\cos^2(\alpha)} = \frac{2}{\sin^2(\beta_H)} = \frac{2}{1 - \cos^2(\beta_H)} \leq 4. \qquad \blacksquare$$

APPENDIX J

PROOF OF PROPOSITION 8

The output of the LR-aided ZF equalizer is given in (83). For QAM symbols, the real and imaginary parts of each symbol are drawn from the set $\{-(\sqrt{\mathcal{M}}-1), \cdots, -1, 1, \cdots, \sqrt{\mathcal{M}}-1\}$. Then, by applying $(\boldsymbol{s}-(1+j)\mathbf{1})/2$, we transfer the real and imaginary parts of the constellation to a consecutive integer set, which makes the real and imaginary parts of $\boldsymbol{z}$ are also consecutive integers. Thus, the estimate of $\boldsymbol{s}$ is expressed as

$$\begin{aligned}\hat{\boldsymbol{s}} &= 2\boldsymbol{T}\left\lfloor \frac{1}{2}\left(\boldsymbol{x}-\boldsymbol{T}^{-1}(1+j)\mathbf{1}\right)\right\rfloor + (1+j)\mathbf{1} \\ &= \boldsymbol{s} + 2\boldsymbol{T}\left\lfloor \frac{1}{2}\tilde{\boldsymbol{H}}^{\dagger}\boldsymbol{w}\right\rfloor . \end{aligned} \tag{128}$$

Apparently, if $\left\lfloor \frac{1}{2}\tilde{\boldsymbol{H}}^{\dagger}\boldsymbol{w}\right\rfloor = \mathbf{0}$, $\boldsymbol{s}$ will be decoded correctly. Therefore, the symbol error probability $P_{e|H}$ for a given $\boldsymbol{H}$ is upper-bounded by

$$P_{e|H} \leq 1 - P\left(\left\lfloor \frac{1}{2}\tilde{\boldsymbol{H}}^{\dagger}\boldsymbol{w}\right\rfloor = \mathbf{0} \middle| \boldsymbol{H}\right). \tag{129}$$

Let us denote $\tilde{\boldsymbol{H}}^{\dagger}$ as $[\boldsymbol{a}_1, \boldsymbol{a}_2, \ldots, \boldsymbol{a}_{N_t}]^T$, where $\boldsymbol{a}_i^T, i \in [1, N_t]$ is the i^{th} row of $\tilde{\boldsymbol{H}}^{\dagger}$. The upper bound can be written as

$$P_{e|H} \leq P\left(\max_{1\leq i\leq N_t} |\boldsymbol{a}_i^T\boldsymbol{w}| \geq 1 \;\middle|\; \boldsymbol{H}\right). \tag{130}$$

From [96, Lemma 1], we obtain the following inequality:

$$\max_{1\leq i\leq N_t} \|\boldsymbol{a}_i^T\| \leq \frac{1}{\sqrt{1-od(\tilde{\boldsymbol{H}})}\cdot \min\limits_{1\leq i\leq N_t}\|\tilde{\boldsymbol{h}}_i\|}, \tag{131}$$

where $\tilde{\boldsymbol{h}}_i, i \in [1, N_t]$ represents the i^{th} column of $\tilde{\boldsymbol{H}}$. Because

$$\begin{aligned}\max_{1\le i\le N_t} |\boldsymbol{a}_i^T \boldsymbol{w}| &\le \max_{1\le i\le N_t} \|\boldsymbol{a}_i^T\| \cdot \|\boldsymbol{w}\| \\ &\le \frac{\|\boldsymbol{w}\|}{\sqrt{1-od(\tilde{\boldsymbol{H}})} \cdot \min\limits_{1\le i\le N_t} \|\tilde{\boldsymbol{h}}_i\|},\end{aligned}$$

$P_{e|H}$ is further bounded by

$$P_{e|H} \le P\left(\frac{\|\boldsymbol{w}\|}{\sqrt{1-od(\tilde{\boldsymbol{H}})} \cdot \min\limits_{1\le i\le N_t} \|\tilde{\boldsymbol{h}}_i\|} \ge 1 \,\middle|\, \boldsymbol{H} \right). \tag{132}$$

Furthermore, since $\tilde{\boldsymbol{H}}$ is reduced from $\boldsymbol{H}$ using the CLLL algorithm with parameter δ and $\boldsymbol{H}$ is full rank with probability one, according to (40) in Proposition 5, we have $\sqrt{1-od(\tilde{\boldsymbol{H}})} \ge c_\delta$. Let $\boldsymbol{h}_{\min}$ represent the vector with minimum non-zero norm of all the vectors in the lattice generated by $\boldsymbol{H}$. Since $\boldsymbol{T}$ is unimodular, $\tilde{\boldsymbol{H}}$ spans the same lattice as $\boldsymbol{H}$ with an infinite coefficient set. From the definition of $\boldsymbol{h}_{\min}$, we know that $\|\boldsymbol{h}_{\min}\|$ is less than or equal to $\min\limits_{1\le i\le N_t} \|\tilde{\boldsymbol{h}}_i\|$. In summary, we have [c.f. (130) and (132)]

$$\begin{aligned}P_{e|H} &\le P\left(\max_{1\le i\le N_t} |\boldsymbol{a}_i^T \boldsymbol{w}| \ge 1 \,\middle|\, \boldsymbol{H} \right) \\ &\le P\left(\|\boldsymbol{w}\| \ge c_\delta \|\boldsymbol{h}_{\min}\| \mid \boldsymbol{H} \right).\end{aligned} \tag{133}$$

Thus, by averaging (133) with respect to the random matrix $\boldsymbol{H}$ (or $\boldsymbol{h}_{\min}$), the average symbol error probability can be simplified as:

$$\begin{aligned}P_e = E_H\left[P_{e|H}\right] &\le E_H\left[P\left(\|\boldsymbol{w}\|^2 \ge c_\delta^2 \|\boldsymbol{h}_{\min}\|^2 \middle|\, \boldsymbol{H}\right)\right] \\ &= E_w\left[P\left(\|\boldsymbol{h}_{\min}\|^2 \le \frac{\|\boldsymbol{w}\|^2}{c_\delta^2} \,\middle|\, \boldsymbol{w} \right) \right].\end{aligned} \tag{134}$$

Since $\boldsymbol{w}$ is an $N_r \times 1$ complex white Gaussian noise vector with covariance matrix $\sigma_w^2 \boldsymbol{I}_{N_r}$, $\|\boldsymbol{w}\|^2$ is a central Chi-square random variable with $2N_r$ degrees of freedom and mean $N_r\sigma_w^2$. To simplify the bound in (134), we need the following lemma.

Lemma 5 *Define a lattice* $\mathbb{L}$ *in* $\mathbb{C}^{N_r \times 1}$ *generated by a set of bases* $\boldsymbol{H} = [\boldsymbol{h}_1, \boldsymbol{h}_2, \ldots, \boldsymbol{h}_{N_t}]$ *and a complex integer coefficient set. If all the entries of* $\boldsymbol{H}$ *are i.i.d. complex Gaussian distributed with zero mean and unit variance, then we have* $P\left(\|\boldsymbol{h}_{\min}\|^2 \leq \epsilon\right) \leq c_{N_r N_t} \epsilon^{N_r}$*, where* $c_{N_r N_t}$ *is a finite constant depending on* N_r *and* N_t*.*

Proof: See Appendix C in [67].

Consequently, we obtain that the average error probability in (134) is bounded as

$$\begin{aligned} P_e &\leq E_w \left[P\left(\|\boldsymbol{h}_{\min}\|^2 \leq \frac{\|\boldsymbol{w}\|^2}{c_\delta^2} \middle| \boldsymbol{w} \right) \right] \\ &\leq E_w \left[c_{N_r N_t} \left(\frac{1}{c_\delta^2} \right)^{N_r} \|\boldsymbol{w}\|^{2N_r} \right] \\ &= c_{N_r N_t} \left(\frac{1}{c_\delta^2} \right)^{N_r} \frac{(2N_r - 1)!}{(N_r - 1)!} \left(\frac{1}{\sigma_w^2} \right)^{-N_r}, \end{aligned} \tag{135}$$

where the last equality comes from the N_r^{th} moment of Chi-square random variable $\|\boldsymbol{w}\|^2$, which can be found in [92, p. 14]. Therefore, the diversity order of the LR-aided ZF equalizer is greater than or equal to N_r. However, as we know, the maximum diversity order for the MIMO V-BLAST system is N_r. Thus, the LR-aided ZF equalizer collects diversity N_r. Similarly, for LR-aided MMSE equalizer, we can show that it also collects diversity N_r. ■

APPENDIX K

PROOF OF PROPOSITION 9

Following the same procedures in Appendix J, to prove Proposition 9, we only need to prove the following lemma to establish the diversity claim of the LR-aided LEs for LP-OFDM systems.

Lemma 6 *Let $\mathbb{L}$ be a lattice in $\mathbb{C}^{K\times 1}$ generated by the set of bases $\boldsymbol{H}_{equ} = \boldsymbol{D}_H\boldsymbol{\Theta}$ in* (2) *with complex integer coefficients. Define $\boldsymbol{h}_{\min}$ as the vector that has the minimum non-zero norm among all vectors in $\mathbb{L}$. Then for any $\epsilon > 0$, we have*

$$P\{\|\boldsymbol{h}_{\min}\|^2 \leq \epsilon\} \leq c_D\epsilon^D, \tag{136}$$

where the finite constant c_D depends on $D = \min(K, \rho_h)$ and the channel covariance matrix.

Proof: Let $\boldsymbol{p}_a = \boldsymbol{H}_{equ}\boldsymbol{a}$ be a $K\times 1$ vector in the lattice $\mathbb{L}$ with finite elements spanned by $\boldsymbol{H}_{equ}$ with $\boldsymbol{a}$ being a $K\times 1$ vector with all entries belonging to the complex integer coefficient set. By definition, $\|\boldsymbol{h}_{\min}\|^2 = \arg\min_{\boldsymbol{p}_a\in\mathbb{L},\ \boldsymbol{p}_a\neq\boldsymbol{0}} \|\boldsymbol{p}_a\|^2$. By putting the diagonal entries of $\boldsymbol{D}_H$ into a $K\times 1$ vector $\boldsymbol{h}_H = [H(1), \ldots, H(K)]$, we have

$$\begin{aligned}\|\boldsymbol{p}_a\|^2 = \|\boldsymbol{H}_{equ}\boldsymbol{a}\|^2 &= \|\boldsymbol{D}_H\boldsymbol{\Theta}\boldsymbol{a}\|^2 \\ &= \boldsymbol{h}_H^{\mathcal{H}}\mathrm{diag}[\boldsymbol{\Theta}\boldsymbol{a}]\mathrm{diag}[\boldsymbol{\Theta}\boldsymbol{a}]^{\mathcal{H}}\boldsymbol{h}_H.\end{aligned} \tag{137}$$

Consider the g^{th} group in (2); let $\boldsymbol{F}$ denote the $N_c\times(L+1)$ DFT matrix; in MATLAB notation, let $\boldsymbol{F}_g := \boldsymbol{F}(g:N_g:N_c, 1:L+1)$ with size $K\times(L+1)$. Then we have $\boldsymbol{h}_H = \boldsymbol{F}_g\boldsymbol{h}$, where the $(L+1)\times 1$ column vector $\boldsymbol{h}$ consists of all the $L+1$ channel taps. The correlation matrix of $\boldsymbol{h}$ is $\boldsymbol{R}_h = E[\boldsymbol{h}^{\mathcal{H}}\boldsymbol{h}]$ with rank ρ_h, and SVD as $\boldsymbol{U}_h\boldsymbol{\Lambda}_h\boldsymbol{U}_h^{\mathcal{H}}$. Define a $\rho_h\times 1$ vector $\tilde{\boldsymbol{h}}$ with i.i.d. complex Gaussian entries. Then,

$\boldsymbol{h}$ and $\boldsymbol{U}_h\boldsymbol{\Lambda}_h^{\frac{1}{2}}\tilde{\boldsymbol{h}}$ have identical distributions and thus the same statistical properties. Hence, we can rewrite (137) as (in the following, equality should be interpreted in the sense of equivalence of distributions)

$$\begin{aligned}\|\boldsymbol{p}_a\|^2 &= \tilde{\boldsymbol{h}}^{\mathcal{H}}\boldsymbol{\Lambda}_h^{\frac{1}{2}}\boldsymbol{U}_h^{\mathcal{H}}\boldsymbol{F}_g^{\mathcal{H}}\mathrm{diag}[\boldsymbol{\Theta}\boldsymbol{a}]\mathrm{diag}[\boldsymbol{\Theta}\boldsymbol{a}]^{\mathcal{H}}\boldsymbol{F}_g\boldsymbol{U}_h\boldsymbol{\Lambda}_h^{\frac{1}{2}}\tilde{\boldsymbol{h}} \\ &= \tilde{\boldsymbol{h}}^{\mathcal{H}}\boldsymbol{A}_a\tilde{\boldsymbol{h}} = \tilde{\boldsymbol{h}}^{\mathcal{H}}\boldsymbol{U}_a^{\mathcal{H}}\boldsymbol{\Lambda}_a\boldsymbol{U}_a\tilde{\boldsymbol{h}} \\ &= \bar{\boldsymbol{h}}^{\mathcal{H}}\boldsymbol{\Lambda}_a\bar{\boldsymbol{h}} = \sum_{k=1}^{\min(K,\rho_h)}\alpha_k|\bar{h}_k|^2, \end{aligned} \tag{138}$$

where $\boldsymbol{A}_a$ with SVD as $\boldsymbol{U}_a^{\mathcal{H}}\boldsymbol{\Lambda}_a\boldsymbol{U}_a$ depends on $\boldsymbol{a}$ and the correlation matrix of the channel taps, and α_k, $k \in [1, \min(K, \rho_h)]$ are the eigenvalues of $\boldsymbol{A}_a$. Since $\boldsymbol{F}_{g+1} = \boldsymbol{F}_g\mathrm{diag}[1, e^{j2\pi/N_c}, \ldots, e^{j2\pi L/N_c}]$, the analysis in (138) holds true for any group g. Since $\boldsymbol{U}_a$ contains the $\min(K, \rho_h)$ rows of a unitary matrix, $\bar{h}_k$'s are still i.i.d. complex Gaussian random variables as the entries in $\tilde{\boldsymbol{h}}$. Thanks to the precoder design of $\boldsymbol{\Theta}$, all α_k's are nonzero if $\boldsymbol{a}$ is not a zero vector, i.e., there exists a nonzero minimum of α_k's which does not depend on $\boldsymbol{a}$ [57]. From the definition of $\boldsymbol{h}_{\min}$, it is easy to show that

$$\|\boldsymbol{h}_{\min}\|^2 \geq \left(\min_{\boldsymbol{a}\in\mathbb{Z}[j]^K,\ \boldsymbol{a}\neq\boldsymbol{0}}\alpha_k\right)\left(\sum_{k=1}^{\min(K,\rho_h)}|\bar{h}_k|^2\right). \tag{139}$$

Eq. (139) provides an upper bound for the probability that $\|\boldsymbol{h}_{\min}\|^2$ is less than ϵ as

$$\begin{aligned}P(\|\boldsymbol{h}_{\min}\|^2 \leq \epsilon) &\leq P\left(\left(\min_{\boldsymbol{a}\in\mathbb{Z}[j]^K,\ \boldsymbol{a}\neq\boldsymbol{0}}\alpha_k\right)\left(\sum_{k=1}^{\min(K,\rho_h)}|\bar{h}_k|^2\right) \leq \epsilon\right) \\ &\leq \frac{1}{2^D D!}\left(\min_{\boldsymbol{a}\in\mathbb{Z}[j]^K,\ \boldsymbol{a}\neq\boldsymbol{0}}\alpha_k\right)^{-D}\epsilon^D := c_D\epsilon^D, \end{aligned} \tag{140}$$

where $D = \min(K, \rho_h)$ and c_D is a finite constant, and the second inequality is based on [48, Eq. (40)] when ϵ is small. ■

Note that the proof for Lemma 6 is quite different from the one for the i.i.d. channel case in [67]. Correlated multipath channels are covered here. Thanks to the

precoder design in [57], the minimum vector $\boldsymbol{h}_{\min}$ has the same degrees of freedom as other vectors in the lattice.

Now we are ready to quantify the diversity order collected by the LR-aided ZF equalizer for the LP-OFDM systems. Given Lemma 6, inserting (136) into [67, Eq. (27)] and following [66, Eq. (28)], one can upper bound the average pairwise error probability of LR-aided ZF equalizer as

$$P_e \leq c_D \left(\frac{4}{c_\delta^2}\right)^D \frac{(2D-1)!}{(D-1)!} \left(\frac{1}{\sigma_w^2}\right)^{-D}, \tag{141}$$

where $D = \min(K, \rho_h)$. Therefore, the diversity order of the LR-aided ZF equalizer is greater than or equal to $\min(K, \rho_h)$. Since the maximum diversity order enabled by each group is $\min(K, \rho_h)$, for LP-OFDM , the LR-aided ZF equalizer collects the full diversity order $\min(K, \rho_h)$. ■

REFERENCES

[1] Agrell, E., Eriksson, T., Vardy, A., and Zeger, K., "Closest point search in lattices," *IEEE Transactions on Information Theory*, vol. 48, pp. 2201–2214, Aug. 2002.

[2] Al-Dhahir, N. and Cioffi, J. M., "Block transmission over dispersive channels: transmit filter optimization and realization, and mmse-dfe receiver performance," *IEEE Transactions on Information Theory*, vol. 42, pp. 137–160, Jan. 1996.

[3] Al-Dhahir, N. and Cioffi, J. M., "Block transmission over dispersive channels: Transmit filter optimization and realization, and MMSE-DFE receiver performance," *IEEE Transactions on Information Theory*, vol. 42, pp. 137–160, Jan. 1996.

[4] Avestimehr, A. S. and Tse, D. N. C., "Outage capacity of the fading relay channel in the low-SNR regime," *IEEE Transactions on Information Theory*, vol. 53, pp. 1401–1415, Apr. 2007.

[5] Barbarossa, S., *Multiantenna wireless communication systems*. Artech House, 2005.

[6] Barbero, L. G. and Thompson, J. S., "Fixing the complexity of the sphere decoder for MIMO detection," *IEEE Transactions on Wireless Communications*, vol. 7, pp. 2131–2142, June 2008.

[7] Belfiore, J.-C., Rekaya, G., and Viterbo, E., "The golden code: A 2 x 2 full-rate space-time code with non-vanishing determinants," *IEEE Transactions on Information Theory*, vol. 51, pp. 1432–1436, Apr. 2005.

[8] Benedetto, S. and Biglieri, E., *Principles of digital transmission with wireless applications*. Kluwer Academic, New York, 1999.

[9] Berrou, C., Glavieux, A., and Thitimajshima, P., "Near shannon limit error-correcting coding and decoding: Turbo-codes. 1," in *Proc. of International Conference on Communications*, vol. 2, (Geneva, Switzerland), pp. 1064–1070, May 23-26 1993.

[10] Burg, A., Seethaler, D., and Matz, G., "VLSI implementation of a lattice-reduction algorithm for multi-antenna broadcast precoding," in *Proc. of IEEE International Symposium on Circuits and Systems*, (New Orleans, LA), pp. 673–676, May 27-30 2007.

[11] Burg, A., Seethaler, D., and Matz, G., "VLSI implementation of a lattice-reduction algorithm for multi-antenna broadcast precoding," in *Proc. of International Symp. on Circuit and Systems*, (New Orleans, LA), pp. 673–676, 2007.

[12] Chen, C.-J. and Wang, L.-C., "On the performance of the zero-forcing receiver operating in the multiuser MIMO system with reduced noise enhancement effect," in *Proc. of Global Telecommunications Conference*, vol. 3, (St. Louis, USA), pp. 1294–1298, Nov. 28-Dec. 2 2005.

[13] Choi, W.-J., Negi, R., and Cioffi, J. M., "Combined ML and DFE decoding for the V-BLAST system," in *Proc. of International Conference on Communications*, vol. 3, (New Orleans, USA), pp. 1243–1248, Jun. 18-22 2000.

[14] Fan, D. Y., "The distribution of the product of independent Beta variables," *Communications in Statistics - Theory and Methods*, vol. 20, pp. 4043–4052, 1991.

[15] Foschini, G. J. and Gans, M. J., "On limits of wireless communications in a fading environment when using multiple antennas," *Wireless Personal Communications*, vol. 6, pp. 311–335, Mar. 1998.

[16] Gallager, R. G., *Low-density parity-check codes*. MIT Press, 1963.

[17] Galliou, S. and Belfiore, J. C., "A new family of full rate, fully diverse space-time codes based on Galois theory," in *Proc. of IEEE International Symposium on Information Theory*, (Lausanne, Switzerland), p. 419, June 30-July 5 2002.

[18] Gamal, H. E. and Damen, M. O., "Universal space-time coding," *IEEE Transactions on Information Theory*, vol. 49, pp. 1097–1119, May 2003.

[19] Gan, Y. H. and Mow, W. H., "Complex lattice reduction algorithms for low-complexity MIMO detection," in *Proc. of Global Telecommunications Conference*, (St. Louis, USA), pp. 2953–2957, Nov. 28-Dec. 2 2005.

[20] Gestner, B. and Anderson, D., "Single newton-raphson iteration-rounded divider for lattice reduction algorithms," in *Proc. IEEE Midwest Symposium on Circuits and Systems*, (Knoxville, TN), pp. 966–969, Aug 10-13 2008.

[21] Gestner, B. and Anderson, D., "Automatic generation of modelsim-matlab interface for rtl debugging and verification," in *IEEE Midwest Symp. on Circuits and Systems*, (Montreal, Canada), pp. 1497–1500, 2007.

[22] Gestner, B., Zhang, W., Ma, X., and Anderson, D., "VLSI implementation of a lattice reduction-aided low-complexity equalizer," in *Proc. IEEE Internatinal Conf. on Circuits and Systems for Communications*, (Shanghai, China), pp. 643–647, May 26-28 2008.

[23] Giannakis, G., Liu, Z., Ma, X., and Zhou, S., *Space-time coding for broadband wireless communications*. Wiley, 2006.

[24] Ginis, G. and Cioffi, J. M., "On the relationship between V-BLAST and the GDFE," *IEEE Communications Letters*, vol. 5, pp. 364–366, Sept. 2001.

[25] Goeckel, D. L., "Coded modulation with non-standard signal sets for wireless OFDM systems," in *IEEE International Conference on Communications*, vol. 2, pp. 791–795, 1999.

[26] Goeckel, D. L. and Ananthaswamy, G., "On the design of multidimensional signal sets for OFDM systems," *IEEE Transactions on Communications*, vol. 50, pp. 442–452, Mar. 2002.

[27] Golden, G. D., Foschini, G. J., Valenzuela, R. A., and Wolniansky, P. W., "Detection algorithm and initial laboratory results using V-BLAST space-time communication architecture," *Electronics Letters*, vol. 35, pp. 14–16, Jan. 7 1999.

[28] Goldsmith, A., Jafar, S., Jindal, N., and Vishwanath, S., "Capacity limits of MIMO channels," *IEEE Journal on Selected Areas in Communications*, vol. 21, pp. 684–702, June 2003.

[29] Gore, D. A., Jr., R. W. H., and Paulraj, A. J., "On performance of the zero forcing receiver in presence of transmit correlation," in *Proc. the International Symp. on Information Theory*, (Lausanne, Switzerland), p. 159, June 30-July 5 2002.

[30] Gore, D. A., Jr., R. W. H., and Paulraj, A. J., "Transmit selection in spatial multiplexing systems," *IEEE Communications Letters*, vol. 6, pp. 491–493, Nov. 2002.

[31] Gupta, A. K. and Nadarajah, S., *Handbook of Beta distribution and its applications*. Marcel Dekker. Inc, 2004.

[32] H. Daudé, P. F. and Vallée, B., "An analysis of the Gaussian algorithm for lattice reduction," in *Proc. 1st International Symposium on Algorithmic Number Theory*, (Ithaca, NY, USA), pp. 144–158, May 1994.

[33] Hassibi, B., "An efficient square-root algorithm for BLAST," in *Proc. of Intl. Conf. on ASSP*, (Istanbul, Turkey), pp. 737–740, Jun. 5-9 2000.

[34] Hassibi, B. and Vikalo, H., "On the sphere-decoding algorithm I. Expected complexity," *IEEE Transactions on Signal Processing*, vol. 53, pp. 2806–2818, Aug. 2005.

[35] Hochwald, B. M. and ten Brink, S., "Achieving near-capacity on a multiple-antenna channel," *IEEE Transactions on Communications*, vol. 51, pp. 389–399, Mar. 2003.

[36] Hsiao, S.-F. and Delosme, J., "Householder cordic algorithms," *IEEE Transactions on Computers*, vol. 44, pp. 990–1001, Aug. 2002.

[37] J. H. Winters, J. S. and Gitlin, R. D., "The impact of antenna diversity on the capacity of wireless communication systems," *IEEE Transactions on Communications*, vol. 42, pp. 1740–1751, Feb/Mar/Apr. 1994.

[38] Jaldén, J., Barbero, L. G., Ottersten, B., and Thompson, J. S., "Full diversity detection in MIMO systems with a fixed-complexity sphere decoder," in *Proc. of Intl. Conf. on ASSP*, vol. 3, (Honolulu, HI), pp. 49–52, Apr. 15-20 2007.

[39] Jaldén, J. and Ottersten, B., "On the complexity of sphere decoding in digital communications," *IEEE Transactions on Signal Processing*, vol. 53, pp. 1474–1484, Apr. 2005.

[40] Jaldén, J., Seethaler, D., and Matz, G., "Worst- and average-case complexity of LLL lattice reduction in MIMO wireless systems," in *Proc. of Intl. Conf. on ASSP*, (Las Vegas, NV, USA), Mar. 30-Apr. 4 2008.

[41] Jiang, Y., Zheng, X., and Li, J., "Asymptotic performance analysis of V-BLAST," in *Proc. of Global Telecommunications Conference*, vol. 6, (St. Louis, USA), pp. 3882–3886, Nov. 28-Dec. 2 2005.

[42] Kaltofen, E. and Villard, G., "Computing the sign or the value of the determinant of an integer matrix, a complexity survey," *Journal on Computational Applied Math.*, vol. 162, no. 1, pp. 133–146, 2004.

[43] Kay, S., *Fundamentals of Statistical Signal Processing: Detection Theory*. Prentice Hall, 1998.

[44] Kisialiou, M. and Luo, Z.-Q., "Performance analysis of quasi-maximum-likelihood detector based on semi-definite programming," in *Proc. of Intl. Conf. on ASSP*, (Philadelphia, USA), pp. 433–436, Mar. 19-23 2005.

[45] Knuth, D. E., *Art of computer programming (2nd ed.)*. Wellesley, MA: Addison-Wesley, Apr. 1998, vol. 3, Sorting and Searching.

[46] Korkine, A. and Zolotareff, G., "Sur les formes quadratiques (in french)," *Math. Ann*, vol. 6, pp. 366–389, 1873.

[47] Kotz, S., Balakrishnan, N., and Johnson, N., *Continuous Multivariate Distributions. Volume 1: Methods and Applications*. Wiley, New York, 2000.

[48] Kotz, S., Johnson, N. L., and Boyd, D. W., "Series representations of distributions of quadratic forms in normal variables. i. central case," *The Annals of Mathematical Statistics*, vol. 38, no. 3, pp. 823–837, 1967.

[49] L. G. Barbero, T. R. and Cowan, C., "A comparison of complex lattice reduction algorithms for MIMO detection," in *Proc. of Intl. Conf. on ASSP*, (Las Vegas, NV), pp. 2705–2708, Mar. 31 - Apr. 4 2008.

[50] LaMacchia, B., "Basis reduction algorithms and subset sum problems," in *Master thesis*, (MIT), May 1991.

[51] Lenstra, A. K., Lenstra, H. W., , and Lovász, L., "Factoring polynomials with rational coefficients," *Math Ann.*, vol. 261, no. 3, pp. 515–534, 1982.

[52] Ling, C., "Approximate lattice decoding: primal versus dual basis reduction," in *Proc. IEEE Int. Symp. Inform. Theory*, (Seattle, WA), July 2006.

[53] Ling, C., "Towards characterizing the performance of approximate lattice decoding in MIMO communications," in *Proc. Int. Symp. Turbo Codes / Int. ITG Conf. Source Channel Coding*, (Munich, Germany), Apr. 2006.

[54] Ling, C. and Howgrave-Graham, N., "Effective LLL reduction for lattice decoding," in *Proc. IEEE Int. Symp. Inform. Theory*, (Nice, France), June 2007.

[55] Litwin, L. R., Endres, T. J., Hulyalkar, S. N., and Zoltowski, M. D., "The effects of finite bit precision for a VLSI implementation of the constant modulus algorithm," in *Proc. of Intl. Conf. on ASSP*, (Phoenix, AZ), pp. 2013–2016, 1999.

[56] Liu, J. and Li, J., "Turbo processing for an OFDM-based MIMO system," *IEEE Transactions on Wireless Communications*, vol. 4, pp. 1988–1993, Sept. 2005.

[57] Liu, Z., Xin, Y., and Giannakis, G. B., "Linear constellation precoding for OFDM with maximum multipath diversity and coding gains," *IEEE Transactions on Communications*, vol. 51, pp. 416–427, Mar. 2003.

[58] Lu, B. and Wang, X., "Space-time code design in OFDM systems," in *Proc. of Global Telecommunications Conference*, vol. 2, (San Francisco, CA), pp. 1000–1004, 2000.

[59] Luethi, P., Burg, A., Haene, S., Perels, D., Felber, N., and Fichtner, W., "VLSI implementation of a high-speed iterative sorted mmse qr decomposition," in *Proc. of International Symp. on Circuit and Systems*, (New Orleans, LA), pp. 1421–1424, 2007.

[60] Luo, J., Pattipati, K. R., Willett, P. K., and Hasegawa, F., "Near-optimal multiuser detection in synchronous CDMA using probabilistic data association," *IEEE Communications Letters*, vol. 5, pp. 361–363, Sept. 2001.

[61] Ma, W. K., Davidson, T. N., Wong, K. M., Luo, Z.-Q., and Ching, P. C., "Quasi-maximum-likelihood multiuser detection using semi-definite relaxation," *IEEE Transactions on Signal Processing*, vol. 50, pp. 912–922, Apr. 2002.

[62] Ma, X. and Giannakis, G. B., "Complex field coded MIMO systems: performance, rate, and tradeoffs," *Wireless Communications and Mobile Computing*, pp. 693–717, Nov. 2002.

[63] Ma, X. and Giannakis, G. B., "Full-diversity full-rate complex-field space-time coding," *IEEE Transactions on Signal Processing*, vol. 51, pp. 2917–2930, Nov. 2003.

[64] Ma, X. and Giannakis, G. B., "Space-time-multipath coding using digital phase sweeping or block circular delay diversity," *IEEE Transactions on Signal Processing*, vol. 53, pp. 1121–1131, Mar. 2005.

[65] Ma, X., Leus, G., and Giannakis, G. B., "Space-time-Doppler coding for correlated time-selective fading channels," *IEEE Transactions on Signal Processing*, vol. 53, pp. 2167–2181, June 2005.

[66] Ma, X. and Zhang, W., "Fundamental limits of linear equalizers: diversity, capacity and complexity," *IEEE Transactions on Information Theory*, vol. 54, pp. 3442–3456, Aug. 2008.

[67] Ma, X. and Zhang, W., "Performance analysis for MIMO systems with lattice-reduction aided linear equalization," *IEEE Transactions on Communications*, vol. 56, pp. 309–318, Feb. 2008.

[68] Ma, X., Zhang, W., and Swami, A., "Lattice-reduction aided linear equalizer design for linear complex-field coded OFDM systems," in *Proc. of MILCOM Conf.*, (Atlantic City, USA), Oct. 17-20 2005.

[69] Ma, X., Zhang, W., and Swami, A., "Lattice-reduction aided equalization for OFDM systems," *IEEE Transactions on Wireless Communications*, vol. 8, pp. 1608–1613, Apr. 2009.

[70] Mathai, A. M. and Provost, S. B., *Quadratic Forms in Random Variables: Theory and Applications*. New York: Marcel Dekker, 1992.

[71] Maurer, J., Matz, G., and Seethaler, D., "Low-complexity and full-diversity MIMO detection based on condition number thresholding," in *Proc. of Intl. Conf. on ASSP*, vol. 3, (Honolulu, HI), pp. 61–64, Apr. 15-20 2007.

[72] Milliner, D. and Barry, J. R., "A lattice-reduction-aided soft detector for multiple-input multiple-output channels," in *Proc. of Global Telecommunications Conference*, (San Francisco, USA), Nov. 27-Dec. 1 2006.

[73] Milliner, D. L., Zimmermann, E., Barry, J. R., and Fettweis, G., "A framework for fixed complexity breadth-first MIMO detection," in *Proc. International Symposium on Spread Spectrum Techniques and Applications*, (Bologna, Italy), Aug. 25-28 2008.

[74] Mow, W. H., "Universal lattice decoding: a review and some recent results," in *Proc. of International Conference on Communications*, pp. 2842–2846.

[75] Narasimhan, R., "Finite-snr diversity-multiplexing tradeoff for correlated rayleigh and rician mimo channels," *IEEE Transactions on Information Theory*, vol. 52, pp. 3965–3979, Sept. 2006.

[76] Niu, J. and Lu, I.-T., "A new lattice-reduction-based receiver for MIMO systems," in *Proc. of 41st CISS*, (John Hopkins University, USA), Mar. 14-16 2007.

[77] Pammer, V., Delignon, Y., Sawaya, W., and Boulinguez, D., "A low complexity suboptimal MIMO receiver: the combined ZF-MLD algorithm," in *Proc. of Personal, Indoor and Mobile Radio Communications*, vol. 3, (Beijing, China), pp. 2271–2275, Sept. 7-10 2003.

[78] Papoulis, A. and Pillai, U. S., *Probability, Random Variables and Stochastic Processes*. McGraw-Hill Science/Engineering/Math, 2001.

[79] Ponnampalam, V., McNamara, D., Lillie, A., and Sandell, M., "On generating soft outputs for lattice-reduction-aided mimo detection," in *Proc. of International Conference on Communications*, (Glasgow, Scotland), pp. 4144–4149, Jun. 24-28 2007.

[80] Proakis, J. G., *Digital communications*. McGraw-Hill, 2000.

[81] Qi, X. and Holt, K., "A lattice-reduction-aided soft demapper for high-rate coded MIMO-OFDM systems," *IEEE Signal Processing Letters*, vol. 14, pp. 305–308, May 2007.

[82] Ryan, W., McPheters, L., and McLaughlin, S., "Combined turbo coding and turbo equalization for pr4-equalized lorentzian channels," in *Proc. of 32nd CISS*, (Princeton University, USA), Mar. 18-20 1998.

[83] Scharnhorst, K., "Angles in complex vector spaces," *Acta Applicandae Mathematicae*, vol. 69, pp. 95–103, Oct. 2001.

[84] Schnorr, C. P. and Euchner, M., "Lattice basis reduction: improved practical algorithms and solving subset sum problems," *Math. Programming*, vol. 66, pp. 181–191, 1994.

[85] Seethaler, D. and Matz, G., "Efficient vector perturbation in multi-antenna multi-user systems based on approximate integer realtions," in *Proc. of European Signal Proc. Conf.*, pp. 673–676, 2006.

[86] Seethaler, D. and Matz, G., "Efficient vector perturbation in multi-antenna multi-user systems based on approximate integer relations," in *Proc. of the European Signal Proc. Conf. (EUSIPCO)*, (Florence, Italy), Sept. 4-8 2006.

[87] Seethaler, D., Matz, G., and Hlawatsch, F., "Low-complexity mimo data detection using Seysen's lattice redution algorithm," in *Proc. of Intl. Conf. on ASSP*, (Honolulu, USA), Apr. 15-20 2007.

[88] Seysen, M., "Simultaneous reduction of a lattice basis and its reciprocal basis," *Combinatorica*, vol. 13, pp. 363–376, 1993.

[89] Sezgin, A., Jorswieck, E. A., and Costa, E., "Lattice-reduction aided detection: spatial multiplexing versus quasi-orthogonal stbc," in *Proc. of Vehicular Technology Conference*, vol. 4, (Los Angels, USA), pp. 2389–2393, Sept. 26-29 2004.

[90] Shin, H. and Lee, J. H., "Capacity of multiple-antenna fading channels: spatial fading correlation, double scattering, and keyhole," *IEEE Transactions on Information Theory*, vol. 49, pp. 2636–2647, Oct. 2003.

[91] Silvola, P., Hooli, K., and Juntti, M., "Suboptimal soft-output map detector with lattice reduction," *IEEE Signal Processing Letters*, vol. 13, pp. 321–324, June 2006.

[92] Simon, M. K., *Probability distributions involving Gaussian random variables*. Kluwer Academic Publishers, 2002.

[93] Singh, C., Prasad, S., and Balsara, P., "A fixed-point implementation for qr decomposition," in *IEEE Dallas/CAS Workshop on Design, Application, Integration and Software*, (Richardson, TX), pp. 75–78, 2006.

[94] Stefanov, A. and Duman, T. M., "Turbo-coded modulation for systems with transmit and receive antenna diversity over block fading channels: system model, decoding approaches, and practical considerations," *IEEE Journal on Selected Areas in Communications*, vol. 19, pp. 958–968, May 2001.

[95] Steingrimsson, B., Luo, Z.-Q., and Wong, K.-M., "Quasi-maximum-likelihood detection for multiple-antenna channels," *IEEE Transactions on Signal Processing*, vol. 51, pp. 2710–2719, Nov. 2003.

[96] Taherzadeh, M., Mobasher, A., and Khandani, A. K., "Lattice-basis reduction achieves the precoding diversity in MIMO broadcast systems," in *Proc. of 39th CISS*, (John Hopkins University, USA), Mar. 15-18 2005.

[97] Tarokh, V., Jafarkhani, H., and Calderbank, A. R., "Space-time block coding for wireless communications: performance results," *IEEE Journal on Selected Areas in Communications*, vol. 17, pp. 451–460, Mar. 1999.

[98] Tarokh, V., Seshadri, N., and Calderbank, A. R., "Space-time codes for high data rate wireless communication: performance criterion and code construction," *IEEE Transactions on Information Theory*, vol. 44, pp. 744–765, Mar. 1998.

[99] Telatar, I. E., "Capacity of multi-antenna gaussian channels," *European Trans. Telecomm*, vol. 10, pp. 585–595.

[100] Tepedelenlioglu, C., "Maximum multipath diversity with linear equalization in precoded OFDM systems," *IEEE Transactions on Information Theory*, vol. 50, pp. 232–235, Jan. 2004.

[101] Tse, D. and Viswanath, P., *Fundamentals of wireless communications*. Cambridge, 2005.

[102] Tulino, A. M. and Verdu, S., *Random matrix theory and wireless communications*. USA: now Publishers Inc., 2004.

[103] Verdu, S., *Multiuser Detection*. Cambridge University Press, 1998.

[104] Vikalo, H. and Hassibi, B., "On the sphere-decoding algorithm II. Generalizations, second-order statistics, and applications to communications," *IEEE Transactions on Signal Processing*, vol. 53, pp. 2819–2834, Aug. 2005.

[105] Vikalo, H., Hassibi, B., and Kailath, T., "Iterative decoding for mimo channels via modified sphere decoder," *IEEE Transactions on Wireless Communications*, vol. 3, pp. 2299–2311, Nov. 2004.

[106] Wang, Z. and Giannakis, G. B., "Complex-field coding for OFDM over fading wireless channels," *IEEE Transactions on Information Theory*, vol. 49, pp. 707–720, Mar. 2003.

[107] Wang, Z. and Giannakis, G. B., "A simple and general parameterization quantifying performance in fading channels," *IEEE Transactions on Communications*, vol. 51, pp. 1389–1398, Aug. 2003.

[108] Wang, Z., Ma, X., and Giannakis, G. B., "OFDM or single-carrier zero-padded block transmissions?," *IEEE Transactions on Communications*, vol. 52, pp. 380–394, Mar. 2004.

[109] Waters, D. W. and Barry, J. R., "A reduced-complexity lattice-aided decision-feedback detector," in *Proc. International Conference on Wireless Networks, Communications and Mobile Computing*, vol. 2, (Maui, HI), pp. 845–850, June 13-16 2005.

[110] Waters, D. W. and Barry, J. R., "The chase family of detection algorithms for MIMO channels," *IEEE Transactions on Signal Processing*, vol. 56, pp. 739–747, Feb. 2008.

[111] Windpassinger, C. and Fischer, R. F. H., "Low-complexity near-maximum-likelihood detection and precoding for MIMO systems using lattice reduction," in *Proc. of Information Theory Workshop*, (Munich, Germany), pp. 345–348, Mar. 31-Apr. 4 2003.

[112] Windpassinger, C. and Fischer, R. F., "Optimum and sub-optimum lattice-reduction-aided detection and precoding for MIMO communications," in *Proc. Canadian Workshop on Information Theory*, (Waterloo, Ontario, Canada), pp. 88–91, May 2003.

[113] Windpassinger, C., Lampe, L., Fischer, R. F. H., and Hehn, T., "A performance study of MIMO detectors," *IEEE Transactions on Wireless Communications*, vol. 5, pp. 2004–2008, Aug. 2006.

[114] Windpassinger, C., Lampe, L., and Fischer, R. F., "From lattice-reduction-aided detection towards maximum-likelihood detection in mimo systems," in *Proc. of International Conference on Wireless and Optical Communications*, (Banff, Canada), July 14-16 2003.

[115] Wong, K.-W., Tsui, C.-Y., Cheng, R.-K., and Mow, W.-H., "A VLSI architecture of a K-best lattice decoding algorithm for MIMO channels," in *Proc. of IEEE International Symposium on Circuits and Systems*, vol. 3, (Scottsdale, USA), pp. 273–276, May 26-29 2002.

[116] Wübben, D., Böhnke, R., Kühn, V., and Kammeyer, K.-D., "MMSE extension of V-BLAST based on sorted QR decomposition," in *Proc. of Vehicular Technology Conference*, vol. 1, (Orlando, USA), pp. 508–512, Oct. 6-9 2003.

[117] Wübben, D., Böhnke, R., Kühn, V., and Kammeyer, K.-D., "Near-maximum-likelihood detection of MIMO systems using MMSE-based lattice reduction," in *Proc. of International Conference on Communications*, vol. 2, (Paris, France), pp. 798–802, Jun. 20-24 2004.

[118] Wübben, D. and Seethaler, D., "On the performance of lattice reduction schemes for MIMO data detection," in *Proc. of Asilomar Conf. on Signals, Systems,and Computers*, (Pacific Grove, CA), pp. 1534–1538, Nov. 4-7 2007.

[119] Xin, Y., Liu, Z., and Giannakis, G. B., "High-rate layered space-time coding based on constellation precoding," in *Proc. of Wireless Communications and Networking Conf.*, vol. 1, (Orlando, France), pp. 471–476, Mar. 17-21 2002.

[120] Xin, Y., Wang, Z., and Giannakis, G. B., "Space-time diversity systems based on linear constellation precoding," *IEEE Transactions on Wireless Communications*, vol. 2, pp. 294–309, Mar. 2003.

[121] Yao, H., "Efficient signal, code, and receiver designs for MIMO communication systems," in *Doctoral Thesis*, (Department of Electrical Engineering and Computer Science, Massachusetts Institute of Technology), 2003.

[122] Yao, H. and Wornell, G. W., "Lattice-reduction-aided detectors for MIMO communication systems," in *Proc. of Global Telecommunications Conference*, vol. 1, (Taipei, Taiwan), pp. 424–428, Nov. 17-21 2002.

[123] Yao, H. and Wornell, G. W., "Achieving the full MIMO diversity-multiplexing frontier with rotation-based space-time codes," in *Proc. of Allerton Conf. on Communications, Control and Computing*, (IL, USA), Oct. 2003.

[124] Yap, C. K., *Fundamental problems in algorithmic algebra*. Oxford University Press, 1999.

[125] Zhang, W., Arnold, F., and Ma, X., "An analysis of Seysen's lattice reduction algorithm," *Signal Processing*, vol. 88, pp. 2573–2577, Oct. 2008.

[126] Zhang, W. and Ma, X., "Performance analysis for V-BLAST systems with linear equalization," in *Proc. of 39th CISS*, (John Hopkins University, MD), Mar. 15-18 2005.

[127] Zhang, W. and Ma, X., "Approaching optimal performance by lattice-reduction aided soft detectors," in *Proc. of 41st CISS*, (John Hopkins University, USA), Mar. 14-16 2007.

[128] Zhang, W. and Ma, X., "A suboptimal equalizer for mimo systems to guarantee maximum diversity and near linear equalization complexity," in *IEEE Workshop on Signal Processing Advances in Wireless Communications*, (Helsinki, Finland), Jun. 5-8 2007.

[129] Zhang, W. and Ma, X., "What determines the diversity order of linear equalizers?," in *Proc. of Intl. Conf. on ASSP*, vol. 3, (Honolulu, HI), pp. 57–60, Apr. 15-20 2007.

[130] Zhang, W. and Ma, X., "Quantifying diversity for wireless systems with finite-bit representation," in *Proc. of Intl. Conf. on ASSP*, (Las Vegas, NV), Mar. 30CApr. 4 2008.

[131] Zhang, W. and Ma, X., "Low-complexity soft-output decoding with lattice-reduction-aided detectors," *IEEE Transactions on Communications*, June 2009 (revised).

[132] Zhang, W., Ma, X., Gestner, B., and Anderson, D. V., "Designing low-complexity equalizers for wireless systems," *IEEE Communications Magazine*, vol. 47, pp. 56–62, Jan. 2009.

[133] Zheng, L. and Tse, D., "Diversity and multiplexing: a fundamental tradeoff in multiple-antenna channels," *IEEE Transactions on Information Theory*, vol. 49, pp. 1073–1196, May 2003.

[134] Zhu, H., Shi, Z., and Farhang-Boroujeny, B., "Mimo detection using markov chain monte carlo techniques for near-capacity performance," in *Proc. of Intl. Conf. on ASSP*, (Philadelphia, USA), Mar. 18-23 2005.

[135] Zou, W. and Wu, Y., "COFDM: an overview," *IEEE Trans. on Broadcasting*, vol. 41, pp. 1–8, Mar. 1995.

VITA

Wei Zhang was born on May 14, 1982 in Qingdao, a beautiful seaside city in China. He graduated from Qingdao No. 2 Middle School in 2000. Then, he attended Zhejiang University in Hangzhou, China, where he got his Bachelor of Engineering degree from the Department of Information Science and Electronic Engineering and Chu Kechen Honors College in 2004. He got his M.S. degree in 2006 from Department of Electrical and Computer Engineering, Auburn University, Auburn, AL, USA. Since then, he has been working towards his Ph.D. degree in Electrical and Computer Engineering at the Georgia Institute of Technology, Atlanta, Georgia, USA.